REINFORCEMENT LEARNING IN SELF ORGANIZING CELLULAR NETWORKS

by

Roohollah Amiri

A dissertation

submitted in partial fulfillment

of the requirements for the degree of

Doctor of Philosophy in Electrical and Computer Engineering

Boise State University

May 2020

© 2020
Roohollah Amiri
ALL RIGHTS RESERVED

BOISE STATE UNIVERSITY GRADUATE COLLEGE

DEFENSE COMMITTEE AND FINAL READING APPROVALS

of the dissertation submitted by

Roohollah Amiri

Dissertation Title: Reinforcement Learning In Self Organizing Cellular Networks

Date of Oral Examination: 29 May 2020

The following individuals read and discussed the dissertation submitted by student Roohollah Amiri, and they evaluated the presentation and response to questions during the final oral examination. They found that the student passed the final oral examination.

Hani Mehrpouyan, Ph.D.	Chair, Supervisory Committee
John Chiasson, Ph.D.	Member, Supervisory Committee
Hao Chen, Ph.D.	Member, Supervisory Committee
Erik Perrins, Ph.D.	External Examiner

The final reading approval of the dissertation was granted by Hani Mehrpouyan, Ph.D., Chair of the Supervisory Committee. This dissertation was approved by the Graduate College.

To my parents who sacrificed too much for me.

ACKNOWLEDGMENTS

I am using this opportunity to express my gratitude to my advisor Dr. Hani Mehrpouyan for his support, guidance, and friendship during the last five years. Dr. Mehrpouyan is one of the sharpest people I know who despite his intelligence does not have a bigoted attitude. Dr. Mehrpouyan always gave me freedom on choosing my research topics and people who I worked with. He always shows genuine excitement in my ideas and supports them on many different levels from idea to analysis and implementation. Dr. Mehrpouyan's scrutiny on writing and presentation of ideas has improved my writing skills enormously. His willingness to collaborate with other researchers has made many opportunities for me. I thank him for his patience in reviewing my papers, and generosity of sharing his technical material with me.

My sincere gratitude goes to Professor Jeffrey G. Andrews who agreed to host me at the University of Texas at Austin for about a year in 2019. Working with Professor Andrews has been a pivot point in my career. During my visit at UT Austin, I had many valuable meetings and discussions with Prof. Andrews and I am grateful for such experience.

I would like to extend my gratitude towards my committee members, Dr. John Chiasson and Dr. Hao Chen. I always enjoyed my technical discussions with them during courses that I took with them. My sincere thanks goes to Dr. Chiasson for his effort in developing great courses in machine learning. I would like to use this opportunity to thank Jenn Ambrose, the ECE department manager, and all her staff.

I have had the chance to work with brilliant researchers during my PhD as collaborations on different projects and technical papers. Here, my sincere thanks goes to Professor David Matolak at the University of South Carolina, Dr. Maged Elkashlan at Queen Mary University of London, Dr. Lex Fridman at Massachusetts Institute of Technology, Professor Ranjan K. Mallik at Indian Institute of Technology, Professor Arumugam Nallanathan at Kings College London, Dr. Eren Balevi at University of Texas at Austin, and Dr. Mojtaba Vaezi at Villanova University.

Special thanks to Dr. Solmaz Niknam, Mojtaba Ahmadi Almasi, and Ruthvik Vaila as my lab mates and close friends and for many technical discussions, arguments, and laughter. I also thank all the lab members and former visitors of High Performance Computing lab for creating a nice environment for research. I have to thank my group mates at UT Austin for great meetings and technical discussions. My special thanks go to my friends Ahmad AlAmmouri, Anum Ali, and Rebal Jurdi who made my visit at UT Austin memorable.

When it comes to living in a foreign country, friends have the potential to be your family. I have been privileged for having such friends who I call family now, Zachariah Vandeventer and Isabella Cohen and their beautiful families. My special thanks goes to Zachariah who has been my partner in crime during my life in Boise. Further, my gratitude goes to Bahareh Badamchi who always treated me with kindness.

Finally and most importantly, I thank my family back home for their unconditional support, their unwavering confidence in my abilities and their encouragement in all of my endeavors. My unconditional love goes to my sister and brother who I wish all the best for. Without you, this journey would not have been possible.

ABSTRACT

Self-organization is a key feature as cellular networks densify and become more heterogeneous, through the additional small cells such as pico and femtocells. Self-organizing networks (SONs) can perform self-configuration, self-optimization, and self-healing. These operations can cover basic tasks such as the configuration of a newly installed base station, resource management, and fault management in the network. In other words, SONs attempt to minimize human intervention where they use measurements from the network to minimize the cost of installation, configuration, and maintenance of the network. In fact, SONs aim to bring two main factors in play: intelligence and autonomous adaptability. One of the main requirements for achieving such goals is to learn from sensory data and signal measurements in networks. Therefore, machine learning techniques can play a major role in processing underutilized sensory data to enhance the performance of SONs.

In the first part of this dissertation, we focus on reinforcement learning as a viable approach for learning from signal measurements. We develop a general framework in heterogeneous cellular networks agnostic to the learning approach. We design multiple reward functions and study different effects of the reward function, Markov state model, learning rate, and cooperation methods on the performance of reinforcement learning in cellular networks. Further, we look into the optimality of reinforcement learning solutions and provide insights into how to achieve optimal solutions.

In the second part of the dissertation, we propose a novel architecture based on spatial indexing for system-evaluation of heterogeneous 5G cellular networks. We develop an open-source platform based on the proposed architecture that can be used to study large scale directional cellular networks. The proposed platform is used for generating training data sets of accurate signal-to-interference-plus-noise-ratio (SINR) values in millimeter-wave communications for machine learning purposes. Then, with taking advantage of the developed platform, we look into dense millimeter-wave networks as one of the key technologies in 5G cellular networks. We focus on topology management of millimeter-wave backhaul networks and study and provide multiple insights on the evaluation and selection of proper performance metrics in dense millimeter-wave networks. Finally, we finish this part by proposing a self-organizing solution to achieve k-connectivity via reinforcement learning in the topology management of wireless networks.

TABLE OF CONTENTS

LIST OF TABLES

LIST OF FIGURES

LIST OF ABBREVIATIONS

SON – Self Organizing Network

RL – Reinforcement Learning

MARL – Multi Agent Reinforcement Learning

HetNet – Heterogeneous Network

MBS – Macro Base Station

SBS – Small Base Station

FBS – Femto Base Station

UE – User Equipment

FUE – Femto User Equipment

MUE – Macro User Equipment

SNR – Signal to Noise Ratio

SINR – Signal to Interference plus Noise Ratio

DL – Deep Learning

DNN – Deep Neural Network

MDP – Markov Decision Process

mmWave – Millimeter Wave

WSN – Wireless Sensor Network

RAN	– Radio Access Network
MIMO	– Multiple Input Multiple Output
LoS	– Line of Sight
NLoS	– Non Line of Sight
IL	– Independent Learning
CL	– Cooperative Learning
CSI	– Channel State Information

Chapter 1

INTRODUCTION

Self-organizing network (SON) technology minimizes the cost of running a mobile network by eliminating manual configuration of network elements at the time of deployment, through dynamic optimization and troubleshooting during operation. Further, SON improves network performance, customer experience, and reduces the cost of mobile operator services. SON started as an approach to improve performance of cellular radio access network (RAN) deployment and optimization in 2008. However, its focus is gradually extending beyond RAN to managing the core network as well. Largely driven by the increasing complexity of new wireless network generation (5G), multi-RAN, densification, and spectrum heterogeneity, global investments in SON technology are expected to grow. By the end of 2022, the research estimates that SON will account for a market worth 5.5 Billion dollars [1].

One of the new developments in SON is increasing its capabilities in self-learning through artificial intelligence techniques. Self-learning is considered to be critical to address 5G requirements. Reinforcement learning [2] is one of the most used approaches from machine learning to make self-learning algorithms viable in SON. This dissertation focuses on developing frameworks, algorithms, and platforms to integrate reinforcement learning methods into algorithms designed for cellular networks. This chapter reviews some of the technologies of 5G, features of SON, and reasons of interest in reinforcement learning. Then, the challenges of developing a reinforcement learning algorithm are described. Finally, the contributions of the dissertation are detailed.

1.1 The Road to 5G

5G is expected to provide multiple folds of data capacity, higher security and better QoS in the next decade. Many new technologies will rely on 5G such as Virtual reality (VR), augmented reality (AR), streaming services such as Chromecast or SanDisk, and connected cars such as OnStar or Autonet. To realize such a vision, three key technologies are under development: millimeter wave (mmWave) communications, massive multiple-input multiple-output (MIMO), and ultra-densificiation [3].

To achieve higher rates promised for 5G there is just one way: Going up in frequency. The mmWave frequency range between 30-300 GHz is almost unused and can provide bandwidth on the range of GHz for communication. However, to be able to use mmWave frequencies, new technologies needed to be developed at link-level and new algorithms need to be designed at the system-level.

Severe path loss at mmWave frequencies was a barrier to not consider it for wireless communication for a long time. However, thanks to the short wavelength at mmWave frequencies, directivity can be achieved by using a large number of antennas at transmitters and receivers to mitigate severe path loss [4]. MmWave has been considered for short-range communications (such as Wi-Fi connections). Further, cost-efficient mmWave communication in cellular networks is promised in a few years. Three beamforming architectures have been proposed for mmWave systems: *digital* [4], *analog* [5], and *hybrid* [6]. Hybrid beamforming is achieved with different architectures such as: (*i*) hybrid beamforming with phase-shifters [6], (*ii*) hybrid beamforming with lens antennas [7], and (*iii*) hybrid beamforming with reconfigurable microelectromechanical systems (MEMS) integrated antennas [8]. Ahmadi *et. al.* have developed new architecture (RA-MIMO) based on lens antennas to generate multiple independent beams simultaneously using a single RF chain [9–11]. RA-MIMO is used to combat small-scale fading and shadowing in mmWave bands. Further, multiple new antenna designs to steer the beam at mmWave frequencies are proposed at [12–14].

At the system-level, one of the basic while effective ways to increase the capacity of a cellular network is to make cells smaller. Cell shrinking results in reusing frequency spectrum across a geographical area and less competition for users over resources. Technically there is no limitation on reducing the cell size, even until the point in which each access point just services one user [3]. In general, *ultra densification* is one main technology to achieve higher data rates. Densification is achieved using nested cells which is the use of low-range small base stations to provide better coverage or higher capacity for the users. These small cells can be picocells (range below 100m), or femtocells (Wi-Fi range). Meanwhile, achieving the full potential of densification to improve the spectral efficiency of access links runs into the significant bottleneck of efficient backhauling.

Wired and wireless technologies can be used as backhaul solutions. Wired technologies such as fiber or xDSL have the advantage of high throughput, high reliability, and low latency. However, wired solutions have high expenses and situational impracticality in providing backhaul to a large number of small cells [15]. On the contrary, wireless technology is a potential solution to provide a cost-efficient and scalable backhaul support when a wired solution is impractical [16, 17]. Wireless backhaul technologies can operate at Sub6GHz or mmWave bands. Sub6GHz wireless backhaul has the advantage of non-line-of-sight (NLoS) transmission with the disadvantage of co-channel interference and variable delay. In contrast, thanks to a large spectrum, high directional transmission, and low delay of line-of-sight (LoS) links, mmWave communications can be modeled as pseudo-wired communications without interference [18]. Therefore, mmWave communications are suitable candidates for the backhaul of dense small cells.

Considering the above, 5G will be heterogeneous on the access and backhaul networks. Further, the number of nodes in a 5G network will increase in multiple folds. As 5G gets more complex, network management procedures need to evolve as well. In the following, we look into the SON as a viable solution for 5G network management.

1.2 Self-Organizing Networks

As 5G networks get more complex, the management of such a system becomes a challenge. In wireless networks, many network elements and associated parameters are manually configured. Planning, commissioning, configuration, and management of these parameters are essential for efficient and reliable network operation. Manual tuning has limitations such as:

- Specialized expertise must be maintained to tune network parameters.
- The existing manual process is time-consuming and error-prone.
- Manual tuning results in long delays in response to the often rapidly-changing network topologies and operating conditions.

- Manual tuning results in sub-optimal network performance.

Considering the above, the big picture vision for the management of large cellular networks raised some questions: Could future networks become intelligent and organize their operations autonomously? What is the definition of intelligence/learning? How do existing nodes adapt their operating parameters when a new node is added (removed) to (from) the network? Such discussion was the introduction of the SON concept in cellular networks.

SON has been discussed and defined in many parts of the literature. Here, we bring our favorite definitions:

- SONs are intelligent systems which **learn** from **environment** and **adapt** to statistical variations [19].

- A phenomenon in which nodes work **cooperatively** in response to changes in the environment in order to achieve certain goals [20].

- A set of entities that obtain a **global** system behavior as a result of **local interactions** without central control [21].

In cellular networks, SON refers to scalable, stable, and agile **mobile network automation** to **minimize human intervention** with three main features: (*i*) scalability: bounded complexity with respect to network size, (*ii*) stability: transition from current state to desired state in limited time, and (*iii*) agility: transition should not be sluggish! In cellular networks, SON aims for improving the network performance while reducing capital and operational expenditures (CAPEX/OPEX).

Self-organization is a key feature as cellular networks densify and become more heterogeneous, through the additional small cells such as pico and femtocells. SON's operations are defined at the deployment phase (self-configuration), optimization phase (self-optimization), and maintenance phase (self-healing) [22]. These operations can cover basic tasks such as the configuration of a newly installed base station, resource management, and fault management in the network [23].

1.3 SON Requirements and Reinforcement Learning

One of the requirements of self-organization in cellular networks is open-loop communication. This means that a transmitter has only access to a channel quality indicator (CQI) signal received from its related receiver. CQI can be translated into signal-to-interference-plus-noise-ration (SINR). Hence, on a high-level definition, many problems in SON can be translated to making the transmitter intelligent enough to configure/adapt itself based on SINR measurements. Further, intelligence can be defined as learning a function/map from measurements (data samples) to a required parameter. For instance, if p_i stands for transmit power for the $(i-1)th$ SINR measurement (γ_{i-1}), self-learning as a power control problem can be defined as follows.

Definition 1. For a given dataset $(\gamma_i, p_i)_{i=1}^{m}$ drawn from fixed and unknown distribution $\rho\left(\Gamma, \mathcal{P}\right)$, find a function f such that

$$f\left(\gamma_{i-1}\right) = p_i,\ \ i = 1, ..., m. \tag{1.1}$$

The above definition relates to the concept of statistical learning or more commonly known as machine learning.

The problem in Definition 1 has the following challenges:

- All signal measurements are not available at the transmitter at once. Hence, the data set needs to be acquired during interaction with the receiver (or environment).

- Correct outputs are unknown. In supervised learning algorithms, the correct label (p_i) for input (γ_{i-1}) is known. However, here there is no model of the network at the transmitter and calculation of correct transmit power potentially ends in a non-convex problem depending on channel coefficients.

- The transmitter needs to adapt the mapping function continuously due to the changes in wireless channels.

Considering the above challenges, reinforcement learning (RL) is a promising approach to attack the problem. RL is a branch of machine learning that concerns with finding an optimal policy to interact with an unknown environment. In RL, the environment is defined as a Markov decision process (MDP) and policy is defined as a mapping between the MDP states and the actions taken at those states [24]. In each time step, t, an agent takes an action (a_t) and receives a reward (R_t) and transits to a new state (s_t) in interaction with the environment. The goal of the RL is to maximize the total received reward by interacting with the environment. In Fig. 1.1, the agent, environment, and their interaction are illustrated.

We can define a learning model comprised of the following elements:

- Agent: which is the transmitter in our problem.

- Environment: the channel, receiver, and all other communication devices affecting the desired link SINR.

- **S**: state space, a finite set of environment states.

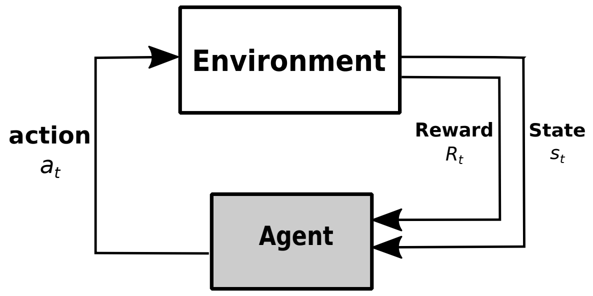

Figure 1.1: Agent and environment interaction in RL

- **A**: action space, a finite set of actions.
- **r**: $\mathbf{S} \rightarrow \mathbf{R}$, a reward function.

And the goal of RL is to find a policy (Π) in a stochastic MDP that maximizes the cumulative received reward

$$\underset{\Pi}{\text{maximize}}\ E\left[R|\Pi\right] \tag{1.2a}$$

$$\text{where } R = \sum_{i=0}^{\infty} r_i. \tag{1.2b}$$

Q-*learning* is a RL method that finds an optimal action-selection policy for a finite MDP with dynamic programming [25]. Q-*learning* learns an action-value function called *Q-function* ($Q(\mathbf{s}, a)$) which ultimately gives the value of taking an action a in state $\mathbf{s}$. The Q-function provides the agent with the optimal policy. One of the main features of Q-*learning* is that it is model-free, which means no information from the environment is known a priori by the agent. This model fits our problem very well, in which the transmitter (for instance a new small base station) can be considered as an agent which is deployed in the cellular network (environment) with no prior information.

The *one-step* Q-*learning* update rule is

$$Q(\mathbf{s}_t, a_t) \leftarrow (1-\alpha)Q(\mathbf{s}_t, a_t) + \alpha \max_a (r_t + \gamma Q(\mathbf{s}_{t+1}, a)), \tag{1.3}$$

where r_t is the received reward, $\mathbf{s}_t$ is the state, a_t is the action at time step t, $0 \leq \gamma \leq 1$ is the discount factor, and α is the learning rate. Algorithm 1 specifies the Q-*learning* in procedural form [2].

Algorithm 1 Q-Learning algorithm

```
1: Initialize $Q(\mathbf{s}_t, a_t)$ arbitrarily
2: Initialize $\mathbf{s}_t$
3: for all episodes do
4:     for all steps of episode do
5:         Choose $a_t$ from set of actions
6:         Take action $a_t$, observe $R_t$, $\mathbf{s}_{t+1}$
7:         $Q(\mathbf{s}_t, a_t) \leftarrow (1-\alpha)Q(\mathbf{s}_t, a_t) + \alpha \max_a(r_t + \gamma Q(\mathbf{s}_{t+1}, a))$
8:         $\mathbf{s}_t \leftarrow \mathbf{s}_{t+1}$;
9:     end for
10: end for
```

1.4 Challenges

Designing an RL algorithm in many situations is not conventional. Prof. Sutton in his book [2], mentions that selecting the state sets and actions varies from one task to another and such representation methods are more of an art than science. Generally, the challenges of designing an RL algorithm can be categorized as follows.

- Defining state and action set based on the problem definitions and context of the environment.

- Designing reward functions that satisfy multiple constraints of an optimization problem.
- Cooperation and coordination method definitions in multi-agent problems.
- Finding proper bounds for sample complexity or the number of samples needed to achieve close to optimal solutions.
- Investigating optimality of an RL solution after designing an algorithm.

Another challenge in machine learning-based algorithms is generating accurate data sets that are close to reality in a simulation environment. Furthermore, the implementation of multi-agent RL algorithms in large networks becomes a challenge. We faced this problem in mmWave backhaul networks, where hundreds of nodes (agents) need to interact with each other.

In this dissertation, we focus on the above challenges on the access and backhaul of cellular networks. The summary of the contributions of this dissertation is in the following.

1.5 Summary of Contributions

In the first part of this dissertation, we focus on reinforcement learning as a viable approach for learning from signal measurements. We develop a general framework in heterogeneous cellular networks agnostic to the learning approach. We design multiple reward functions and study different effects of reward function, Markov state model, learning rate, and cooperation methods on the performance of reinforcement learning in cellular networks. Further, we look into optimality of reinforcement learning solutions and provide insights of how to achieve optimal solutions.

In the second part of the dissertation, we propose a novel technique based on spatial indexing for system-evaluation of heterogeneous 5G cellular networks. Further, we develop an open-source platform that can be used to study large scale directional cellular networks. The proposed platform is used for generating training data sets of accurate signal-to-interference-plus-noise-ratio (SINR) values in millimeter-wave communications. Then, with taking advantage of the developed platform, we look into dense millimeter wave networks as one of the key technologies in 5G cellular networks. We focus on topology management of millimeter wave backhaul networks and study and provide multiple insights on evaluation and selection of proper performance metrics in dense millimeter wave networks. Finally, we finish this part by proposing a self-organizing solution to achieve k-connectivity in topology management of wireless networks.

We summarize our contributions in this dissertation as follows.

⋆ Chapter 2: Reinforcement Learning for Self Organization and Power Control of Heterogeneous Networks

1. We propose a framework that is agnostic to the choice of learning method but also connects the required RL analogies to wireless communications. The proposed framework models a multi-agent network with a single MDP that contains the joint action of the all the agents as its action set. Next, we introduce MDP factorization methods to provide a distributed and scalable architecture for the proposed framework. The proposed framework is used to benchmark the performance of different learning rates, Markov state models, or reward functions in two-tier wireless networks.

2. We present a systematic approach for designing a reward function based on the optimization problem and the nature of RL. In fact, due to scarcity of resources in a dense network, we propose some properties for a reward function to maximize sum transmission rate of the network while considering minimum requirements of all users. The procedure is simple and general and the designed reward function is in the shape of low complexity polynomials. Further, the designed reward function results in increasing the achievable sum transmission rate of the network while consuming considerably less power compared to greedy based algorithms.

3. We propose Q-DPA as an application of the proposed framework to perform distributed power allocation in a dense femtocell network. Q-DPA uses the factorization method to derive independent and cooperative learning from the optimal solution. Q-DPA uses local signal measurements at the femtocells to train the FBSs in order to: (i) maximize the transmission rate of femtocells, (ii) achieve minimum required QoS for all femtocell users with a high probability, and (iii) maintain the QoS of macrocell users in a densely deployed femtocell network. In addition, we determine the minimum number of samples that is required to achieve an ϵ-optimal policy in Q-DPA as its sample complexity.

4. We introduce four different learning configurations based on different combinations of independent/cooperative learning and Markov state models. We conduct extensive simulations to quantify the effect of different learning configurations on the performance of the network. Simulations show that the proposed Q-DPA algorithm can decrease power usage and as a result reduce the interference to the macrocell user.

– This work was published in [26, 27].

⋆ Chapter 3: Power Allocation in Interference-Limited Networks via Coordinated Learning

1. We model the whole small cell network as a Markov decision process (MDP) with the small base stations (SBSs) being represented as the agents of the MDP. Then, we define a coordination graph according to the interference model of the network. The global MDP is factorized to local ones and the value function of the MDP is approximated by a linear combination of local value functions.
2. Each SBS uses a model-free reinforcement learning approach, i.e., Q-learning. Q-learning is used to update the SBS's local value function. Subsequently, we leverage the ability of SBSs to communicate over the backhaul network to build a simple message passing structure to select a transmit power action based on the variable elimination method.
3. Finally, we propose a distributed algorithm which finds an optimal joint power allocation to maximize the sum transmission rate.

– This work was published in [28].

⋆ Chapter 4: Spatial Indexing for System-Level Evaluation of 5G Heterogeneous Cellular Networks

1. We propose a multi-level inheritance based structure to be able to store different nodes of a HetNet on a single geometry tree. The proposed structure is polymorphic in a sense that different levels of a node can be accessed via dynamic casting.

2. We focus on potentials of spatial indexing in accelerating the simulation of directional communications. We introduce different spatial queries and show that spatial indexing significantly accelerates simulation time in orders of magnitude when it comes to location-based searches over azimuth, and elevation as well as its traditional usage in searches over distance.

– This work is submitted for possible publication in [29].

⋆ Chapter 5: Topology Management in Millimeter Wave Wireless Backhaul in 5G Cellular Networks

1. We focus on the effect of selecting signal-to-noise-ratio (SNR) vs signal-to-interference-plus-noise-ratio (SINR) as mmWave link quality performance in dense mmWave networks. In fact, in directional communications, the links are sometimes assumed to be interference-free, and the SNR metric is used in simulations. Here, we show that despite the fact that in directional communications, the interference-free assumption is reasonable, however, in cases of occurrence of interference, SNR is not a valid metric and SINR should be considered to make a correct decision.

2. We design a self-organizing algorithm based on reinforcement learning to achieve k-connectivity in a backhaul network. Redundancy in a backhaul network is one of the requirements of a fail-safe topology, and k-connectivity is a key performance factor in topology management. Hence, we use Q-learning to design a transmission range control algorithm to achieve k-connectivity in a backhaul network.

1.6 Dissertation Organization

We organize the remainder of this dissertation as follows. In Chapter 2, we present a learning framework for power control problem in a two-tier HetNet. In Chapter 3 a coordinated learning method based on message-passing is proposed to achieve optimal power control in an interference-limited network. Chapter 4, designs a new architecture for system-level evaluation of large 5G HetNets. Chapter 5 focuses on mmWave wireless backhauling and proposes a multi-agent based topology management solution to achieve k-connectivity in backhaul networks. Finally, Chapter 6 concludes the dissertation and discusses potential future works based on this dissertation.

Chapter 2

REINFORCEMENT LEARNING FOR POWER CONTROL OF TWO-TIER HETEROGENEOUS NETWORKS

Self-organizing networks (SONs) can help manage the severe interference in dense heterogeneous networks (HetNets). Given their need to automatically configure power and other settings, machine learning is a promising tool for data-driven decision making in SONs. In this chapter, a HetNet is modeled as a dense two-tier network with conventional macrocells overlaid with denser small cells (e.g. femto or pico cells). First, a distributed framework based on multi-agent Markov decision process is proposed that models the power optimization problem in the network. Second, we present a systematic approach for designing a reward function based on the optimization problem. Third, we introduce Q-*learning* based distributed power allocation algorithm (Q-DPA) as a self-organizing mechanism that enables ongoing transmit power adaptation as new small cells are added to the network. Further, the sample complexity of the Q-DPA algorithm to achieve ϵ-optimality with high probability is provided. We demonstrate, at density of several thousands femtocells per km^2, the required quality of service of a macrocell user can be maintained via the proper selection of independent or cooperative learning and appropriate Markov state models. This work was published in [26, 27].

2.1 Introduction

Self-organization is a key feature as cellular networks densify and become more heterogeneous, through the additional small cells such as pico and femtocells [30–34]. Self-organizing networks (SONs) can perform self-configuration, self-optimization and self-healing. These operations can cover basic tasks such as configuration of a newly installed base station (BS), resource management, and fault management in the network [35]. In other words, SONs attempt to minimize human intervention where they use measurements from the network to minimize the cost of installation, configuration and maintenance of the network. In fact SONs bring two main factors in play: *intelligence* and *autonomous adaptability* [30, 31]. Therefore, machine learning techniques can play a major role in processing underutilized sensory data to enhance the performance of SONs [36, 37].

One of the main responsibilities of SONs is to configure the transmit power at various small BSs to manage interference. In fact, a small BS needs to configure its transmit power before joining the network (as self-configuration). Subsequently, it needs to dynamically control its transmit power during its operation in the network (as self-optimization). To address these two issues, we consider a macrocell network overlaid with small cells and focus on autonomous distributed power control, which is a key element of self-organization since it improves network throughput [38–42] and minimizes energy usage [43–45]. We rely on local measurements, such as signal-to-interference-plus-noise ratio (SINR), and the use of machine learning to develop a SON framework that can continually improve the above performance metrics.

2.1.1 Related Work

In wireless communications, dynamic power control with the use of machine learning has been implemented via reinforcement learning (RL). In this context, RL is an area of machine learning that attempts to optimize a BS's transmit power to achieve a certain goal such as throughput maximization. One of the main advantages of RL with respect to supervised learning methods is its training phase, in which there is no need for correct input/output data. In fact, RL operates by applying the experience that it has gained through interacting with the network [2]. RL methods have been applied in the field of wireless communications in areas such as resource management [46–51], energy harvesting [52], interference mitigation [53], and opportunistic spectrum access [54,55]. A comprehensive review of RL applications in wireless communications can be found in [56].

Q-*learning* is a model-free RL method [25]. The model-free feature of Q-*learning* makes it a proper method for scenarios in which the statistics of the network continuously change. Further, Q-*learning* has low computational complexity and can be implemented by BSs in a distributed manner [26]. Therefore, Q-*learning* can bring *scalability*, *robustness*, and *computational efficiency* to large networks. However, designing a proper reward function which accelerates the learning process and avoids false learning or unlearning phenomena [57] is not trivial. Therefore, to solve an optimization problem, an appropriate reward function for Q-*learning* needs to be determined.

In this regard, the works in [46–51] have proposed different reward functions to optimize power allocation between femtocell base stations (FBSs). The method in [46] uses independent Q-*learning* in a cognitive radio system to set the transmit power of secondary BSs in a digital television system. The solution in [46] ensures that the minimum quality of service (QoS) for the primary user is met by applying Q-*learning* and using the SINR as a metric. However, the approach in [46] does not take the QoS of the secondary users into considerations. The work in [47] uses cooperative Q-*learning* to maximize the sum transmission rate of the femtocell users while keeping the transmission rate of macrocell users near a certain threshold. Further, the authors in [48] have used the proximity of FBSs to a macrocell user as a factor in the reward function. This results in a fair power allocation scheme in the network. Their proposed reward function keeps the transmission rate of the macrocell user above a certain threshold while maximizing the sum transmission rate of FBSs. However, by not considering a minimum threshold for the FBSs' rates, the approach in [48] fails to support some FBSs as the density of the network (and consequently interference) increases. The authors in [49] model the cross-tier interference management problem as a non-cooperative game between femtocells and the macrocell. In [49], femtocells use the average SINR measurement to enhance their individual performances while maintaining the QoS of the macrocell user. In [50], the authors attempt to improve the transmission rate of cell-edge users while keeping the fairness between the macrocell and the femtocell users by applying a round robin approach. The work in [51] minimizes power usage in a Long Term Evolution (LTE) enterprise femtocell network by applying an exponential reward function without the requirement to achieve fairness amongst the femtocells in the network.

In the above works, the reward functions do not apply to dense networks. That is to say, first, there is no minimum threshold for the achievable rate of the femtocells. Second, the reward functions are designed to limit the macrocell user rate to its required QoS and not more than that. This property encourages an FBS to use more power to increase its own rate by assuming that the caused interference just affects the macrocell user. However, the neighbor femtocells suffer from this decision and overall the sum rate of the network decreases. Further, they do not provide a generalized framework for modeling a HetNet as a multi-agent RL network or a procedure to design a reward function which meets the QoS requirements of the network. In this chapter, we focus on dense networks and try to provide a general solution to the above challenges.

2.1.2 Contributions

We propose a learning framework based on multi-agent Markov decision process (MDP). By considering an FBS as an agent, the proposed framework enables FBSs to join and adapt to a dense network autonomously. Due to unplanned and dense deployment of femtocells, providing the required QoS to all the users in the network becomes an important issue. Therefore, we design a reward function that trains the FBSs to achieve this goal. Furthermore, we introduce a Q-*learning* based distributed power allocation approach (Q-DPA) as an application of the proposed framework.Q-DPA uses the proposed reward function to maximize the transmission rate of femtocells while prioritizing the QoS of the macrocell user. More specifically the contributions of the paper can be summarized as:

1. We propose a framework that is agnostic to the choice of learning method but also connects the required RL analogies to wireless communications. The proposed framework models a multi-agent network with a single MDP that contains the joint action of the all the agents as its action set. Next, we introduce MDP factorization methods to provide a distributed and scalable architecture for the proposed framework. The proposed framework is used to benchmark

the performance of different learning rates, Markov state models, or reward functions in two-tier wireless networks.

2. We present a systematic approach for designing a reward function based on the optimization problem and the nature of RL. In fact, due to scarcity of resources in a dense network, we propose some properties for a reward function to maximize sum transmission rate of the network while considering minimum requirements of all users. The procedure is simple and general and the designed reward function is in the shape of low complexity polynomials. Further, the designed reward function results in increasing the achievable sum transmission rate of the network while consuming considerably less power compared to greedy based algorithms.

3. We propose Q-DPA as an application of the proposed framework to perform distributed power allocation in a dense femtocell network. Q-DPA uses the factorization method to derive independent and cooperative learning from the optimal solution. Q-DPA uses local signal measurements at the femtocells to train the FBSs in order to: (i) maximize the transmission rate of femtocells, (ii) achieve minimum required QoS for all femtocell users with a high probability, and (iii) maintain the QoS of macrocell user in a densely deployed femtocell network. In addition, we determine the minimum number of samples that is required to achieve an ϵ-optimal policy in Q-DPA as its sample complexity.

4. We introduce four different learning configurations based on different combinations of independent/cooperative learning and Markov state models. We conduct extensive simulations to quantify the effect of different learning configurations on the performance of the network. Simulations show that the

proposed Q-DPA algorithm can decrease power usage and as a result reduce the interference to the macrocell user.

The chapter is organized as follows. In Section 5.2, the system model is presented. Section 2.3 introduces the optimization problem and presents the existing challenges in solving this problem. Section 2.4 presents the proposed learning framework which models a two-tier femtocell network with a multi-agent MDP. Section 2.5.1 presents the Q-DPA algorithm as an application of the proposed framework. Section 3.6 presents the simulation results while Section 3.7 concludes the chapter.

Notation: Lower case, boldface lower case, and calligraphic symbols represent scalars, vectors, and sets, respectively. For a real-valued function $Q : \mathcal{Z} \to \mathbb{R}$, $\|Q\|$ denotes the max norm, i.e., $\|Q\| = \underset{z \in \mathcal{Z}}{max} \; |Q\left(z\right)|$. $\mathbb{E}_x\left[\cdot\right]$, $\mathbb{E}_x\left[\cdot|\cdot\right]$, and $\frac{\partial f}{\partial x}$ denote the expectation, the conditional expectation, and the partial derivation with respect to x, respectively. Further, $\Pr\left(\cdot|\cdot\right)$ and $|\cdot|$ denote the conditional probability and absolute value operators, respectively.

2.2 Downlink System Model

Consider the downlink of a single cell of a HetNet operating over a set $\mathcal{S} = \{1, ..., S\}$ of S orthogonal subbands. In the cell a single macro base station (MBS) is deployed. The MBS serves one macrocell user equipment (MUE) over each subband while guaranteeing this user a minimum average SINR over each subband which is denoted by Γ_0. A set of FBSs are deployed in area of coverage of the macrocell. Each FBS selects a random subband and serves one femtocell user equipment (FUE). We assume that overall, on each subband $s \in \mathcal{S}$, a set $\mathcal{K} = \{1, ..., K\}$ of K FBSs are operating. Each FBS guarantees a minimum average SINR denoted by Γ_k to its related FUE.

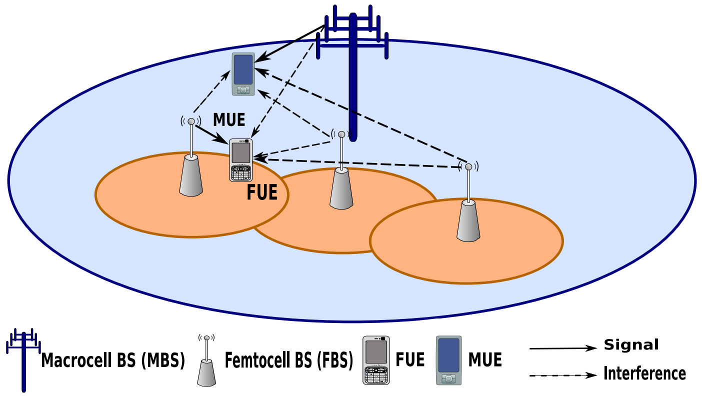

Figure 2.1: Macrocell and femtocells operating over the same frequency band.

We consider a dense network in which the density results in both cross-tier and co-tier interference. Therefore, in order to control the interference-level and provide the users with their required minimum SINR, we focus on power allocation in the downlink of the femtocell network. Uplink results can be obtained in a similar fashion but are not included for brevity. The overall network configuration is presented in Fig. 2.1. We focus on one subband, meanwhile the proposed solution can be extended to a case in which each FBS supports multiple users on different subbands.

We denote the MBS-MUE pair by the index 0 and the FBS-FUE pairs by the index k from the set $\mathcal{K}$. In the downlink, the received signal at the MUE operating over subband s includes interference from the femtocells and thermal noise. Hence, the SINR at the MUE operating over subband $s \in \mathcal{S}$, γ_0, is calculated as

$$\gamma_0 = \frac{p_0 |h_{0,0}|^2}{\underbrace{\sum_{k \in \mathcal{K}} p_k |h_{k,0}|^2}_{\text{femtocells' interference}} + N_0}, \tag{2.1}$$

where p_0 denotes the power transmitted by the MBS and $h_{0,0}$ denotes the channel gain from the MBS to the MUE. Further, the power transmitted by the kth FBS is denoted by p_k and the channel gain from the kth FBS to the MUE is denoted by $h_{k,0}$. Finally, N_0 denotes the variance of the additive white Gaussian noise. Similarly, the SINR at the kth FUE operating over subband $s \in \mathcal{S}$, γ_k, is obtained as

$$\gamma_k = \frac{p_k |h_{k,k}|^2}{\underbrace{p_0 |h_{0,k}|^2}_{\text{macrocell's interference}} + \underbrace{\sum_{j \in \mathcal{K} \setminus \{k\}} p_j |h_{j,k}|^2}_{\text{femtocells' interference}} + N_k}, \tag{2.2}$$

where $h_{k,k}$ denotes the channel gain between the kth FBS and the kth FUE, $h_{0,k}$ denotes the channel gain between the MBS and the kth FUE, p_j denotes the transmit power of the jth FBS, $h_{j,k}$ is the channel gain between the jth FBS and the kth FUE, and N_k is the variance of the additive white Gaussian noise. Finally, the transmission rates, normalized by the transmission bandwidth, at the MUE and the FUE operating over subband $s \in \mathcal{S}$, i.e., r_0 and r_k, respectively, are expressed as $r_0 = \log_2(1+\gamma_0)$ and $r_k = \log_2(1+\gamma_k)\,,\ k \in \mathcal{K}$.

2.3 Problem Formulation

Each FBS has the objective of maximizing its transmission rate while ensuring that the SINR of the MUE is above the required threshold, i.e., Γ_0. Denoting $\mathbf{p} = \{p_1, ..., p_K\}$ as the vector of the transmit powers of the K FBSs operating over the subband $s \in \mathcal{S}$, the power allocation problem is presented in (2.3). In (2.3), p_{max} defines the maximum available transmit power at each FBS. The objective (2.3a) is to maximize the sum transmission rate of the FUEs. Constraint (3.4b) refers to the power limitation of every FBS. Constraints (2.3c) and (2.3d) ensure that the minimum SINR requirement is satisfied for the MUE and the FUEs. The addition of constraint (2.3d) to the optimization problem is one of the differences between the proposed approach in this paper and that of [46–51].

$$\begin{aligned}
\underset{\mathbf{p}}{\text{maximize}} \quad & \sum_{k\in\mathcal{K}} \log_2\left(1+\gamma_k\right) && \text{(2.3a)}\\
\text{subject to} \quad & 0 \le p_k \le p_{max},\ k\in\mathcal{K}, && \text{(2.3b)}\\
& \gamma_0 \ge \Gamma_0, && \text{(2.3c)}\\
& \gamma_k \ge \Gamma_k,\ k\in\mathcal{K}, && \text{(2.3d)}
\end{aligned}$$

Considering (2.2), it can be concluded that the optimization in (2.3) is a non-convex problem for dense networks. This follows from the SINR expression in (2.2) and the objective function (2.3a). More specifically, the interference term due to the neighboring femtocells in the denominator of (2.2) ensures that the optimization problem in (2.3) is not convex [58]. This interference term may be ignored in low density networks but cannot be ignored in dense networks consisting of a large number of femtocells [59]. However, non-convextiy is not the only challenge of the above problem. In fact, many iterative algorithms are developed to solve the above optimization problem with excellent performance. However, their algorithms contains expensive computations such as matrix inversion and bisection or singular value decomposition in each iteration which makes their real-time implementation challenging [60]. Besides, the kth FBS is only aware of its own transmit power, p_k, and does not know the transmit powers of the remaining FBSs. Therefore, the idea here is to treat the given problem as a black-box and try to learn the relation between the transmit power and the resulting transmission rate gradually by interacting with the network and simple computations.

To realize self-organization, each FBS should be able to operate autonomously. This means an FBS should be able to connect to the network at anytime and to continuously adapt its transmit power to achieve its objectives. Therefore, our optimization problem requires a self-adaptive solution. The steps for achieving self-adaptation can be summarized as: (i) the FBS measures the interference level at its related FUEs, (ii) determines the maximum transmit power to support its FUEs while not greatly degrading the performance of other users in the network. In the next section, the required framework to solve this problem will be presented.

2.4 The Proposed Learning Framework

Here, first we model a multi-agent network as an MDP. Then the required definitions, evaluation methods, and factorization of the MDP to develop a distributed learning framework are explained. Subsequently, the femtocell network is modeled as a multi-agent MDP and the proposed learning framework is developed.

2.4.1 Multi-Agent MDP and Policy Evaluation

A single-agent MDP comprises an agent, an environment, an action set, and a state set. The agent can transition between different states by choosing different actions. The trace of actions that is taken by the agent is called its policy. With each transition, the agent will receive a reward from the environment, as a consequence of its action, and will save the discounted summation of rewards as a cumulative reward. The agent will continue its behavior with the goal of maximizing the cumulative reward and the value of cumulative reward evaluates the chosen policy. The discount property increases the impact of recent rewards and decreases the effect of later ones.

If the number of transitions is limited, the non-discounted summation of rewards can be used as well.

A multi-agent MDP consists of a set, $\mathcal{K}$, of K agents. The agents select actions to move between different states of the model to maximize the cumulative reward received by all the agents. Here, we again formulate the network of agents as one MDP, e.g., we define the action set as the joint action set of all the agents. Therefore, the multi-agent MDP framework is defined with a tuple as $(\mathcal{A}, \mathcal{X}, Pr, \mathbf{R})$ with the following definitions.

- $\mathcal{A}$ is the joint set of all the agents' actions. An agent k selects its action a from its action set $\mathcal{A}_k$, i.e., $a_k \in \mathcal{A}_k$. The joint action set is represented as $\mathcal{A} = \mathcal{A}_1 \times \cdots \times \mathcal{A}_K$, with $\mathbf{a} \in \mathcal{A}$ as a single joint action.

- The state of the system is defined with a set of random variables. Each random variable is represented by X_i with $i = 1, ..., n$, and the state set is represented as $\mathcal{X} = \{X_1, X_2, ..., X_n\}$, where $\mathbf{x} \in \mathcal{X}$ denotes a single state of the system. Each random variable reflects a specific feature of the network.

- The transition probability function, $\Pr(\mathbf{x}, \mathbf{a}, \mathbf{x}')$, represents the probability of taking joint action $\mathbf{a}$ at state $\mathbf{x}$ and ending in state $\mathbf{x}'$. In other words, the transition probability function defines the environment which agents are interacting with.

- $\mathbf{R}(\mathbf{x}, \mathbf{a})$ is the reward function such that its value is the received reward by the agents for taking joint action $\mathbf{a}$ at state $\mathbf{x}$.

We define $\pi : \mathcal{X} \rightarrow \mathbf{A}$ as the policy function, where $\pi(\mathbf{x})$ is the joint action that is taken at the state $\mathbf{x}$. In order to evaluate the policy $\pi(\mathbf{x})$, a value function $V_\pi(\mathbf{x})$

and an action-value function $\mathbf{Q}_{\pi}(\mathbf{x}, \mathbf{a})$ are defined. The value of the policy π in state $\mathbf{x}' \in \mathcal{X}$ is defined as [2]

$$V_{\pi}(\mathbf{x}') = \mathbb{E}_{\pi}\left[\sum_{t=0}^{\infty} \beta^{t} \mathbf{R}^{(t+1)} \left| \mathbf{x}^{(0)} = \mathbf{x}' \right.\right], \tag{2.4}$$

in which $\beta \in (0, 1]$ is a discount factor, $\mathbf{R}^{(t+1)}$ is the received reward at time step $t+1$, and $\mathbf{x}^{(0)}$ is the initial state. The action-value function, $\mathbf{Q}_{\pi}(\mathbf{x}, \mathbf{a})$, represents the value of the policy π for taking joint action $\mathbf{a}$ at state $\mathbf{x}$ and then following policy π for subsequent iterations. According to [2], the relation between the value function and the action-value function is given by

$$\mathbf{Q}_{\pi}(\mathbf{x}, \mathbf{a}) = \mathbf{R}(\mathbf{x}, \mathbf{a}) + \beta \sum_{\mathbf{x}' \in \mathcal{X}} \Pr(\mathbf{x}' | \mathbf{x}, \mathbf{a}) V_{\pi}(\mathbf{x}'). \tag{2.5}$$

For the ease of notation, we will use V and $\mathbf{Q}$ for the value function and the action-value function of policy π, respectively. Further, we use the term *Q-function* to refer to the action-value function. The optimal value of state $\mathbf{x}$ is the maximum value that can be reached by following any policy and starting at this state. An optimal value function V^{*}, which gives an optimal policy π^{*}, satisfies the Bellman optimality equation as [2]

$$V^{*}(\mathbf{x}) = \max_{\mathbf{a}} \mathbf{Q}^{*}(\mathbf{x}, \mathbf{a}), \tag{2.6}$$

where $\mathbf{Q}^{*}(\mathbf{x}, \mathbf{a})$ is an optimal Q-function under policy π^{*}. The general solution for (2.6) is to start from an arbitrary policy and using the *generalized policy iteration* (GPI) [2] method to iteratively evaluate and improve the chosen policy to achieve an optimal policy. If the agents have *a priori* information of the environment, i.e.,

$Pr(\mathbf{x}, \mathbf{a}, \mathbf{x}')$ is known to the agents, dynamic programming is the solution for (2.6). However, the environment is unknown in most practical applications. Hence, we rely on reinforcement learning (RL) to derive an optimal Q-function. RL uses temporal-difference to provide a real-time solution for the GPI method [2]. As a result, in Section 2.5.1, we use Q-*learning*, as a specific method of RL, to solve (2.6).

2.4.2 Factored MDP

To this point, we defined the Q-function over the joint state-action space of all the agents, i.e., $\mathcal{X} \times \mathcal{A}$. We refer to this Q-function as the global Q-function. According to [25], Q-*learning* finds the optimal solution to a single MDP with probability one. However, in large MDPs, due to exponential increase in the size of the joint state-action space with respect to the number of agents, the solution to the problem becomes intractable. To resolve this issue, we use *factored* MDPs as a decomposition technique for large MDPs. The idea in factored MDPs is that many large MDPs are generated by systems with many parts that are weakly interconnected. Each part has its associated state variables and the state space can be factored into subsets accordingly. The definition of the subsets affects the optimality of the solution [61], and investigating the optimal factorization method helps with understanding the optimality of multi-agent RL solutions [28]. In [62] power control of a multi-hop network is modeled as an MDP and the state set is factorized into multiple subsets each referring to a single hop. The authors in [63] show that the subsets can be defined based on the local knowledge of the agents from the environment. Meanwhile, we aim to distribute the power control to the nodes of the network. Therefore, due to the definition of the problem in Section 2.3 and the fact that each FBS is only aware of its own power, we use the assumption in [63] and define the individual action set of the agents, i.e., $\mathcal{A}_k$, as the subsets of the joint action set. Consequently, the resultant Q-function for the kth agent is defined as $Q_k\left(\mathbf{x}_k, a_k\right)$, in which $a_k \in \mathcal{A}_k$, $\mathbf{x}_k \in \mathcal{X}_k$ is the state vector of the kth agent, and $\mathcal{X}_k,\ k \in \mathcal{K}$, are the subsets of the global state set of the system, i.e., $\mathcal{X}$.

In factored MDPs, We assume that the reward function is factored based on the subsets, i.e.,

$$\mathbf{R}\left(\mathbf{x}, \mathbf{a}\right) = \sum_{k \in \mathcal{K}} R_k\left(\mathbf{x}_k, a_k\right), \tag{2.7}$$

where, $R_k\left(\mathbf{x}_k, a_k\right)$ is the local reward function of the kth agent. Moreover, we also assume that the transition probabilities are factored, i.e., for the kth subsystem we have

$$\begin{aligned} &\Pr\left(\mathbf{x}'_k | \mathbf{x}, \mathbf{a}\right) = \Pr\left(\mathbf{x}'_k | \mathbf{x}_k, a_k\right), \\ &\left(\mathbf{x}, \mathbf{a}\right) \in \mathcal{X} \times \mathcal{A},\ \left(\mathbf{x}_k, a_k\right) \in \mathcal{X}_k \times \mathcal{A}_k,\ \mathbf{x}'_k \in \mathcal{X}_k. \end{aligned} \tag{2.8}$$

The value function for the global MDP is given by

$$\begin{aligned} \mathbf{V}\left(\mathbf{x}\right) &= \mathbb{E}\left[\sum_{t=0}^{\infty} \beta^t \mathbf{R}^{(t+1)}\left(\mathbf{x}, \mathbf{a}\right)\right] \\ &= \mathbb{E}\left[\sum_{t=0}^{\infty} \beta^t \sum_{k \in \mathcal{K}} R_k^{(t+1)}\left(\mathbf{x}_k, a_k\right)\right] \\ &= \sum_{k \in \mathcal{K}} V_k\left(\mathbf{x}_k\right), \end{aligned} \tag{2.9}$$

where, $V_k\left(\mathbf{x}_k\right)$ is the value function of the kth agent. Therefore, the derived policy has the value function equal to the linear combination of local value functions. Further, according to (3.6), for each agent $k \in \mathcal{K}$

$$Q_k\left(\mathbf{x}_k, a_k\right) = R_k\left(\mathbf{x}_k, a_k\right) + \beta \sum_{\mathbf{x}'_k} \Pr\left(\mathbf{x}'_k | \mathbf{x}_k, a_k\right) V_k\left(\mathbf{x}'_k\right), \tag{2.10}$$

and for the global Q-function

$$\begin{aligned}
\mathbf{Q}\left(\mathbf{x}, \mathbf{a}\right) &= \mathbf{R}\left(\mathbf{x}, \mathbf{a}\right) + \beta \sum_{\mathbf{x}' \in \mathcal{X}} \Pr\left(\mathbf{x}' | \mathbf{x}, \mathbf{a}\right) \mathbf{V}\left(\mathbf{x}'\right) \\
&= \sum_{k \in \mathcal{K}} R_k\left(\mathbf{x}_k, a_k\right) + \beta \sum_{\mathbf{x}' \in \mathcal{X}} \Pr\left(\mathbf{x}' | \mathbf{x}, \mathbf{a}\right) \sum_{k \in \mathcal{K}} V_k\left(\mathbf{x}_k\right) \\
&= \sum_{k \in \mathcal{K}} R_k\left(\mathbf{x}_k, a_k\right) + \beta \sum_{k \in \mathcal{K}} \sum_{\mathbf{x}'_k \in \mathcal{X}_k} \Pr\left(\mathbf{x}'_k | \mathbf{x}, \mathbf{a}\right) V_k\left(\mathbf{x}_k\right) \\
&= \sum_{k \in \mathcal{K}} R_k\left(\mathbf{x}_k, a_k\right) + \beta \sum_{k \in \mathcal{K}} \sum_{\mathbf{x}' \in \mathcal{X}_k} \Pr\left(\mathbf{x}'_k | \mathbf{x}_k, a_k\right) V_k\left(\mathbf{x}_k\right) \\
&= \sum_{k \in \mathcal{K}} Q_k\left(\mathbf{x}_k, a_k\right).
\end{aligned} \tag{2.11}$$

Therefore, based on the assumptions in (2.7) and (2.8), the global Q-function can be approximated with the linear combination of local Q-functions. Further, (2.11) results in a distributed and scalable architecture for the framework.

2.4.3 Femtocell Network as Multi-Agent MDP

In a wireless communication system, the resource management policy is equivalent to the policy function in an MDP. To integrate the femtocell network in a multi-agent MDP, we define the followings according to Fig. 2.2.

- **Environment**: From the view point of an FBS, the environment is comprised of the macrocell and all other femtocells.

- **Agent**: Each FBS is an independent agent in the MDP. In this paper, the terms of agent and FBS are used interchangeably. An agent has three objectives: (i)

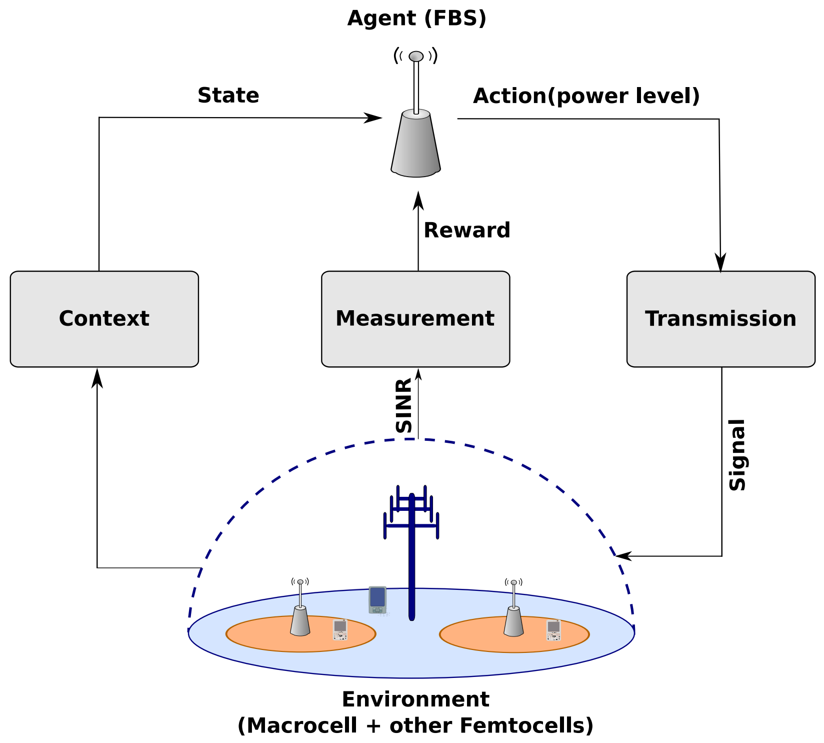

Figure 2.2: The proposed learning framework: the environment from the point of view of an agent (FBS), and its interaction with the environment in the learning procedure. Context defines the data needed to derive the state of the agent. Measurement refers to calculations needed to derive the reward of the agent.

improving its sum transmission rate, (ii) guaranteeing the required SINR for its user (i.e., Γ_k), and (iii) meeting the required SINR for the MUE.

- **Action set** ($\mathcal{A}_k$): The transmit power level is the action of an FBS. The kth FBS chooses its transmit power from the set $\mathcal{A}_k$ which covers the space between $p_{\min}$ and $p_{\max}$. $p_{\min}$ and $p_{\max}$ denote the minimum and maximum transmit power of the FBS, respectively. In general, the FBS has no knowledge of the environment and it chooses its actions with the same probability in the training mode. Therefore, equal step sizes of Δp are chosen between p_{min} and p_{max} to construct the set $\mathcal{A}_k$.

- **State set** ($\mathcal{X}_k$): State set directly affects the performance of the MUE and the FUEs. To this end, we define four variables to represent the state of the network. The state set variables are defined based on the constraints of the optimization problem in (2.3). We define the variables X_1 and X_2 as indicators of the performance of the FUE and the MUE. On the other hand, the relative location of an FBS with respect to the MUE and the MBS is important and affects the interference power at the MUE caused by the FBS, and the interference power at the FBS causes by the MBS. Therefore, we define X_3 as an indicator of the interference imposed on the MUE by the FBS, and X_4 as an indicator of interference imposed on the femtocell by the MBS. The state variables are defined as

  – $X_1 \in \{0, 1\}$: The value of X_1 indicates whether the FBS is supporting its FUE with the required minimum SINR or not. X_1 is defined as $X_1 = \mathbb{1}_{\{\gamma_k \geq \Gamma_k\}}$.

  – $X_2 \in \{0, 1\}$: The value of X_2 indicates whether the MUE is being supported with its required minimum SINR or not. X_2 is defined as $X_2 = \mathbb{1}_{\{\gamma_0 \geq \Gamma_0\}}$.

  – $X_3 \in \{0, 1, 2, ..., N_1\}$: The value of X_3 defines the location of the FBS compared to N_1 concentric rings around the MUE. The radius of rings are d_1, d_2, ..., d_{N_1}.

  – $X_4 \in \{0, 1, 2, ..., N_2\}$: The value of X_4 defines the location of the FBS compared to N_2 concentric rings around the MBS. The radius of rings are d'_1, d'_2, ..., d'_{N_2}.

The kth FBS calculates γ_k based on the channel equality indicator (CQI) received from its related FUE to assess X_1. The MBS is aware of the SINR of the MUE user, i.e., γ_0, and the relative location of the FBS concerning itself and the MUE. Therefore, the FBS obtains the required information to asses the X_2, X_3, and X_4 variables via backhaul and feedback from the MBS.

Here, we defined the state variables as a function of each FBS's SINR and location. Therefore, in high SINR regime, the state of FBSs can be assumed to be independent of each other.

In Section 3.6, we will examine different possible state sets to investigate the effect of the above state variables on the performance of the network.

2.5 Q-DPA, Reward Function, and Sample Complexity

In this section, we present Q-DPA, which is an application of the proposed framework. Q-DPA details the learning method, the learning rate, and the training procedure. Then, the proposed reward function is defined. Finally, the required sample complexity for the training is derived.

2.5.1 Q-learning Based Distributed Power Allocation (Q-DPA)

To solve the Bellman equation in (2.6), we use Q-*learning*. The reasoning for choosing the RL method and advantages of Q-*learning* are explained in Sections 2.4.1 and 2.1.1, respectively. The Q-*learning* update rule to evaluate a policy for the global Q-function can be represented as (2.12)

$$\mathbf{Q}(\mathbf{x}^{(t)},\mathbf{a}^{(t)}) \leftarrow \mathbf{Q}(\mathbf{x}^{(t)},\mathbf{a}^{(t)}) + \alpha^{(t)}(\mathbf{x},\mathbf{a})\left(\mathbf{R}^{(t+1)}\left(\mathbf{x}^{(t)},\mathbf{a}^{(t)}\right) + \underbrace{\beta\max_{\mathbf{a}'}\mathbf{Q}(\mathbf{x}^{(t+1)},\mathbf{a}')}_{(M)} - \mathbf{Q}(\mathbf{x}^{(t)},\mathbf{a}^{(t)})\right), \tag{2.12}$$

where $\mathbf{a}' \in \mathcal{A}$, $\alpha^{(t)}(\mathbf{x},\mathbf{a})$ denotes the learning rate at time step t, and $\mathbf{x}^{(t+1)}$ is the new state of the network [25]. The term M is the maximum value of the global Q-function that is available at the new state $\mathbf{x}^{(t+1)}$. After each iteration, the FBSs will receive the delayed reward $\mathbf{R}^{(t+1)}\left(\mathbf{x}^{(t)},\mathbf{a}^{(t)}\right)$ and then the global Q-function will be updated according to (2.12).

In the prior works [46–48, 50, 51], a constant learning rate was used for Q-*learning* to solve the required optimization problems. However, according to [64], in finite number of iterations, the performance of Q-*learning* can be improved by applying a decaying learning rate. Therefore, we use the following learning rate

$$\alpha^{(t)}(\mathbf{x},\mathbf{a}) = \frac{1}{[1 + t(\mathbf{x},\mathbf{a})]}, \tag{2.13}$$

in which $t(\mathbf{x},\mathbf{a})$ refers to the number of times, until time step t, that the state-action pair $(\mathbf{x},\mathbf{a})$ is visited. It is worth mentioning that, by using the above learning rate, we need to keep track of the number of times each state-action pair has been visited during training, which requires more memory. Therefore, at the cost of more memory, a better performance can be achieved.

There are two alternatives available for the training of new FBSs as they join the network, they can use independent learning or cooperative learning. In independent learning, each FBS tries to maximize its own Q-function. In other words, using the factorization method in Section 2.4.2, the term M in (2.12) is approximated as

$$M = \max_{\mathbf{a}'} \sum_{k \in \mathcal{K}} Q_k(\mathbf{x}_k^{(t+1)}, a_k') \approx \sum_{k \in \mathcal{K}} \max_{a_k'} Q_k\left(\mathbf{x}_k^{(t+1)}, a_k'\right). \tag{2.14}$$

In cooperative learning, the FBSs share their local Q-functions and will assume that the FBSs with the same state make the same decision. Hence, term M is approximated as

$$M = \max_{\mathbf{a}'} \sum_{k \in \mathcal{K}} Q_k(\mathbf{x}_k^{(t+1)}, a_k') \approx \max_{a_k'} \sum_{k \in \mathcal{K}'} Q_k\left(\mathbf{x}_k^{(t+1)}, a_k'\right), \tag{2.15}$$

where $\mathcal{K}'$ is the set of FBSs with the same state $\mathbf{x}_k^{(t+1)}$. Cooperative Q-*learning* may result in a higher cumulative reward [65]. However, cooperation will result in the same policy for FBSs with the same state and additional overhead since the Q-functions between FBSs need to be shared over the backhaul network. The local update rule for the kth FBS can be derived from (2.12) as in (2.16)

$$\begin{aligned} Q_k(\mathbf{x}_k^{(t)}, a_k^{(t)}) \leftarrow & Q_k(\mathbf{x}_k^{(t)}, a_k^{(t)}) + \\ & \alpha^{(t)}\left(R^{(t+1)}\left(\mathbf{x}_k^{(t)}, a_k^{(t)}\right) + \beta Q_k\left(\mathbf{x}_k^{(t+1)}, a_k^{*}\right) - Q_k(\mathbf{x}_k^{(t)}, a_k^{(t)})\right), \end{aligned} \tag{2.16}$$

where, $R^{(t+1)}\left(\mathbf{x}_k^{(t)}, a_k^{(t)}\right)$ is the reward of the kth FBS, and a_k^* is defined as

$$\arg\max_{a_k'} Q_k\left(\mathbf{x}_k^{(t+1)}, a_k'\right), \tag{2.17}$$

and

$$\arg\max_{a_k'} \sum_{k \in \mathcal{K}'} Q_k\left(\mathbf{x}_k^{(t+1)}, a_k'\right), \tag{2.18}$$

for independent and cooperative learning, respectively.

In this paper, a tabular representation is used for the Q-function in which the rows of the table refer to the states and the columns refer to the actions of an agent. Generally, for large state spaces, neural networks are more efficient to use as Q-functions, however, part of this work is focused on the effect of state space variables. Therefore, we avoid large number of state variables. On the other hand, we provide exhaustive search solution to investigate the optimality of our solution which is not possible for large state spaces.

The training for an FBS happens over L frames. In the beginning of each frame, the FBS chooses an action, i.e., transmit power. Then, the FBS sends a frame to the intended FUE. The FUE feeds back the required measurements such as CQI so the FBS can estimate the SINR at the FUE, and calculate the reward based on (2.24). Finally, the FBS updates its Q-table according to (2.16).

Due to limited number of training frames, each FBS needs to select its actions in a way that covers most of the action space and improves the policy at the same time. Therefore, the FBS chooses the actions with a combination of exploration and exploitation, known as an e-greedy exploration. In the e-greedy method, the FBS acts greedily with probability $1-e$ (i.e., exploiting) and randomly with probability e (i.e., exploring). In exploitation, the FBS selects an action that has the maximum value in the current state in its own Q-table (independent learning) or in the summation of Q-tables (cooperative learning). In exploring, the FBS selects an action randomly to cover action space and avoid biasing to a local maximum. In [2], it is shown that for a limited number of iterations the e-greedy policy results in a closer final value to the optimal value compared to only exploiting or exploring.

It is worth mentioning that the overhead of sharing Q-tables depends on the definition of the state model $\mathcal{X}_k$ according to Section 2.4.3. For instance, assuming the largest possible state model as $\mathcal{X}_k = \{X_1, X_2, X_3, X_4\}$. The variables X_3 and X_4 depend on the location of the FBS and are fixed during training. Therefore, one training FBS uses four rows of its Q-table and just needs the same rows from other FBSs. Hence, if the number of active FBSs is $|\mathcal{K}|$, the number of messages to the FBS in each training frame is $4 \times (|\mathcal{K}| - 1)$, each of size $|\mathcal{A}_k|$.

2.5.2 Proposed Reward Function

The design of the reward function is essential because it directly impacts the objectives of the FBS. Generally, there has not existed a quantitative approach to designing the reward function. Here, we present a systematic approach for deriving the reward function based on the nature of the optimization problem under consideration. Then, we compare the behavior of the designed reward function to the ones in [46–48].

The reward function for the kth FBS is represented as R_k. According to the Section 2.4.3, the kth FBS has knowledge of the minimum required SINR for the MUE, i.e. Γ_0, and minimum required SINR for its related FUE, i.e. Γ_k. Also, after taking an action in each step, the kth FBS has access to the rate of the MUE, i.e. r_0 and the rate of its related FUE, i.e. r_k. Therefore, R_k is considered as a function of the above four variables as $R_k : (r_0, r_k, \Gamma_0, \Gamma_k) \to \mathbb{R}$.

In order to design the appropriate reward function, we need to estimate the progress of the kth FBS toward the goals of the optimization problem. Based on the input arguments to the reward function, we define two progress estimators, one for the MUE as $(r_0 - \log_2(1 + \Gamma_0))$ and one for the kth FUE as $(r_k - \log_2(1 + \Gamma_k))$. To reduce computational complexity, we define the reward function as a polynomial function of the defined progress estimators as

$$R_k = \left(r_0 - \log_2\left(1+\Gamma_0\right)\right)^{k_1} + \left(r_k - \log_2\left(1+\Gamma_k\right)\right)^{k_2} + C, \tag{2.19}$$

where, k_1 and k_2 are integers and $C \in \mathbb{R}$ is a constant referred to as the bias of the reward function.

The constant bias, C, in the reward function has two effects on the learning algorithm: (i) The final value of the states for a given policy π, and (ii) the behavior of the agent in the beginning of the learning process as follows:

1. Effect of bias on the final value of the states: Assume the reward function, $R_1 = f(\cdot)$, and the reward function $R_2 = f(\cdot) + C$, $C \in \mathbb{R}$. We define the value of state $\mathbf{x}$ for a given policy π using R_1 as $V_1(\mathbf{x})$ and the value of the state $\mathbf{x}$ for the same policy using R_2 as $V_2(\mathbf{x})$. According to (2.4), we have

$$\begin{aligned} V_2(\mathbf{x}) &= \mathbb{E}_\pi\left[\sum_{t=0}^{\infty} \beta^t \left(f^{(t+1)}(\cdot) + C\right)\right] \\ &= \mathbb{E}_\pi\left[\sum_{t=0}^{\infty} \beta^t f^{(t+1)}(\cdot)\right] + C\sum_{t=0}^{\infty}\beta^t \\ &= V_1(\mathbf{x}) + \frac{C}{1-\beta}. \end{aligned} \tag{2.20}$$

   Therefore, bias of the reward function adds the constant value $\frac{C}{1-\beta}$ to the value of the states. However, all the states are affected the same after the convergence of the algorithm.

2. Effect of bias in the beginning of the learning process: This effect is studied using the action-value function of an agent, i.e., the Q-function. Assume that the Q-function of the agent is initialized with zero values and the reward function is defined as $R = f(\cdot) + C$. Further let us consider the first transition of the

agent from state $\mathbf{x}'$ to state $\mathbf{x}''$ happens by taking action a at time step t, i.e., $\mathbf{x}^{(t)} = \mathbf{x}'$ and $\mathbf{x}^{(t+1)} = \mathbf{x}''$. The update rule at time step t is given by (2.16) as in (2.21)

$$\begin{aligned} Q(\mathbf{x}', a) &\leftarrow Q(\mathbf{x}', a) + \alpha^{(t)}(\mathbf{x}', a)\Big(R(\mathbf{x}', a) + \beta \max_{a'} Q(\mathbf{x}'', a') - Q(\mathbf{x}', a)\Big) \\ &\leftarrow \alpha^{(t)}(\mathbf{x}', a)\Big(f(\cdot) + \beta \max_{a'} Q(\mathbf{x}'', a')\Big) + \underbrace{\alpha^{(t)}(\mathbf{x}', a)\, C}_{(A)}. \end{aligned} \tag{2.21}$$

According to the above, after the first transition from the state $\mathbf{x}'$ to the state $\mathbf{x}''$, the Q-value for the state $\mathbf{x}'$ is biased by the term (A). If $(A > 0)$, the value of the state $\mathbf{x}'$ increases and if $(A < 0)$, the value of the state $\mathbf{x}'$ decreases. Therefore, the already visited states will be more or less attractive to the agent in the beginning of the learning process as long as the agent has not explored the state-space enough.

The change of behavior of the agent in the learning process can be used to bias the agent towards the desired actions or states. However, in basic Q-learning the agent has no knowledge in prior about the environment. Therefore, we select the bias equal to zero, $C = 0$, and define the reward function as follows.

Definition 2. The reward function for the kth FBS, $R_k : (r_0, r_k, \Gamma_0, \Gamma_k) \to \mathbb{R}$, is a continuous and differentiable function on $\mathbb{R}^2$ defined as (2.22)

$$R_k(r_0, r_k, \Gamma_0, \Gamma_k) = (r_0 - \log_2(1 + \Gamma_0))^{k_1} + (r_k - \log_2(1 + \Gamma_k))^{k_2}, \tag{2.22}$$

where k_1 and k_2 are integers.

The objective of the FBS is to maximize its transmission rate. On the other hand, high transmission rate for the MUE is a priority for the FBS. Therefore, R_k should have the following property

$$\frac{\partial R_k}{\partial r_i} \geq 0, \;\; i = 0, k. \tag{2.23}$$

The above property implies that higher transmission rate for the FBS or the MUE results in higher reward. Hence, considering Definition 2, we design a reward function that motivates the FBSs to increase r_k and r_0 as much as possible even more than the required rate as follow

$$R_k = \left(r_0 - \log_2\left(1 + \Gamma_0\right)\right)^{2m-1} + \left(r_k - \log_2\left(1 + \Gamma_k\right)\right)^{2m-1}, \tag{2.24}$$

where m is an integer. The above reward function considers the minimum rate requirements of the FUE and the MUE, while encourages the FBS to increase transmission rate of both.

To further understand the proposed reward function, we discuss reward functions that are used by [46–48]. We refer to the designed reward function in [46] as quadratic, in [47] as exponential, and in [48] as proximity reward functions. The quadratic reward function is designed based on a conservative approach. In fact, the FBS is enforced to select actions that result in transmission rate close to the minimum requirement. Therefore, higher or lower rate than the minimum requirement results in a same amount of reward. The behavior of the quadratic reward function can be explained as follow

$$\frac{\partial R_k}{\partial r_i} \times (r_i - \log_2(1+\Gamma_i)) \leq 0,\ \ i = 0, k. \tag{2.25}$$

The above property implies that if the rate of the FBS or the MUE is higher than the minimum requirement, the actions that increase the rate will decrease the reward. Hence, this property is against increasing sum transmission rate of the network. The exponential and proximity reward functions have the property in (2.23) for the rate of the FBS, and the property in (2.25) for the rate of the MUE. In another words, they satisfy the following properties

$$\begin{aligned} &\frac{\partial R_k}{\partial r_0} \times (r_0 - \log_2(1+\Gamma_0)) \leq 0, \\ &\frac{\partial R_k}{\partial r_k} \geq 0. \end{aligned} \tag{2.26}$$

As the density of the FBSs increases, the above properties result in increasing transmit power to achieve higher individual rate for a FUE while introducing higher interference for the MUE and other neighbor FUEs. In fact, as increasing the FUE rate is rewarded, taking actions that result in increasing the MUE rate decreases the reward. However, the FBS should have the option of decreasing its transmit power to increase the rate of the MUE. This behavior is important since it causes an FBS to produce less interference for its neighboring femtocells. Therefore, we give equal opportunity for increasing the rate of the MUE or the FUE.

The value of reward functions for different FBSs is different, however they have the same behavior. Here, we plot the value of the four reward functions that are discussed above. The plots refers to the proposed (Fig. 2.3(a)), quadratic (Fig. 2.3(b)), exponential (Fig. 2.3(c)), and proximity (Fig. 2.3(d)) reward functions. The important information that can be obtained from these plots are the maximal points of the

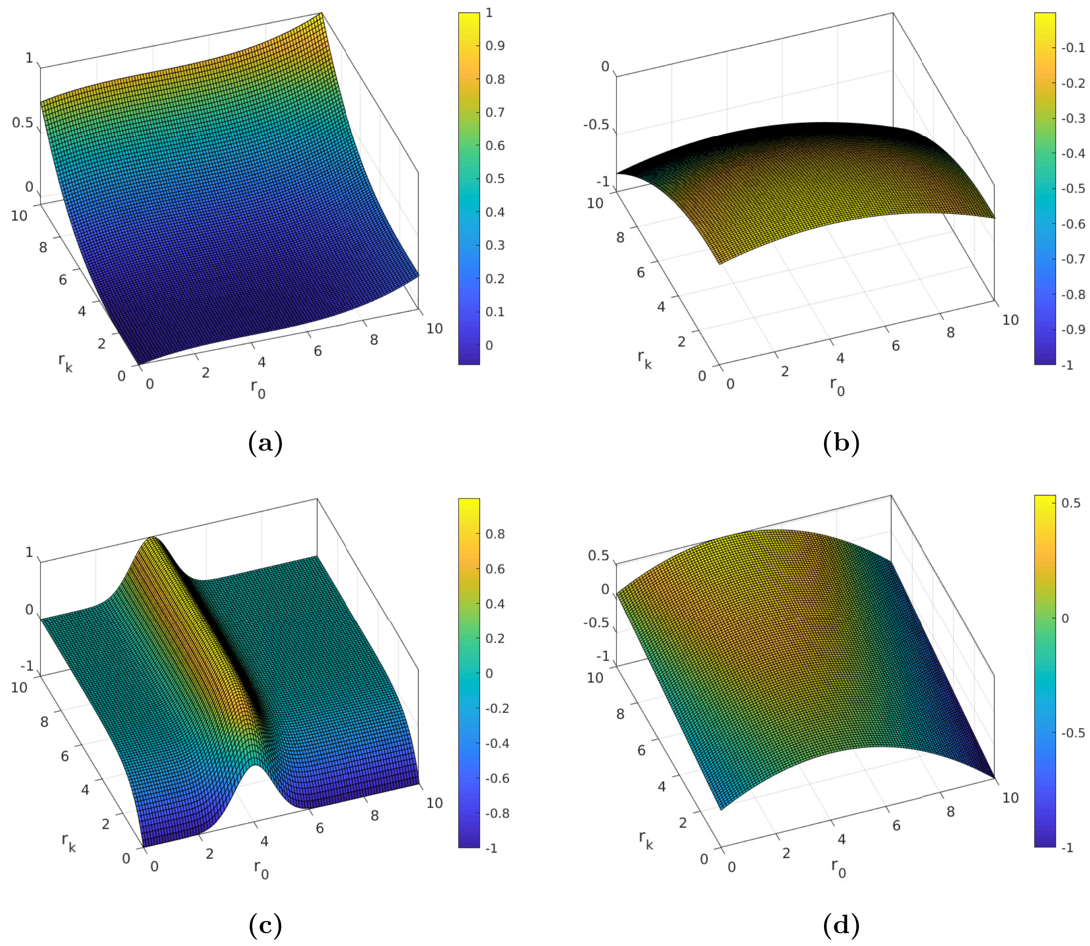

Figure 2.3: Reward functions: (a) Proposed reward function with $m = 2$, (b) Quadratic reward function with zero maximum at $(4.0, 0.5)$, (c) Exponential reward function, (d) Proximity reward function.

reward functions, behavior of the reward functions around minimum requirements, and behavior of the reward functions by increasing r_k or r_0. The proposed reward function in Fig. 2.3(a) shows pushing the FBS to select transmit power levels that increase both r_k and r_0, while other reward functions have their maximum around the minimum rate requirements.

2.5.3 Sample Complexity

In each training frame, Q-DPA collects one sample from the environment represented as the state-action pair in the Q-function. Sample complexity is defined as the minimum number of samples that is required to train the Q-function to achieve an ϵ-optimal policy. For $\epsilon > 0$ and $\delta \in (0, 1]$, π is an ϵ-optimal policy if [66]

$$\Pr\left(\|Q^* - Q_\pi\| < \epsilon\right) \geq 1 - \delta. \tag{2.27}$$

The sample complexity depends on the exploration policy that is generating the samples. In Q-DPA, e-greedy policy is used as the exploration policy. However, e-greedy policy depends on the Q-function of the agent which is being updated. In fact, the distribution of e-greedy policy is unknown. Here, we provide a general bound on the sample complexity of Q-*learning*.

Proposition 1. Assume R_{max} is the maximum of the reward function for an agent and $Q^{(T)}$ is the action-value for state-action pair (x, a) after T iterations. Then, with probability at least $1 - \delta$, we have

$$\|Q^* - Q^{(T)}\| \leq \frac{2R_{max}}{(1-\beta)} \left[\frac{\beta}{T\,(1-\beta)} + \sqrt{\frac{2}{T} \ln \frac{2|\mathcal{X}|.|\mathcal{A}|}{\delta}} \right]. \tag{2.28}$$

Proof. See Appendix A.1. □

This proposition proves the stability of Q-*learning* and helps us to provide a minimum number of iterations to achieve $\epsilon > 0$ error with respect to Q^* with probability $1 - \delta$ for each state-action pair. By assuming the right term of the above inequality as ϵ, the following Corollary is concluded.

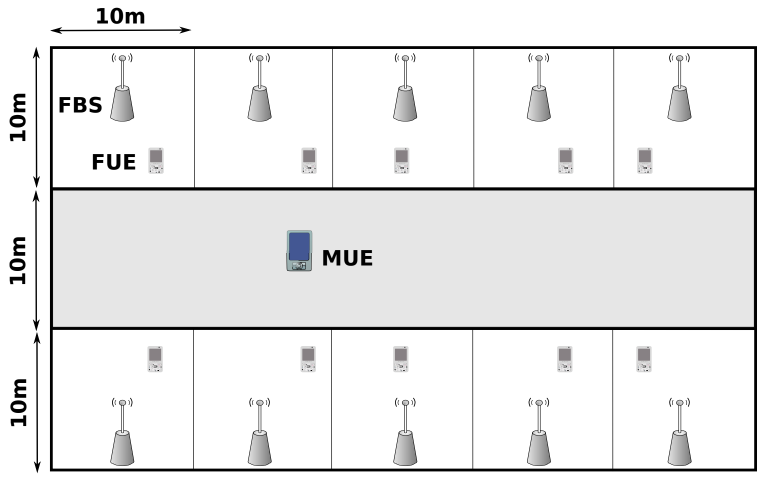

Figure 2.4: Dense urban scenario with a dual strip apartment block located at distance of 350 m of the MBS; FUEs are randomly located inside each apartment.

Corollary 1. For any $\epsilon > 0$, after

$$T = \Omega\left(\frac{8R_{max}^2}{\epsilon^2\left(1-\beta\right)^2}\ln\frac{2|\mathcal{X}|.|A_k|}{\delta}\right) \tag{2.29}$$

number of iterations, $Q^{(T)}$ reaches ϵ-optimality with probability at least $1-\delta$.

2.6 Simulation Results

The objective of this section is to validate the performance of the Q-DPA algorithm with different learning configurations in a dense urban scenario. We first introduce the simulation setup and parameters. Then, we introduce four different learning configurations and we analyze the trade-offs between them. Finally, we investigate the performance of the Q-DPA with different reward functions introduced in Section 2.5.2. For the sake of simplicity, we use the notation IL as independent learning and CL as cooperative learning.

Table 2.1: Urban dual strip pathloss model

Link	**PL(dB)**
MBS to MUE	$15.3 + 37.6 \log_{10} R$,
MBS to FUE	$15.3 + 37.6 \log_{10} R + L_{ow}$,
FBS to FUE (same apt strip)	$56.76 + 20 \log_{10} R + 0.7 d_{2D,indoor}$,
FBS to FUE (different apt strip)	$max(15.3 + 37.6 \log_{10} R,$ $38.46 + 20 \log_{10} R) + 18.3 + 0.7 d_{2D,indoor} + L_{ow}.$

Table 2.2: Simulation Parameters

parameters	**Value**	**parameters**	**Value**
Frame time	2 ms	d'_1, d'_2, d'_3	50, 150, 400 m
Thermal noise	-174 dBm/Hz	d_1, d_2, d_3	17.5, 22.5, 45 m
Traffic model	Fullbuffer		
Q-DPA parameters	**Value**	**parameters**	**Value**
Training period (iterations) L	$T \times \lvert\mathcal{X}\rvert.\lvert\mathcal{A}_k\rvert$	$p_{\min}$	5 dBm
Learning parameter β	0.9	$p_{\max}$	15 dBm
Exploratory probability (e)	10%	Δp	1 dBm

2.6.1 Simulation Setup

We use a dense urban scenario as the setup of the simulation as illustrated in Fig. 2.4. We consider one macrocell with radius 350 m which supports multiple MUEs. The MBS assigns a subband to each MUE. Each MUE is located within a block of apartments and each block contains two strip of apartments. Each strip has five apartments of size 10 m×10 m. There is one FBS located in the middle of each apartment which supports an FUE within a 5 m distance. We assume that the FUEs are always inside the apartments. The FBSs are closed-access, therefore, the MUE is not able to connect to any FBS, however, it receives interference from the FBSs working on the same subband as itself.

Here, we assume that the MUE and all the FBSs work on the same sub-carriers to consider the worst case scenario (high interference scenario). However, the extension of the simulation to the multi-carrier scenario is straight forward but does not affect our investigations. We assume the block of apartments is located on the edge of the macrocell, i.e., 350 m distance from the MBS, and the MUE is assumed to be in between the two strip of apartments.

In these simulations, in order to initiate the state variables X_3 and X_4 in Section 2.4.3, the number of rings around the MBS and the MUE are assumed to be three ($N_1 = N_2 = 3$). Although, as the density increases, more rings with smaller diameters can be used to more clearly distinguish between the FBSs.

It is assumed that the FBSs and the MBS operate at $f = 2.0$ GHz. The MBS allocates 33 dBm as its transmit power, and the FBSs choose their transmit power from a range of 5 dBm to 15 dBm with power steps of 1 dB. In order to model the pathloss, we use the urban dual strip model from 3GPP TR 36.814 [67]. The pathloss model of different links are provided in Table 2.1. In Table 2.1, R is the distance between a transmitter and a receiver in meters, L_{ow} is the wall penetration loss which is set to 20 dB [67]. $d_{2D,indoor}$ is the 2-dimensional distance. We assume that the apartments are single floor, therefore, $d_{2D,indoor} \approx R$. The fourth row of the pathloss models is used for the links between the FBSs and the MUE.

The minimum SINR requirements for the MUE and the FUEs are defined based on the required rate needed to support their corresponding user. In our simulations, the minimum required transmission rate to meet the QoS of the MUE is assumed to be 4 (b/s/Hz), i.e., $\log_2(1+\Gamma_0) = 4$ (b/s/Hz). Moreover, for the FUEs the minimum required rate is set to 0.5 (b/s/Hz), i.e, $\log_2(1+\Gamma_k) = 0.5$ (b/s/Hz), $k \in \mathcal{K}$. It is worth mentioning that by knowing the media access control (MAC) layer parameters, the values of the required rates can be calculated using [68, Eqs. (20) and (21)].

To perform Q-*learning*, the minimum number of required frames, i.e., L, is calculated based on achieving 90% optimality, with probability of at least 0.9, i.e., $\delta = 0.1$. The simulation parameters are given in Table 2.2. The value of the Q-*learning* parameters are selected according to our simulations and references [46–51].

The simulation starts with one femtocell. The FBS starts running Q-DPA in Section 2.5.1 using IL. After convergence, the next FBS is added to the network. The new FBS runs Q-DPA, while the other FBS is already trained, and will just act greedy to choose its transmit power. After convergence of the second FBS, the next one is added to the network, and so on. We represent all the results versus the number of active femtocells in the system, from one to ten. Considering the size of the apartment block, and the assumption that all femtocells operate on the same frequency range, the density of deployment varies approximately from 600 FBS/km^2 to 6000 FBS/km^2.

2.6.2 Performance of Q-DPA

Here, we show the simulation results of distributed power allocation with Q-DPA. First, we define two different state sets. The sets are defined as $\mathcal{X}_1 = \{X_1, X_3, X_4\}$ and $\mathcal{X}_2 = \{X_2, X_3, X_4\}$. In both sets, FBSs are aware of their relative location to the MUE and the MBS due to the presence of X_3 and X_4, respectively. The state set $\mathcal{X}_1$ gives knowledge of the status of the FUE to the FBS, and the state set $\mathcal{X}_2$ provides knowledge of the status of the MUE to the FBS.

In order to understand the effect of independent and cooperative learning, and the effect of different state sets, we use four different learning configurations as: independent learning with each of the two state sets as IL+$\mathcal{X}_1$ and IL+$\mathcal{X}_2$, and cooperative learning with each of the two state sets as CL+$\mathcal{X}_1$ and CL+$\mathcal{X}_2$. The

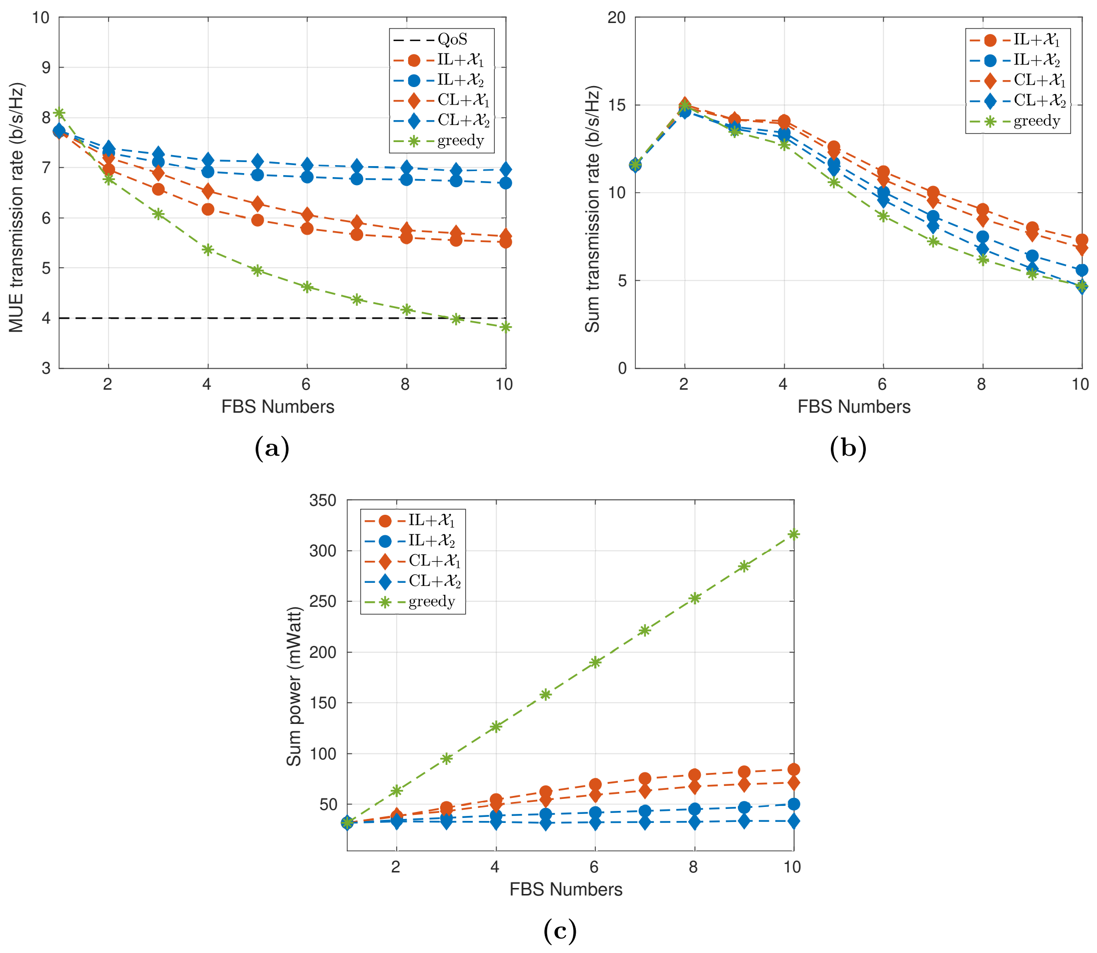

Figure 2.5: Performance of different learning configurations: (a) transmission rate of the MUE, (b) sum transmission rate of the FUEs, (c) sum transmit power of the FBSs.

results are compared with *greedy* approach in which each FBS chooses maximum transmit power. The simulation results are shown in three figures as: transmission rate of the MUE (Fig. 2.5(a)), sum transmission rate of the FUEs (Fig. 2.5(b)), and sum transmit power of the FBSs (Fig. 2.5(c)).

According to Fig. 2.5(c), in the greedy algorithm, each FBS uses the maximum available power for transmission. Therefore, the greedy method introduces maximum interference for the MUE and has the lowest MUE transmission rate in Fig. 2.5(a).

On the other hand, despite using maximum power, the greedy algorithm does not achieve highest transmission rate for the FUEs either (Fig. 2.5(b)). This is again due to the high level of interference.

The state set $\mathcal{X}_2$ provides knowledge of MUE's QoS status to the learning FBSs. Therefore, as we see in Fig. 2.5(a), the performance of IL with $\mathcal{X}_2$ is higher than the ones with $\mathcal{X}_1$. This statement is true for CL too. We can see the reverse of this conclusion in the FUEs' sum transmission rate in Fig. 2.5(b). The performance of IL with $\mathcal{X}_1$ is higher than IL with $\mathcal{X}_2$. This is because the FBSs are aware of the status of the FUE, therefore, they consider actions that result in the state variable $X_1 = \mathbb{1}_{\{\gamma_k \geq \Gamma_k\}}$ to be 1. This is true in comparison of the states in CL too. In conclusion, the state set $\mathcal{X}_1$ works in favor of femtocells and the state set $\mathcal{X}_2$ benefits the MUE.

We conclude from the simulation results that IL and CL present different trade-offs. More specifically, IL supports a higher sum transmission rate for the FBSs and a lower transmission rate for the MUE, while CL can support a higher transmission rate for the MUE at the cost of an overall lower sum transmission rate for the FBSs. From a power consumption point of view, IL results in a higher power consumption when compared to that of CL. In general, IL trains an FBS to be selfish compared to CL. IL can be very useful when there is no means of communication between the agents. On the other hand, CL trains an FBS to be more considerate about other FBSs at the cost of communication overhead.

In Table 2.3, we have compared the performance of the four learning configurations. In each column, number 1 is used as a metric to refer to the highest performance achieved and number 4 is used to refer to the lowest performance observed. The first column represents the summation of transmit powers of FBSs, the second column

Table 2.3: Performance of different learning configurations. 1 is the best, and 4 is the worst.

Learning configuration	$\sum p_k$	$\sum r_k$	r_0
IL+$\mathcal{X}_1$	4	1	4
CL+$\mathcal{X}_1$	3	3	3
IL+$\mathcal{X}_2$	2	2	2
CL+$\mathcal{X}_2$	1	4	1

indicates the summation of transmission rates of the FUEs, and the third column denotes the transmission rate of the MUE.

2.6.3 Reward Function Performance

Here, we compare the performance of the four reward functions discussed in Section 2.5.2. Since the objective is to maximize the sum transmission rate of the FUEs, according to Table 2.3, we choose the combination IL+$\mathcal{X}_1$ as the learning configuration. The performance of the reward functions are provided as the MUE transmission rate (Fig. 2.6(a)), sum transmission rate of the FUEs (Fig. 2.6(b)), and sum transmission power of the FBSs (Fig. 2.6(c)). In each figure, the solution of the optimization problem with exhaustive search and the performance of greedy method are provided. The exhaustive search provides us with the highest achievable sum transmission rate for the network. The quadratic, exponential, and proximity reward functions result in fast decaying of MUE transmission rate, while the proposed reward function results in a much slower decrease of the rate for the MUE. The proposed reward function manages to achieve a higher sum transmission rate compared to that of the other three reward functions as well. Fig. 2.6(c) indicates that the proposed reward function reduces the sum transmitted power at the FBSs which in turn could

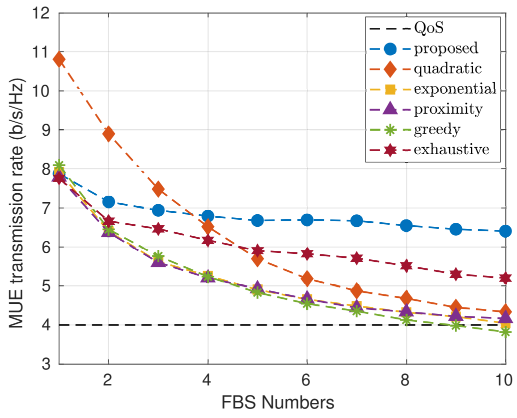

(a)

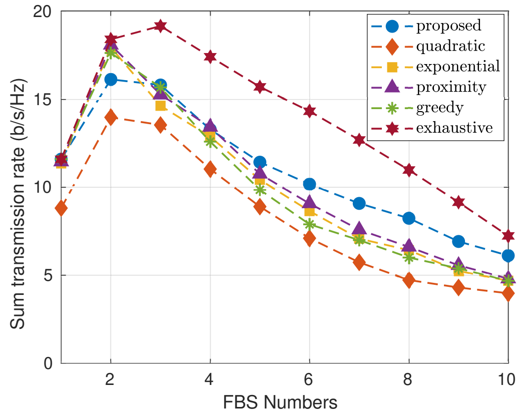

(b)

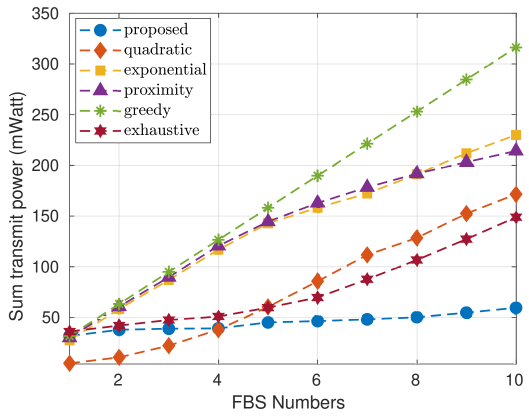

(c)

Figure 2.6: Performance of the proposed reward function compared to quadratic, exponential and proximity reward functions: (a) transmission rate of the MUE, (b) sum transmission rate of the FUEs, (c) sum transmit power of the FBSs.

result in lower levels of interference at the FUEs. In comparison with the exhaustive search solution as the optimal solution, there is a gap of performance. For instance according to Fig. 2.6(c), for eight number of FBSs, the proposed reward function uses an average of 50 mWatt less sum transmit power than the optimal solution. However, as we see in Fig. 2.6(b) and Fig. 2.6(a), by using more power, the sum transmission rate can be improved and the transmission rate of the MUE can be decreased to the level of exhaustive solution without violating its minimum required rate. In our future works, we wish to cover this gap by using neural networks as the function approximator of the learning method.

2.7 Conclusion

In this chapter, we proposed a learning framework for a two-tier femtocell network. The framework enables addition of a new femtocell to the network, while the femtocell trains itself to adapt its transmit power to support its serving user while protecting the macrocell user. On the other hand, the proposed method as a distributed approach can solve the power optimization problem in dense HetNets, while significantly reducing power usage. The proposed framework is generic and motivates the design of machine learning based SONs for management schemes in femtocell networks. Besides, the framework can be used as a bench test for evaluating the performance of different learning configurations such as Markov state models, reward functions and learning rates. Further, the proposed framework can be applied to other interference-limited networks such as cognitive radio networks as well.

Chapter 3

POWER ALLOCATION IN INTERFERENCE-LIMITED NETWORKS VIA COORDINATED LEARNING

In Chapter 2, we focused on transmit power control in a two-tier HetNet and modeled the whole network as a single Markov decision problem (MDP). With introduction of independent and cooperative learning, the MDP was factorized into local Q-functions. However, there was a performance gap between the independent/cooperative learning and the exhaustive search. In this chapter, we focus on transmit power control in an interference-limited network of small base stations (SBSs). We follow the same procedure and define a global Q-function relating to the whole network. However, in order to fill the performance gap, we feed the interference model of the network to the factorization process. In fact, we investigate the effect of accurate MDP factorization on the optimality of the solution. The proposed method leverages coordination through simple message passing between SBSs to achieve an optimal joint power allocation. Simulation results show the optimality of the proposed method for a two-user case. This work was published in [28].

3.1 Introduction

Supporting the expected cellular traffic growth is one of the main tasks for the next generation (a.k.a "5G") wireless cellular networks and densification is one of the main technologies to achieve such growth [3]. A key driver for densification will be deployment of small base stations (SBSs) [69]. The SBSs might be mounted by users in a plug-and-play fashion, and their backhaul may be supported by broadband connections. The user-mounted feature, introduces unplanned deployment of SBSs, which may result in unavoidable co-channel interference. In a dense network, in which the architecture of the network changes sporadically, a self-organizing method is a viable solution to manage the network resources.

One of the requirements of algorithms designed for self-organizing networks (SONs) is working under open loop communication conditions. This means transmitter has access to the signal-to-interference-plus-noise ratio (SINR) values while does not have access to the channel state information (CSI). In fact, radio measurements such as SINR, are part of the Big data in cellular networks [36]. In this regard, one of the main advantages of multi-agent reinforcement learning (MARL) solutions is to utilize the measured SINR values. Generally most of the classic optimization solutions are based on channel coefficients. Thus, the prior methods require full CSI to find the solution while the MARL methods only need access to existing radio measurements, i.e., the measured SINR values. To this end, cooperative MARL methods have been used in resource management of communication networks [27, 70–72]. However, the existing MARL approaches in communication network management do not address the optimality of their cooperation methods. This is an important research topic to address since finding the optimal joint power allocation is directly impacted by the nature of the cooperation approach. In this chapter, we focus on an interference-limited network. We propose a factorization method to achieve optimal solution in transmit power control to maximize sum transmission rate of the system.

3.1.1 Related Work

The problem of power allocation in an interference-limited network has been investigated widely in the literature. In [73] and [74], the optimal power allocation for a two-user interference channel is derived for sum and individual power constraints, respectively. In [75] a more general solution is proposed for multi-transmitter systems with individual power constraints. The solution depends on the SINR value. In high SINR regime, the optimal solution is derived through transforming the problem into a geometric programming (GP) problem, while in the low SINR regime, a heuristic solution based on solving multiple GPs is used. It is important to note that all of these prior approaches are based on interior point methods. Hence, they require a centralized network management approach which may be impossible in dense networks. In [75], a distributed method based on decomposing the optimization problem into local problems is proposed. The solution is based on message-passing and applies to high SINR case with full CSI. Nonetheless, in a dense plug-and-play network, with a changing architecture, the assumptions of high SINR and the availability of full CSI at all nodes may not hold.

3.1.2 Contributions

In this chapter, we find an optimal joint power allocation solution via coordination between deployed SBSs. To address the optimality of the MARL approach, we model the whole system as a Markov decision process (MDP) with the SBSs being represented as the agents of the MDP. Then, we define a coordination graph according to the interference model of the network. Subsequently, MDP is factorized to local ones and the value function of the MDP is approximated by a linear combination of local value functions. As we mentioned before, in order to remove the need for access to CSI, and develop an adaptable algorithm that handles a changing network architecture, each SBS uses a model-free reinforcement learning approach, i.e., Q-learning. Q-learning is used to update the SBS's local value function. Subsequently, we leverage the ability of SBSs to communicate over the backhaul network to build a simple message passing structure to select a transmit power action based on the variable elimination method. Finally, we propose a distributed algorithm which finds an optimal joint power allocation to maximize the sum transmission rate.

This chapter is organized as follows. In Section 5.2, the system model is presented. Section 3.3 first introduces the optimization problem, then analyzes the convexity of the problem. Section 3.4 presents the general framework of the proposed solution. Section 3.5 outlines the proposed power allocation scheme while Section 3.6 presents simulation results. Finally, Section 3.7 concludes the chapter.

3.2 System Model

We consider downlink transmission in a dense deployment of N SBSs. We assumed each SBS supports one user equipment (UE), and all SBSs share the same frequency resource block. This system can represent a single cluster of a large network, which uses different frequency in each cluster to avoid interference between clusters. It is also assumed the SBSs are interconnected via a backhaul network supported by, for example, a broadband connection. Here, we use the same model of interference as [73]. Thus, the received signal at the ith UE, r_i is given by

$$r_i = \sqrt{g_i P_i} d_i + \sum_{j \in D_i} \sqrt{g_i P_j \beta_{ji}} d_j + n_i, \tag{3.1}$$

where g_i represents the channel gain between the ith SBS and the UE it is serving, d_i is the transmitted signal from the ith SBS, P_i is the transmitted power at the ith SBS, D_i represents the set of interfering SBSs to the ith UE, β_{ji} $(0 \leq \beta_{ji} \leq 1)$ for $1 \leq i \leq N$ and $j \in D_i$ is the ratio of the unintended power of the jth SBS when measured at the ith UE, and n_i is the zero mean additive white Gaussian noise (AWGN) at the ith UE with variance σ^2. According to the signal representation in (3.1), the SINR at the ith UE, SINR_i, can be determined as

$$\mathrm{SINR}_i = \frac{g_i P_i}{\sum_{j \in D_i} g_i P_j \beta_{ji} + \sigma^2}, \tag{3.2}$$

and the throughput at the ith UE normalized by the transmission bandwidth, R_i, is calculated as

$$R_i = \log_2 \left(1 + \mathrm{SINR}_i\right). \tag{3.3}$$

It is worth noting that the proposed solution will use the measured SINR, and does not need to estimate the values of channel gains.

3.3 Problem Analysis

Let us define $\underline{\mathbf{P}} = \{P_1, P_2, ..., P_N\}$ as the set containing the transmitted power of the SBSs. The goal of the optimization is to find the optimal joint power allocation between SBSs, $\underline{\mathbf{P}}^* = \{P_1^*, P_2^*, ..., P_N^*\}$, that maximizes the total throughput of the network. The optimization problem ($\mathbf{OP}_1$) can be formulated as

$$\underset{\underline{\mathbf{P}}}{\text{maximize}} \quad \sum_{i=1}^{N} R_i = \sum_{i=1}^{N} \log_2 \left(1 + \text{SINR}_i\right), \tag{3.4a}$$

$$\text{subject to} \quad P_i \leq P_{i,max},\ i = 1, \ldots, N. \tag{3.4b}$$

Here, the objective function in (3.4a) maximizes the sum throughput of the network. The constraint (3.4b) refers to the individual power limitation of every SBS.

3.3.1 Problem Analysis

The optimization problem ($\mathbf{OP}_1$) is a non-convex optimization problem. Here, first we will investigate the non-convexity of $\mathbf{OP}_1$, and then we will examine the approximate solutions to the problem in two regimes : (1) high SINR, and low to medium SINR.

Non-Convexity of $\mathbf{OP}_1$

The objective function in (3.4a) contains the interference term in the denominator of SINR term. In a dense network the interference term cannot be ignored [59]. Due to the presence of the interference term, the objective function (3.4a) is a non-concave function [58], which leads to non-convexity of the optimization problem.

Approximate Problems

- *High SINR* : If the condition SINR $\gg$ 1 holds, which means signal level is much higher than the interference level, the objective function in $\mathbf{OP}_1$ can be approximated as

$$\sum_{i=1}^{N} \log_2 (1 + \mathrm{SINR}_i) = \sum_{i=1}^{N} \log_2(\mathrm{SINR}_i) = \log_2(\prod_{i=1}^{N} \mathrm{SINR}_i). \qquad (3.5)$$

By using the above approximation, and representing the objective function and the constraints using posynomials, $\mathbf{OP}_1$ can be represented in the form of geometric programming (GP) problem. GP is a nonlinear, nonconvex optimization problem which can be transformed into a convex optimization problem and can be solved in efficient time [75].

- *Low to medium SINR* : If the SINR value is not much larger than 0dB, the approximation in (3.5) does not hold. Although by using the posynomial format, $1 + \mathrm{SINR}_i$ can be represented as a ratio of two posynomials. In this format, the optimization problem falls into a nonconvex class of problems called Complementary GP [75]. The Complementary GP problems are intractable NP-hard problems.

As we mentioned before, in both of the above cases, the solutions are based on the availability of CSI at the transmitters (SBSs). However, the assumption of open-loop communication which is one of the features of SONs disqualifies availability of CSI at the transmitter. Hence, SBSs need to select their transmit power just based on the measured SINR fed back from their assigned users.

3.3.2 Nash Equilibrium and Pareto Optimality

Since the goal of the optimization problem is to maximize the sum throughput of the network, $\mathbf{OP}_1$ can be viewed as a fully cooperative game. A fundamental solution to a game is the Nash equilibrium [76]. The Nash equilibrium is a joint action in a game, where deviating from this action when considering the actions of other agents is not profitable to the agent taking the action. Any game can have multiple solutions for the Nash equilibrium. Another concept is the Pareto optimality of a solution. A joint action is Pareto optimal, if an agent can not gain more performance without reducing the performance of at least one other agent in the game. In a fully cooperative game, each Pareto optimal solution is a Nash equilibrium, which can be achieved using coordination between agents [77].

3.4 Distributed Coordinated Q-*learning*

In this section, the proposed optimal solution based on the Markov decision process (MDP) is presented. Then, the dimensionality issues of the optimal solution will be investigated. The dimensionality is important since it affects the tractability of the problem. Next, we use the coordination method introduced by [78] to solve the problem in a distributed fashion. We show that the resulting method, provides a joint solution for the MDP via message passing between the agents of the network.

3.4.1 Optimal Solution via Q-*learning*

Consider a system with N agents, where each agent j selects its actions from its action set, A_j. Further, $\mathbf{X} = \{X_1, X_2, ..., X_n\}$ is the set of state variables which define the state of the system. Let us denote $\underline{x} \subset X$ to represent a single state of the system. In a fully cooperative game, we look for an optimal joint solution that is a Pareto optimal Nash equilibrium. One obvious solution to this problem is to model the whole system as a large MDP with its action set representing the joint action set of all the agents in the system. We consider $\mathbf{A}$ as the joint action set of all the agents, and $\underline{a} \subset \mathbf{A}$ as a single joint action of this set.

The MDP framework will be modeled as $(\mathbf{X}, \mathbf{A}, Pr, \mathbf{R})$, where $\mathbf{X}$ denotes the finite set of states of the system, $\mathbf{A}$ is a finite set of joint actions, Pr is the transition model which represents the probability of taking action $\underline{a}$ at state $\underline{x}$ and ending up in state $\underline{x}'$, $Pr\left(\underline{x}, \underline{a}, \underline{x}'\right)$, and $\mathbf{R}$ is the immediate reward received by taking action $\underline{a}$ at state $\underline{x}$, $\mathbf{R}\left(\underline{x}, \underline{a}\right)$.

A policy, $\pi : \mathbf{X} \rightarrow \mathbf{A}$, for an MDP is defined as a function which shows at state $\underline{x}$, action $\pi\left(\underline{x}\right)$ will be taken. In order to evaluate a policy, a value function $V\left(\underline{x}\right)$, is defined which defines the value of policy at each state. In order to compute the value function for a given policy, we need to calculate the action-value function, also known as Q-function, defined as follows

$$\mathbf{Q}\left(\underline{x}, \underline{a}\right) = \mathbf{R}\left(\underline{x}, \underline{a}\right) + \gamma \sum_{\underline{x}'} Pr\left(\underline{x}' | \underline{x}, \underline{a}\right) V\left(\underline{x}'\right), \tag{3.6}$$

in which $\gamma \in [0, 1]$ is a discount factor. The optimal value at state $\underline{x}$ is the maximum value that can be reached by taking any action at this state. The optimal value function V^*, which gives the optimal policy π^*, satisfies the Bellman operation as follows [2]

$$V^*\left(\underline{x}\right) = \max_{\underline{a}} \mathbf{Q}^*\left(\underline{x}, \underline{a}\right). \tag{3.7}$$

Q-*learning* is a model-free reinforcement learning, which solves the Bellman equation through direct observations without knowledge of the transition model. In Q-*learning*, the agent observers the state, $\underline{x}$, takes an action, $\underline{a}$, receives a reward, $\mathbf{R}$, and ends in a next state, $\underline{x}'$. Then, it will update its Q-function as follows

$$\mathbf{Q}\left(\underline{x},\underline{a}\right)=\mathbf{Q}\left(\underline{x},\underline{a}\right)+\alpha[\mathbf{R}\left(\underline{x},\underline{a}\right)+\gamma\max_{\underline{a}'}\mathbf{Q}\left(\underline{x}',\underline{a}'\right)-\mathbf{Q}\left(\underline{x},\underline{a}\right)], \tag{3.8}$$

where, α is the learning rate of the algorithm. If any action-state pair is repeatedly visited, the Q-function will converge to the optimal value [25].

One issue with this method is that the size of the joint action set is exponential with respect to the number of agents. If there are N agents in the network, and each one has $|A|$ number of actions as the size of their action set, the size of the joint action set, $|\mathbf{A}|$, will be $|A|^N$. The exponential size of the joint action set makes the computation of the Q-function expensive and in most cases intractable.

3.4.2 Factored MDP

In most cases, for both representational and computational advantages, the state and action sets of an MDP can be factored into subsets based on the structure of the problem [61]. In large MDPs, the global Q-function can be approximated by the linear combination of local Q-functions, i.e. $\mathbf{Q} = \sum_j Q_j(\underline{a_j})$ [78]. The jth local Q-function, Q_j, has the joint action set which is a subset of the global joint action set, $\mathbf{A}$. Here, we will define the joint action set of Q_j by $\mathit{Scope}\left[Q_j\right] \subset \mathbf{A}$ for which $\underline{a_j}$ is a joint action of this set.

In a communication network, each SBS plays the role of an agent in the multi-agent network. The action of SBS j, is the transmit power, P_j, that is used to transmit its signal to the intended user. From this point, an agent in a communication network, refers to the SBS. Generally, in wireless communication systems, each access point receives interference from specific local access points. Therefore, the approximation of global Q-function by linear combination of local Q-functions, applies to interference-limited communication networks. In cellular networks, the interferers can be all the neighbor transmitters working on the same frequency band. However, in some cases, we can assume that there is a dominant interferer which allows us to neglect the interference from other neighbors. In this chapter, we follow the assumption of a dominant interferer for each receiver.

3.4.3 Decomposition of Global Q-function

The decomposition of the global Q-function, relies on the dependencies between the agents of the network. These dependencies can be represented by *coordination graphs* (CGs) [78]. Generally, there are two decomposition methods: agent-based and edge-based. The agent-based decomposition provides a suitable architecture for a distributed system with exact solution, while the edge-based decomposition is recommended for coordination graphs with densely connected nodes [79] and provides suboptimal solution. Here, we choose the agent-based decomposition since we are focused on achieving the optimal solution. Further, considering the dominant interferer assumption mentioned in 3.4.2, the coordination graph would be sparse and suitable for agent-based decomposition.

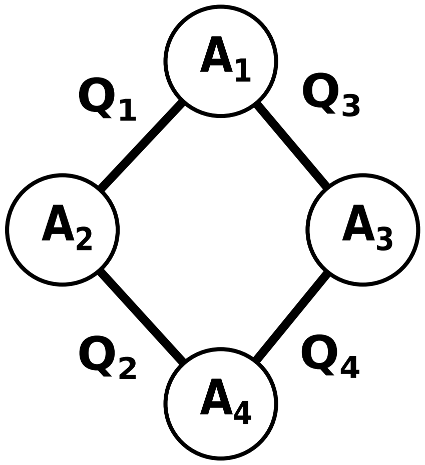

Figure 3.1: Coordination graph.

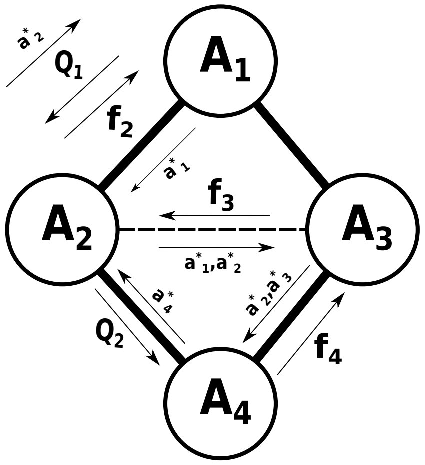

Figure 3.2: Message passing.

In a wireless network, the $Scope\,[Q_j]$ for agent j, is determined based on the interference model of the system, which is related to set D in (3.1). In order to be able to explain the proposed solution, we pick an example as in Fig. 3.1, in which four agents interfere with each other. Assume that agent A_1, receives interference from A_2 and A_3, and A_4 receives its interference from A_2 and A_3. Based on this model, the coordination graph of the system is shown in Fig. 3.1. Each edge between agents, shows a dependency between the two agents.

Here, we assume that all agents have the same state $\underline{x}$, hence, $Q\,(x, a)$ is written as $Q\,(a)$. According to the coordination graph in Fig. 3.1, the global Q-function, $\mathbf{Q}\,(\underline{\mathbf{a}})$, can be written as

$$\mathbf{Q}(\underline{\mathbf{a}}) = Q_1(a_1, a_2) + Q_2(a_2, a_4) + Q_3(a_1, a_3) + Q_4(a_3, a_4). \tag{3.9}$$

3.4.4 Coordinated Action Selection

In multi-agent Q-*learning*, according to (3.8), the agents select a joint action that maximizes the global Q-function. By using the agent-based decomposition, the joint action selection at state $\underline{x}$, $\max_{\underline{a}} \mathbf{Q}\,(\underline{a})$, is written as

$$\max_{a_1,a_2,a_3,a_4} Q_1(a_1, a_2) + Q_2(a_2, a_4) + Q_3(a_1, a_3) + Q_4(a_3, a_4). \tag{3.10}$$

This maximization problem, can be solved via variable elimination (VE) algorithm, which is basically similar to variable elimination in a Bayesian network [80]. Here, we review this method for the network in Fig. 3.1. The key idea is to maximize over one variable at a time, find conditional solutions, passing conditional functions to other agents, and sending back the results of local optimization to the related agents to recover their joint action choices. The steps of the joint maximization solution are presented in Fig. 3.2 as they are described below.

We start from agent A_4. a_4 influences Q_2 and Q_4, so the maximization problem can be written as

$$\max_{a_1,a_2,a_3} Q_1(a_1,a_2) + Q_3(a_1,a_3) + [\max_{a_4} Q_2(a_2,a_4) + Q_4(a_3,a_4)]. \tag{3.11}$$

Agent A_2 communicates Q_2 to A_4, and A_4 solves its local maximization, which results in two functions: $f_4\left(a_2,a_3\right)$, and $b_4\left(a_2,a_3\right)$. These functions are defined as follows

$$f_4\left(a_2,a_3\right) = \max_{a_4} Q_2\left(a_2,a_4\right) + Q_4\left(a_3,a_4\right), \tag{3.12}$$

$$b_4\left(a_2,a_3\right) = \arg\max_{a_4} Q_2\left(a_2,a_4\right) + Q_4\left(a_3,a_4\right). \tag{3.13}$$

At his stage, the A_4 has a conditional solution for a_4 based on a_2, and a_3, represented as the function b_4. Therefore, A_4 keeps b_4 and sends f_4 to its connecting agent, A_3. Then, A_4 is removed from the coordination graph, and the maximization problem is translated to

$$\max_{a_1,a_2,a_3} Q_1\left(a_1,a_2\right) + Q_3\left(a_1,a_3\right) + f_4\left(a_2,a_3\right), \tag{3.14}$$

f_4 brings a new edge in the coordination graph, an induced edge, which is shown with dashed line between A_2 and A_3 in Fig. 3.2. The next agent to be removed is A_3. The maximization problem is rewritten as

$$\max_{a_1,a_2} Q_1(a_1,a_2) + \left[\max_{a_3} Q_3(a_1,a_3) + f_4(a_2,a_3)\right]. \tag{3.15}$$

With the same procedure, A_3 introduces $f_3(a_1,a_2)$, and $b_3(a_1,a_2)$. Accordingly, the problem reduces to

$$\max_{a_1,a_2} Q_1(a_1,a_2) + f_3(a_1,a_2). \tag{3.16}$$

Next agent to choose its action is A_2, for which the problem results in

$$f_1 = \max_{a_1} f_2(a_1), \tag{3.17}$$

where, $f_2(a_1) = \max_{a_2} Q_1(a_1,a_2) + f_3(a_1,a_2)$. Finally, A_1 chooses its action based on maximizing the function $f_2(a_1)$. The results at this stage are f_1, and a_1^*. f_1 represents the maximum value of the global Q-function over a_1, a_2, a_3, and a_4, and a_1^* is the optimal joint action for A_1. To recover the joint action choices, A_1 sends a_1^* to A_2. Then A_2 chooses its action, $a_2 = b_2(a_1^*)$, and sends a_1^*, a_2^* to A_3. A_3 and A_4 will choose their actions with the same procedure, $a_3^* = b_3(a_1^*, a_2^*)$, and $a_4^* = b_4(a_2^*, a_3^*)$.

In general, the elimination algorithm maintains a set of functions in each step, $\mathbf{Q}$. It starts with all local Q-functions, $\{Q_1, Q_2, ..., Q_N\}$, and eliminates agents one by one. The algorithm steps can be summarized as follows

1. Choose an uneliminated agent, for example A_l.

2. Choose all functions, $Q_1, Q_2, ..., Q_l \in \mathbf{Q}$ whose *Scope* contains A_l.

3. Define a new function, $f_l = \max_{a_l} \sum_j Q_j$ and add it to $\mathbf{Q}$. The *Scope* of Q_l is $\cup_{j=1}^{L} \text{Scope}[Q_j] - \{A_l\}$.

3.4.5 Local Update Rule

After finding the joint action, each agent will update its local Q-function. The update rule in (3.8) can be written as

$$\sum_j Q_j\left(\underline{x}, \underline{a_j}\right) = \sum_j Q_j\left(\underline{x}, \underline{a_j}\right) + \alpha\left[\sum_j R_j\left(\underline{x}, \underline{a_j}\right) + \gamma \max_{\underline{a}} \sum_j Q_j\left(\underline{x}', \underline{a}'\right) - \sum_j Q_j\left(\underline{x}, \underline{a_j}\right)\right], \quad (3.18)$$

where, the joint maximization is solved through VE according to the last section. By assuming $\underline{a}^*$ as the solution to the VE, and $\underline{a_j}^* \subset \underline{a}^*$ as the optimal joint action set for Q_j, the update rule for each local Q-function can be derived as

$$Q_j(\underline{x}, \underline{a_j}) = Q_j(\underline{x}, \underline{a_j}) + \alpha[R_j(\underline{x}, \underline{a_j}) + \gamma Q_j(\underline{x}', \underline{a_j}^*) - Q_j(\underline{x}, \underline{a_j})]. \quad (3.19)$$

The Fig. 3.2 illustrates all messages passed between the agents to solve VE and update local Q-functions.

3.5 Power Allocation Using Coordinated Q-Learning

To integrate the idea of coordinated multi-agent learning into a communication network, we will model the SBS as an agent, and the whole network as a multi-agent MDP. The goal of the agents is to maximize total throughput of the network, as a cooperative game. In the following we introduce the power allocation scheme based on coordinated Q-learning as Q-CoPA.

3.5.1 Q-CoPA Algorithm

The proposed solution of this paper, Q-CoPA, can be summarized as follows

The interference model of the network will be used to derive the coordination graph of the agents. The entire network is modeled as an MDP, and the global Q-function of the MDP is approximated by linear combination of local Q-functions of the agents. Each agent, based on the coordination graph, knows its *Scope*. Local Q-functions are learned by the agents using cooperative Q-*learning*. The cooperation method between the agents is to maximize the summation of local Q-functions by choosing an appropriate joint action. This action selection is implemented using variable elimination and message passing between the agents. The backhaul of the network is used as the required infrastructure for message passing. The proposed method is represented in Algorithm 1. In the Algorithm 1, the loops at lines 5 and 10 are independent, and could be executed in parallel by the agents.

Algorithm 1 The proposed Q-CoPA algorithm

```
1: Initialize $\underline{x}$
2: Initialize All $Q_j(\underline{x}, \underline{a_j})$ arbitrarily
3: for all episodes do
4:     Choose $\underline{a}^*$ according to VE
5:     for all agents do
6:         Take action $\underline{a_j}$, observe $R_j$
7:     end for
8:     Observe $\underline{x}'$
9:     Calculate $\max_{\underline{a}'} \mathbf{Q}$ according to VE
10:    for all agents do
11:        Update local Q-function according to Eq. 3.19
12:    end for
13:    $x_j \leftarrow x_j^{'}$
14: end for
```

3.5.2 Q-*learning* Configurations

In the following the actions, and the reward of the Q-*learning* algorithm implemented by each agent is defined.

- *Actions* : Each SBS has a set of actions, which is defined as the transmit power levels. We define this set as $\{p_1, p_2, ..., p_{\mathrm{N_{power}}}\}$. The number of power levels is defined as $\mathrm{N_{power}}$.

- *Reward* : In each episode, SBS chooses a power level, and transmits its data to its intended user. The user measures the SINR of the signal, and will feedback it to the SBS. Then the reward of the SBS j is calculated as $r_j = \log_2(1 + \mathrm{SINR}_j)$.

3.6 Simulation Results

In this section, we implement the proposed power allocation for a two transmitter and two receiver with interfering channels scenario. In fact, since there are only two SBSs in the system, the assumption of one dominant interferer is accurate. Hence, we can investigate the optimality of the proposed solution in this case. We consider each SBS supports one UE. Each transmitter has omni-directional antenna and separate power source. The channel model is assumed to be time-invariant, i.e. slow fading. The channel gains are assumed to be $g_1 = 2.5$, and $g_2 = 1.5$. The $P_{1,\max} = 10$ dBm, $P_{2,\max} = 13$ dBm, and $\sigma^2 = 0$ dBm. Without loss of generality we assume that $\beta_{1,2} = \beta_{2,1} = \beta$ in (3.1). The objective of the optimization is to find the power allocation to maximize the sum throughput of the network under individual power constraints.

In executing the Q-CoPA algorithm, each Q-function is defined as a table, Q-table. The learning rate is $\alpha = 0.5$, the discount factor as $\gamma = 0.9$, $\mathrm{N_{power}} = 100$, and the

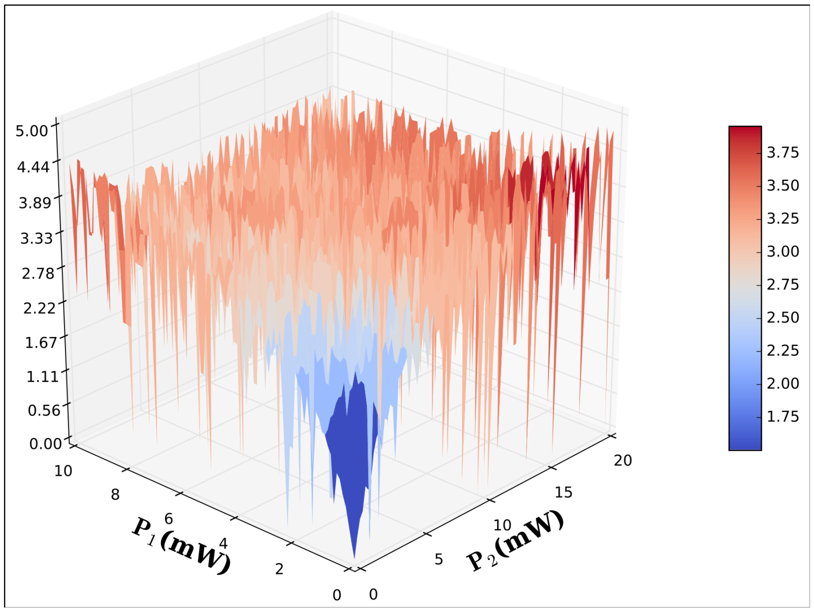

Figure 3.3: Global action-value function.

maximum number of episodes is set to 50 times the size of a Q-table. The MDP of this problem is assumed to be stateless. The actions of agents are the transmit powers, $a_1 = \mathrm{P}_1$, and $a_2 = \mathrm{P}_2$, Q-functions are defined as: $Q_1(\mathrm{P}_1, \mathrm{P}_2)$ and $Q_2(\mathrm{P}_1, \mathrm{P}_2)$, and the global Q-function is defined as: $\mathbf{Q}\,(P_1, P_2) = Q_1(P_1, P_2) + Q_2(P_1, P_2)$.

According to [74], the optimal power allocation to maximize the sum-rate of the above network is derived as

$$(\mathrm{P}_1^*, \mathrm{P}_2^*) = \begin{cases} (\mathrm{P}_{1,\max}, 0), & \text{if } g_1\mathrm{P}_{1,\max} \geq \max\left(g_2\mathrm{P}_{2,\max}, 1/\beta^2\right), \\ (0, \mathrm{P}_{2,\max}), & \text{if } g_2\mathrm{P}_{2,\max} \geq \max\left(g_1\mathrm{P}_{1,\max}, 1/\beta^2\right), \\ (\mathrm{P}_{1,\max}, \mathrm{P}_{2,\max}), & \text{otherwise.} \end{cases} \tag{3.20}$$

First we will execute our proposed algorithm for $\beta = 0.3$. According to the optimal solution, $(0, \mathrm{P}_{2,\max})$ is the optimal solution. According to Q-CoPA, the SBSs will choose the powers that maximizes the global Q-function. The learned global

Q-function, $\mathbf{Q}(\mathrm{P}_1, \mathrm{P}_2)$, is plotted in Fig. 3.3 with maximum value at $\mathrm{P}_1 = 0$ and $\mathrm{P}_2 = \mathrm{P}_{2,\max}$, which is optimal.

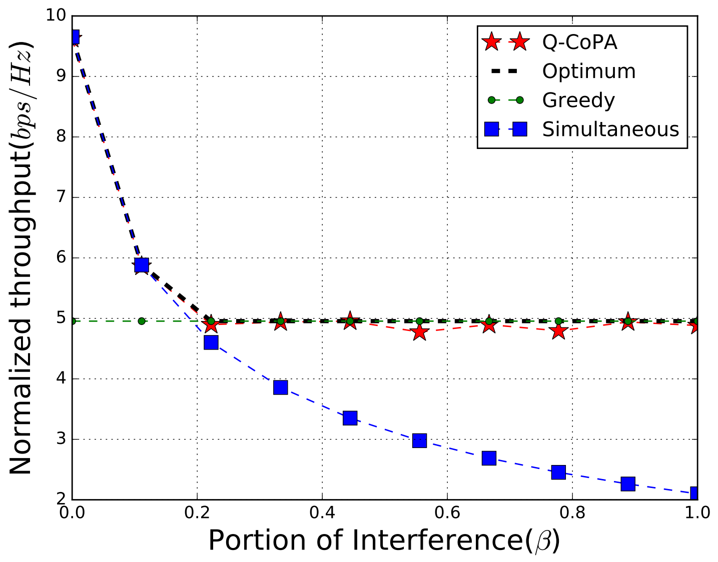

Figure 3.4: Normalized throughput versus portion of interference (β).

In Fig. 3.4, the solution of the power allocation for different values of the portion of interference between two channels, $\beta \in [0, 1]$, is plotted. The greedy approach is defined to allocate full power to the transmitter with higher peak power, and zero to the other one. The simultaneous allocation is defined to use maximum power at both transmitters. According to Fig. 3.4, the Q-CoPA finds the optimal solution for all values of β.

3.7 Conclusion

In this chapter, we used message-passing and variable elimination to coordinate the power allocation in order to maximize a common goal in an interference-limited network. The variable elimination algorithm is exact, so as long as the local Q-functions' action set covers all interfering SBSs, the proposed solution is optimal. Although, when each node of the coordination graph gets densely connected, i.e., the size of action set of local Q-function grows, for the sake of computational complexity we need to approximate local Q-functions' action set with smaller sets, which results in suboptimal solution. Therefore, the proposed solution is suitable for indoor applications, or networks in which the number of interferes is low.

Chapter 4

SPATIAL INDEXING FOR SYSTEM-LEVEL EVALUATION OF 5G HETEROGENEOUS CELLULAR NETWORKS

System level simulations of large 5G networks are essential to evaluate and design algorithms related to network issues such as scheduling, mobility management, interference management, and cell planning. In this chapter, we look back to the idea of spatial indexing and its advantages, applications, and future potentials in accelerating large 5G network simulations. We introduce a multi-level inheritance based architecture which is used to index all elements of a heterogeneous network (HetNet) on a single geometry tree. Then, we define spatial queries to accelerate searches in distance, azimuth, and elevation. We demonstrate that spatial indexing can accelerate location-based searches by 3 orders of magnitude. Further, the proposed design is implemented as an open source platform freely available to all. This work is submitted for possible publication in [29]

4.1 Introduction

Supporting the expected cellular traffic growth is one of the main tasks for the next generation (a.k.a "5G") wireless cellular networks and densification is one of the main technologies to achieve such growth [3]. A key driver for densification in the next 5-10 years will be small base stations (SBSs) operating at millimeter wave (mmWave) frequencies. These SBSs will also support conventional communication below 6 GHz (Sub6GHz) frequencies and possibly use mmWave for the backhauling as well as some user equipment (UE) connections. Furthermore, due to propagation features in mmWave bands, usage of highly directional antennas at the transceivers is a necessity [16]. Hence, 5G will contain directional heterogeneous networks (HetNets) with large number of nodes working on different frequency bands.

In the development and standardization of 5G, simulations are necessary to implement and design new algorithms and protocols. Considering the above features of 5G, system-level simulations need platforms which deliver accurate results in short time in large HetNets. These simulations are needed to evaluate the performance of scheduling algorithms, mobility managements procedures, interference management methods, and cell planning algorithms [81].

In simulation of large networks, operations that require searches over various nodes of the network may be extremely time consuming, where spatial indexing has been one of the methods to address this issue [82]. In fact, spatial indexing has been used instead of traditional array indexing in order to accelerate location-based searches in the simulation of large homogeneous networks such as wireless sensor networks (WSNs). Wireless sensors are indexed based on their location on a geometry tree to provide fast search queries. This method can not be trivially applied in HetNets since a single geometry tree cannot be used for spatial indexing of different nodes.

4.1.1 Contributions

In this chapter, first, we propose a multi-level inheritance based structure to be able to store different nodes of a HetNet on a single geometry tree. The proposed structure is polymorphic in a sense that different levels of a node can be accessed via dynamic casting [83]. Second, we focus on potentials of spatial indexing in accelerating the simulation of directional communications. We introduce different spatial queries and show that spatial indexing significantly accelerates simulation time in orders of magnitude when it comes to location-based searches over azimuth, and elevation as well as its traditional usage in searches over distance.

4.1.2 Motivation

Traditional wireless network simulators such as Network Simulator (NS-2, NS-3) [84, 85] do not take into consideration the relationship between a terminal and its location in the indexing procedure. In other words, nodes are indexed based on features such as identification numbers or the order in which they are added to the network. Nodes are simply stored in an array (array indexing) and there is no pre-processing (sorting or classification) based on the location of the nodes. Consequently, in a network with n nodes, the search size of any algorithm related to the location of the nodes equals the total number of the nodes in the network, i.e., $\mathcal{O}(n)$. Hence, if all nodes run such an algorithm, the exhaustive search complexity would be $\mathcal{O}(n^2)$. This is important since in dynamic wireless networks, location-dependent searches are called frequently in simulations. Examples of location-dependent searches in a simulation environment are: finding the nearest neighboring users for association or handover purposes, finding the k-nearest neighboring BSs for coordinated multipoint (CoMP) transmission, or finding the potential interferers to evaluate signal-to-interference-plus-noise-ratio (SINR) of a communication link. While the above searches are defined over distance, in mmWave applications the direction of communication is important as well. This means searching over distance, azimuth, and elevation at the same time which can increase the complexity of the overall algorithm significantly. In practice, decreasing the order of search complexity can potentially change the computation time from hours to seconds of computation in large networks. In order to achieve this goal, location-transparency can be changed into location-dependency in the indexing of nodes [86–88]. To this aim, spatial indexing has been used in homogeneous networks with the intent of accelerating distance queries. In this work, we take advantage of polymorphic programming to use spatial indexing in heterogeneous cellular networks and to provide fast spatial search queries in distance, azimuth, and elevation.

4.1.3 Related Works

There are several open-source simulators developed for different purposes in wireless networks. In this category, with the focus on open-source platforms, we have Network Simulators (NS-2, NS-3) [84, 85], OMNET++ [89], J-Sim [90], and SHOX [91] platforms. These common simulators focus on preparing a platform for design and evaluation of communication protocols in the network layer or layers above it. The physical layer modules in the above platforms are not appropriate for mmWave or directional communications. The full-stack mmWave module proposed by [92] alleviates this shortcoming, by adding this module to the NS-3 platform for support of the mmWave communications. The physical-layer module presented by [92] is extensive. However, the added module is built on the core of the NS-3 and is not designed to calculate directional interference in networks with dynamic topology. Nevertheless, none of the above simulators takes advantage of spatial indexing. In fact, the nodes of the network are simply stored in an array.

Spatial indexing has been used in two major applications in wireless communications: (*i*) location-aware data indexing in wireless broadcast systems and (*ii*) location-dependent indexing in simulation platforms. Location awareness is naturally the first step of context-awareness in broadcast systems and spatial indexing is used in wireless broadcast systems where efficient indexing of data segments is essential for mobile users to find their required query from the broadcast data [93–95]. Apart from the application of spatial indexing in broadcast systems, its advantage in simulation environments has been noticed in a few works [96, 97]. Fast distance query of spatial indexing is used in high fidelity large-scale simulation of wireless communications [96]. Also, [97] changed the indexing procedure of NS-3 in the simulation of a large-scale (more than 1000 nodes) vehicular ad-hoc network (VANET) to provide fast distance queries as well. However, wireless networks and more specifically cellular networks are heterogeneous. This means elements of the network can vary from macro base stations to small base stations and mobile users. Further, there are certain phenomena that need to be considered in system-level simulations such as blockages. Also, in 5G, features of millimeter-wave communications such as directionality changes the complexity of location-dependent searches. In fact, search queries are not just in distance but also in azimuth and elevation as well. Therefore, we need an architecture that uses spatial indexing in a HetNet and supports the above features. In the following, we introduce a generic architecture that uses multi-level inheritance and polymorphism to enable indexing a heterogeneous network on a single geometry tree. Then we evaluate the performance of the proposed architecture with respect to traditional array indexing.

It is worth mentioning that acceleration of high-fidelity wireless communication simulations has been investigated through geography-based partitioning for parallel implementation on multiple processors as well [98]. However, parallel computing is not the focus of this work.

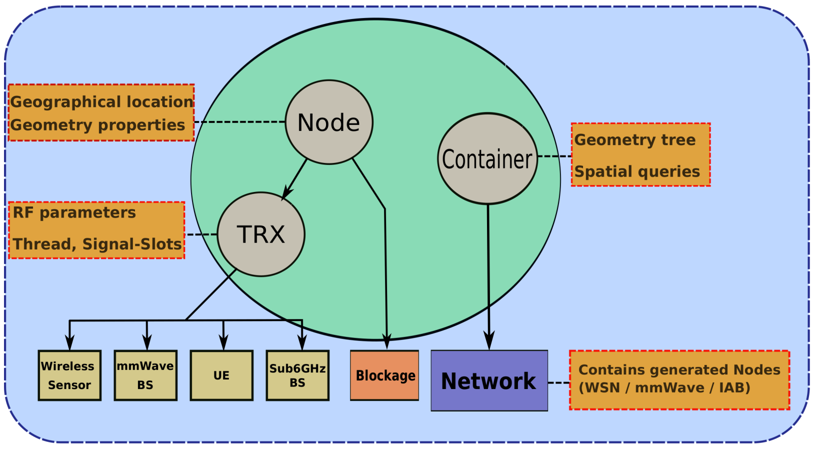

Figure 4.1: The proposed multi-level architecture. Location and geometry properties of elements of the network are abstracted in the *Node* object. The *Container* stores the elements of the network on a geometry tree. From the view of the geometry tree, all elements are the same and represented as polygons. The Network basically represents any wireless network which can be a WSN, mmWave, or an integrated access and backhaul (IAB) network.

4.2 Spatial Indexing and Queries in HetNets

In this section, we first introduce the architecture which enables us to use spatial indexing for a HetNet. Then, the indexing procedure and the defined spatial queries are explained.

4.2.1 Architecture

In order to store heterogeneous nodes on a single geometry tree, nodes of the network need to be represented just by their geometry. In fact, the elements of the network are abstracted as polygons regardless of their higher level nature which can be a UE, BS, or even a blockage. The proposed architecture is shown in Fig. 4.1. All the elements of the network are generated based on inheritance from an object named *Node*. The *Node* object contains location and geometry (length, width, and height) of the elements and is the lowest level in the platform and is stored on the geometry tree. *Node* is inherited by the *TRX* and the *Blockage* objects. The *TRX* object contains related parameters to a transceiver such as the carrier frequency, transmit power, and antenna properties. Also, the *TRX* contains an independent standard thread with signal-slot capabilities. The signal-slot methods are used to implement message-passing and event-based processes such as asynchronous procedures of the network. Wireless sensors, mmWave or Sub6GHz BSs, and UEs can be generated by inheriting from the *TRX*. The blockage objects are generated by directly inheriting from the *Node*. The proposed design consists of a class named *Container* which is used to manage all the created nodes in the simulation. The *Container* holds a geometry tree which indexes all the generated elements and provides the spatial queries over the geometry tree. Since just the Node data is saved on the geometry tree, one single tree can be used for any type of element in the network. The designed architecture and indexing procedure is applicable to any object-oriented language that supports multilevel inheritance. However, the code snippets that we use are based on C++ language.

4.2.2 Indexing a HetNet With single Geometry Tree

In order to use spatial indexing, a proper spatial data structure should be selected. Most of the spatial data structures work based on the principle of space partitioning and storing data on a tree-like structure such as R-tree or K-d tree [99]. K-d tree can only contain points and does not handle adding and removing points. However, in R-tree nodes are represented as polygons. Since, we need to provide dimensions for the nodes of the network as well as dynamic removal of them, we use R-tree [100] for spatial indexing. R-tree is a geometry tree proposed by Guttman as a dynamic indexing structure designed for spatial searching in multi-dimensional datasets. Basi-

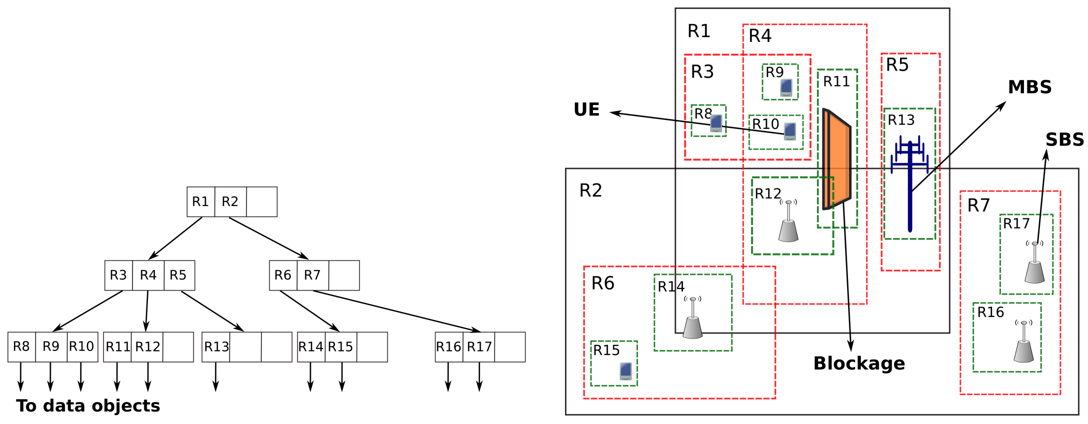

Figure 4.2: Example of a HetNet indexed with a single R-tree with $n = 10$ and $M = 3$. (a) The tree containing different levels of MBRs which partition a network of one macro BS (MBS), four SBSs, four UEs, and one blockage. (b) The rectangles R1 to R17 represent MBRs, the black MBRs (R1, R2) are the roots, the red MBRs (R3-R7) are the second layer, and the green MBRs (R8-R17) are the leaf nodes which contain the data objects of the network. The MBRs R1 and R2 cover total area of the network.

cally, R-tree groups the objects using minimum bounding rectangles (MBR). Objects are added to an MBR within the index that will lead to the smallest increase in its size. R-tree records the indices in its leaf nodes with pointers to the data objects as in Fig. 4.2(a). Data objects refer to the polygons of the elements of the network which is detailed below. Further, by defining M as the maximum number of entries in an element of the tree, the average search complexity of R-tree is $\mathcal{O}(\log_M n)$. A representation of the R-tree and MBRs over a HetNet is illustrated in Fig. 4.2(a) and Fig. 4.2(b), respectively.

According to Fig. 4.2(a), the leaf nodes store data objects related to the elements of the network. The data objects are 2-tuples containing first the location of the element, and second a pointer to the *Node* object of the element. We name the 2-tuple, *value* pairs in the code snippets. We define the following *value* pair as the input of the R-tree.

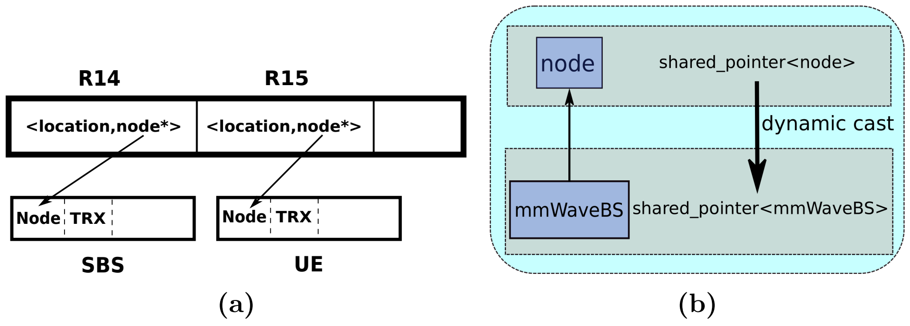

Figure 4.3: (a) The *value* pairs of the R-tree leaves and their relationship with the elements of the network. Each leaf contains location and a pointer which stores the *Node* information of the respective element of the network. Here, R14 contains the location of a SBS and its *Node* data. (b) Retrieving higher levels of an object from a query result.

```
typedef pair<point,shared_ptr<node>>value;
```

According to the above, an element of the network is added to the R-tree based on its location (point variable) and a pointer (shared_ptr) to its *Node* object and the R-tree indexes the elements of the network based on their corresponding locations. Fig. 4.3(a) shows the *value* pairs of MBRs R14 and R15 defined in Fig. 4.2(a). For details of inserting elements to the R-tree see Appendix B.1.

4.2.3 Spatial Queries

A spatial query is a query which considers the spatial relationship between the elements of the network such as relative location-based searching, k-nearest neighbors, and ray tracing. Spatial queries have significant applications in map servers where there are continuous queries over the database based on the location of the objects. Google Maps and Quantum Geographic Information Systems (QGIS) are examples of applications which use spatial queries frequently. Considering the above, any location-dependent search can be defined as a spatial query over the polygons of the elements of the network. For instance, finding fixed-radius neighbors can be defined as a circle-shaped polygon query over the nodes of the network. Therefore, we can represent the association of users to base stations as a spatial query. The same applies to finding the potential interferers in a certain direction which can be stated as a triangular-shaped polygon query. In the following, we describe these queries.

After inserting all the elements (BSs, UEs, blockages) in the R-tree, any element is able to define customized spatial queries over the network. The general format of a spatial query is defined as follows.

```
m_tree.query(Condition, Results)
```

In the above, the *Condition* can be any function defined based on the *point* variables. *Results* is a standard vector containing the *value* pairs of the elements that their locations satisfy the defined *Condition*. Due to the indexing method, any query over the network results in a vector containing pointers to *Node* objects. In order to derive the higher levels of a *Node* object, for example a mmWave BS from the pointer of its *Node*, we use *dynamic_cast* as in Fig. 4.3(b). It is important to note that since we use downcasting to derive classes from the shared pointer of the *Node*, the *Node* class should be polymorphic [83], i.e., *Node* should at least contain one virtual method.

Here, we use spatial queries to define two common location-dependent searches in wireless networks: search for fixed-radius near neighbors and search for interferer BSs residing in the boresight of a receiver. However, any customized query can be defined as well. The two queries are implemented as follows.

(i) Fixed-radius near neighbors: This query is used in association, coordination, and routing problems. The *Condition* for this query is written based on the euclidean distance from the desired point. In fact, any point that is in distance R of the desired point is in a circular polygon with radius R around the desired point. If the MBR of any element of the network intersects with the defined circular polygon, then the

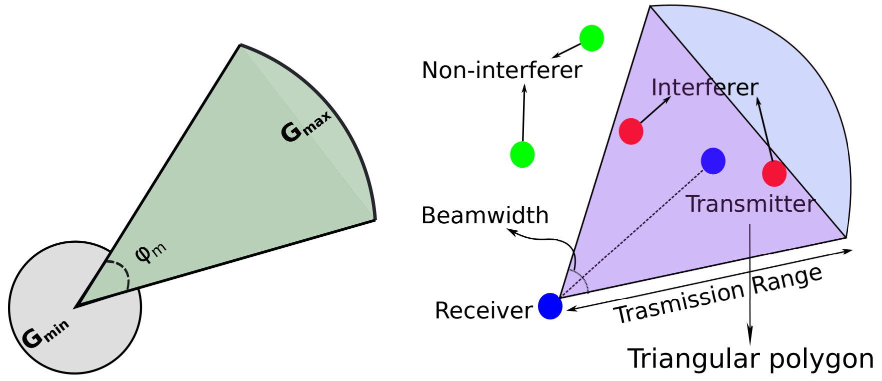

Figure 4.4: (a) Sectored-pattern antenna model with the beamwidth of ϕ_m, main-lobe gain of $G_{\max}$, and side-lobe gain of $G_{\min}$. (b) Polygon estimating the area in which potential interferer BSs reside.

element is in distance R of the desired point (center of the circular polygon). In the following the elements located in the defined distance R of the *desired* point are derived.

```
// Defining the result vector
std::vector<value>results;
// The desired location.
point desired(xx,yy);
m_tree.query(bgi::satisfies([&](value const& v){return bg::distance(v.
    first, sought)<R;}),std::back_inserter(results));
```

(*ii*) Directional interferer neighbors: This query is used for SINR calculation of a directional wireless link. In another terms, search for neighbors in distance and azimuth (or elevation) at the same time. In directional communications, the power received at the receiver depends on the combined antenna gain of the receiver and transmitter. Directional communication is viable with large antenna arrays and using different MIMO transmission techniques such as fully digital, analog or hybrid beamforming. Here, we use the sectored-pattern antenna gain shown in Fig. 4.4(a) which is practically accepted for single stream analog beamforming [16]. In order to accurately calculate the antenna gain at a receiver, we need to figure out if the interfering transmitter is in the main lobe of the receiver or not. We solve this problem with a polygon query. In order to define this query, we define a triangular polygon estimating the area in which the BSs causing interference are located as in Fig. 4.4(b). The nodes residing inside the triangular polygon are in the main lobe of the receiver. After finding the interferer nodes, we can initiate the same query from the interfering nodes to see if the receiver is in their main lobe as well. This query can be implemented as follows.

```
// Defining the result vector.
std::vector<value> results;
// Performing the query to search for any node intersecting with the
    derived polygon.
m_tree.query(bgi::intersects(triangular_polygon), std::back_inserter(
    result));
```

In the above, the *triangular_polygon* is defined for a transmitter-receiver pair based on the direction of transmission, beamwidth, and the maximum transmission range according to Fig. 4.4(b). The neighbors whose MBR intersect with the *triangular_polygon* are returned in the *results* vector. By using *dynamic_cast* the *TRX* related object of the neighbors can be derived. Finally, the interference can be calculated based on the interference model of the network. It is worth mentioning that the polygon query can be used for other purposes such as user association for BSs which have multiple sectors as well.

4.3 Simulation Acceleration with Spatial Indexing

The goal of this section is to compare the performance of spatial indexing versus array indexing in location-dependent searches in large directional wireless networks. The network under study contains mmWave SBSs which are distributed with fixed density of 100 SBS/Km^2. We assume SBSs are equipped with directional antennas. Without loss of generality, we assume all SBSs are on the same horizon plane. Thus, we do not consider beams variations in the elevation and define the antenna gain pattern with widely-adopted sectorized-pattern as [16, 101].

Generally, in cellular communication, the measured signal at a receiver is a combination of the desired signal, the interference, and noise, hence SINR. In mmWave communications, due to narrow beams, the links are sometimes assumed to be interference-free and the SNR metric is used in simulations. Despite the fact that the interference-free assumption is reasonable, the probability of occurrence of interference increases as the density of the network increases [59,102]. Selection of the right metric is important in certain applications such as path selection and routing algorithms. Hence, we assume two scenarios: (i) SNR and (ii) SINR calculation of all potential links between any two pair of SBSs with maximum transmission range of 200 m.

In the following we provide performance time comparison and complexity analysis in both scenarios. Experiments are carried out in C++ with an Intel(R) Core(TM) i5-6300HQ @ 2.30 GHz processor powered by Fedora 31 operating system and Linux kernel 5.4.18.

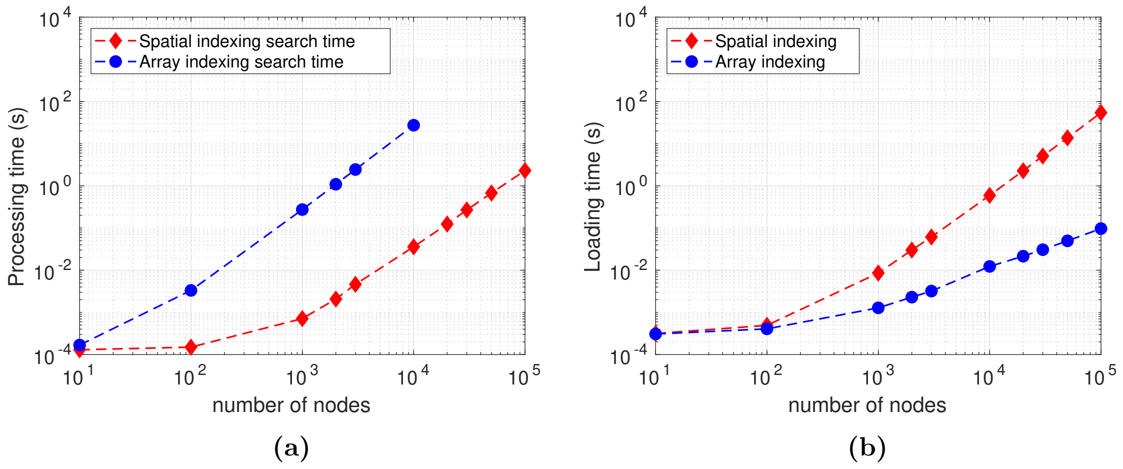

Figure 4.5: (a) Processing times to calculate SNR of all existing links. (b) Loading time to generate and store all nodes.

4.3.1 SNR calculation

In order to calculate the SNR of all potential links between SBSs in a network, we need to measure distance of all pairs of SBSs and calculate SNR of the ones in transmission range of each other. In array indexing, complexity of finding potential links between one SBS and its neighbors is $\mathcal{O}(n)$, which contains measuring the distance between the node and all existing nodes. Hence, the total complexity for all the nodes is $\mathcal{O}(n^2)$. However, with spatial indexing, finding neighbors can simply be implemented with a fixed-radius neighbor query as in 4.2.3 which is a spatial query over the distance. The complexity of one query is $\mathcal{O}(\log n)$ and hence for the whole network is $\mathcal{O}(n \log n)$ on average. In Fig. 4.5(a) the processing time for finding the potential links for calculating SNR of the network is presented. As shown, spatial indexing outperforms array indexing.

It is worth mentioning that, when using spatial indexing, loading the nodes on the R-tree introduces an overhead to the simulation. However, loading time is a *one-time* overhead, however, location-dependent searches are called frequently during

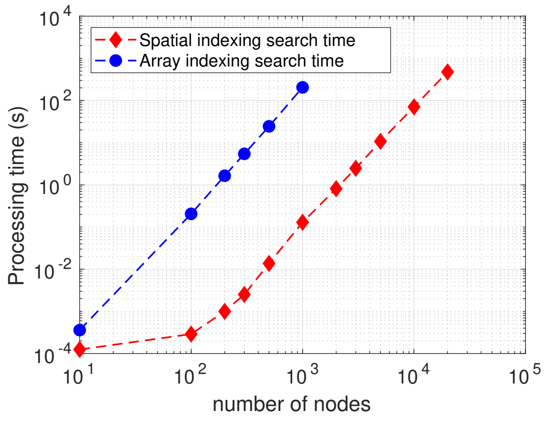

Figure 4.6: Processing time to calculate SINR of all existing links.

a simulation. In Fig. 4.5(b), we have compared the required time of storing nodes on an array and a R-tree with respect to the number of nodes.

4.3.2 SINR calculation

In directional communication, the calculation of SINR for a link contains one additional search compared to SNR calculation. In fact, after finding the potential neighbors, we need to search for interferers for each link. This search is in distance and azimuth according to Fig. 4.4(b). With array indexing, finding directional interferers for each link leads to another search which increases the complexity to $\mathcal{O}(n^2)$. Hence, the computational complexity for the whole network can go up to $\mathcal{O}(n^3)$. On the other hand, spatial indexing provides a systematic approach to accelerate the calculation of SINR. SINR calculation can be simply implemented as a combination of fixed-radius near neighbors query followed by a triangular polygon query over the results of the first query. This systematic approach is one of the advantages of spatial indexing. In Fig. 4.6, the processing time of SINR calculation in large wireless networks with directional communication is plotted. As it is shown in Fig. 4.6, spatial indexing has clear advantage in processing time of searches in distance and azimuth. This advantage can be used to enormously accelerate system-simulation of large systems. For the implementation details see Appendix B.3.

4.4 Conclusion

In this chapter, we propose the use of spatial indexing in system-level evaluation of 5G heterogeneous cellular networks. We introduced an inheritance based polymorphic architecture which enables us to index a wireless heterogeneous network with a single R-tree. This structure enables us to take advantage of spatial queries to accelerate simulation of large-scale directional heterogeneous wireless networks. Researchers can use spatial indexing in their platforms to accelerate system-level simulations enormously. Acceleration can be achieved in any search defined in distance, azimuth or even elevation. Further, due to the ability of considering the blockage, spatial indexing can accelerate system-level simulations which account for the spatial correlation of blocking such as [103, 104]. Another main application of spatial indexing could be generating training data sets of accurate SINR values in millimeter-wave communications for machine learning purposes. Further, spatial indexing can accelerate simulation in multiple applications such SINR evaluations in ad-hoc networks, node deployment [105–107], routing, clustering, implementation of self-organizing networks (SONs) [27], and generating communication graphs. We are currently developing an open-source platform based on the introduced structure in Fig. 4.1 which implements some of the applications of spatial indexing in [108].

Chapter 5

TOPOLOGY MANAGEMENT IN MILLIMETER WAVE WIRELESS BACKHAUL IN 5G CELLULAR NETWORKS

The dynamic and autonomous connections of a mmWave backhaul network is similar as an ad hoc network. In ad hoc networks, the topology of a network is the set of communication links between the nodes that is used by the routing algorithm. According to ad hoc related literature, weeding out redundant and unnecessary topology information is called *topology management*. Topology management plays a key role in performance of routing, scheduling, broadcasting. The wrong topology information can reduce the capacity, increase the end-to-end delay, and decrease the robustness to node failure. As the above factors are important in ad hoc networks, they have the same importance in mmWave backhaul networks as well. In this chapter, we investigate the effect of using signal-to-noise-ratio (SNR) instead of signal-to-interference-plus-noise-ratio (SINR) in topology management of dense mmWave networks. Further, we design a multi-agent reinforcement learning algorithm to achieve k-connecitivty as one of the requirements of fail-safe wireless backhauling in mmWave networks.

5.1 Introduction

Supporting the expected cellular traffic growth via densification is one of the main tasks for the next generation (a.k.a "5G") wireless cellular networks [3]. A key driver for densification in the next 5-10 years will be small base stations (SBSs) operating at millimeter wave (mmWave) frequencies. These SBSs will also support conventional communication below 6 GHz (Sub6GHz) frequencies and possibly use mmWave for the backhauling as well as some UE connections. Small cells construct an underlay of low-power and short-range, indoor and outdoor microcells, femtocells or picocells [109]. New small cells are deployed in public and private infrastructures with the vision of aggressive densification to provide the high speculated rate requirements of 5G networks. Meanwhile, achieving the full potential of densification to improve the spectral efficiency of access links runs into the significant bottleneck of efficient backhauling.

Wired and wireless technologies can be used as backhaul solutions. Wired technologies such as fiber or xDSL have the advantage of high throughput, high reliability, and low latency. However, wired solutions have high expenses and situational impracticality in providing backhaul to a large number of small cells [15]. On the contrary, wireless technology is a potential solution to provide a cost-efficient and scalable backhaul support when wired solution is impractical [16]. Wireless backhaul technologies can operate at Sub6GHz or mmWave bands. Sub6GHz wireless backhaul has the advantage of non-line-of-sight (NLoS) transmission with the disadvantage of co-channel interference and variable delay. In constrast, thanks to huge spectrum, high directional transmission, and low delay of line-of-sight (LoS) links, mmWave communications can be modeled as pseudo-wired communications without interference [18]. Therefore, mmWave communications are suitable candidates for the backhaul of dense small cells.

As mmWave communication is a potential technology for the backhaul of dense small cell networks, its high path loss and susceptibility to blockage needs to be considered in backhaul management (planning) procedures. High path loss results in a limited range of effective communication which is resolved by multi-hop transmissions [110]. Multi-hop transmission increases the reliability of the links while introducing more delay [111]. Severe vulnerability to blockage at mmWave transmission decreases link availability [16]. Link blockage is solely dependent on the placement of transceivers and the context of the environment. Surviving a blocked link can be done via beam switching and finding new unblocked directions between the transceivers. However, due to *channel sparsity* in mmWave communications, the number of strong feasible beam directions between a transmitter and a receiver is mostly on the order of two or three [112]. On the other hand, due to *spatial correlation* of beams, there is good chance of blockage for all beams in case of severe blockage for one of them [113]. Hence, detouring the blockage by using another SBS as a relay is a viable option in wireless backhauling [114].

Therefore, a SBS needs to be aware of all possible links that it can establish to provide its backhaul in case of failure of one of them. Thus, we need an autonomous backhauling algorithm to realize a wireless backhaul which is fast (low latency), reliable (failure resilient), and scalable. We can simplify such definition as a self-organizing wireless backhaul algorithm. In fact, due to unplanned and high density deployment of small cells, self-organizing network (SON) procedures and tools are becoming essential including backhaul managements. SON promises self-configuration, self-optimization, and self-healing procedures for wireless backhaul.

Self-configuration establishes the backhaul links with the appropriate neighboring cells and alignment of transceiver antennas. Self-optimization manages possible interference with neighboring radios. Self-healing features in avoiding possible link failures and contains necessary procedures in case of link failures due to specific propagation features of mmWave communications such as susceptibility to blockage.

The dynamic and autonomous connections of a mmWave backhaul network is similar as ad hoc network. In ad hoc networks, the topology of a network is the set of communication links between the nodes that is used by the routing algorithm. According to ad hoc related literature, weeding out redundant and unnecessary topology information is called *topology management* [115,116]. Topology management plays a key role in performance of routing, scheduling, broadcasting. The wrong topology information can reduce the capacity, increase the end-to-end delay, and decrease the robustness to node failure. As the above factors are important in ad hoc networks, they have the same importance in mmWave backhaul networks as well. This is part of the reason, in recent literature, researchers model mmWave backhaul networks with graph theory and use the same protocols and concepts in ad hoc networks to manage the topology of the network [117]. However, specific propagation characteristics of mmWave communications and 3GPP requirements for mmWave backhaul in 5G NR [118] brings certain features that need to be considered in topology management of mmWave networks. In this chapter, we aim to review and analyze the requirements and possible topologies of mmWave networks.

5.1.1 Related Work

A great deal of research exists in different aspects of wireless backhauling. We can roughly categorize recent works as in wireless backhaul technologies [18, 119], rate and coverage analysis [120–123], optimal node deployment [124, 125], routing and scheduling [126, 127], and management algorithms [117, 128–132]. In [18] heterogeneous backhaul operating on both Sub6GHz and mmWave bands is proposed as a potential solution to backhauling of dense small cells due to their diverse characteristics. Sub6GHz wireless backhaul has the advantage of NLoS transmission with disadvantage of co-existence interference and unpredictable delay. MmWave offers high capacity and reliability in LoS transmissions. The authors in [18] suggest Sub6GHz band for modest length and mmWave as a competitive candidate for short length communications. Meanwhile, the authors in [119] point to high licensing cost of Sub6GHz wireless backhauling compared to the license-exempt nature of 60 GHz from an operator's perspective.

In [120] the advantage of short-hop wireless backhauling is analyzed in terms of the number of antenna requirements for the SBSs and throughput scalability. Sing *et al.* [121] derive rate distribution of a mmWave wireless backhaul network with orthogonal sharing of resources between access and backhaul, and show that the spectral efficiency of mmWave networks increases with density of SBSs. In [122] and [123] integrated access backhaul (IAB) in mmWave communication is analyzed in which access and backhaul share time and bandwidth resources, respectively. More particularly, in [122] static and dynamic, synchronized and unsynchronized time division duplexing (TDD) schemes and in [123] bandwidth sharing based on the backhaul load are analyzed. In both scenarios, the higher achievable rate in dynamic schemes are approved while [123] shows a cell-load beyond which the performance of the IAB scheme starts decreasing.

Authors in [124] and [125] find optimal location of aggregator nodes (ANs), SBSs with fiber-backhaul, to provide wireless backhaul to other SBSs of the network.

In [124] joint problem of minimizing deployment cost while maximizing coverage via ANs is solved with Tabu search. In [125], wireless backhaul support for SBSs in downtown Manhattan is considered. The authors find optimal location for deployment of ANs that can establish LoS mmWave (60 GHz) links to gateways. The required rate is delivered to the SBSs with deployment of two ANs that establish LoS mmWave links to the SBSs in a noise-limited scenario, and six ANs that connect to SBSs via NLoS Sub6GHz links in an interference-limited scenario. [126] and [127] consider the problem of backhaul routing (path selection) in a wireless backhauled mmWave network with already established links. The authors consider latency requirements of the networks and find optimal routes via minimizing defined regret functions in [126] and matching theory in [127].

In management of wireless backhaul, we need to make sure of a topology that is configured cost-effectively, provides the required flow demand, and can restore itself from link failures (self-healing) [128]. Generally, backhaul topology can be one of the ring, tree or mesh topologies. The authors in [129] provide an analytical study of the advantages of the mesh over tree and ring topologies in multiple aspects. They characterize their problem with minimizing installation cost of wireless backhaul links under traffic flow constraints and show that: (i) mesh topology can accommodate higher traffic demands than tree and ring topology, (ii) mesh topology has higher value for maximum feasible traffic fluctuations. Hence, mesh topology is of common interest as the topology of wireless backhauls. As in terms of self-healing, in the current cellular network and their predecessors, restorability is achieved with adding backup links to the mesh of the network [130]. Authors in [117] and [131] follow the same approach and design central organizing algorithms that add backup/redundant links to achieve restorability and minimize packet loss in case of link failures. The work in [131] considers a mmWave wireless backhaul network in which each SBS's antenna array is able to rotate mechanically. The work proposes a central software defined solution to reconfigure the antennas' alignment when the topology of the network changes due to addition or reduction of SBSs or change of flow demand. The work in [117] proposes a central solution to select some of the SBSs as cluster heads to design a two-layer hierarchical mesh topology between the SBSs. Meanwhile, by adding redundant paths for each non-cluster head SBS, they make sure of robustness against blockage or link failures. The work in [132] focuses on the same idea of selecting cluster heads, and provides a heuristic search algorithm to find a trade-off between faster backhaul links or more cluster heads. However, their architecture does not provide link failure restoration.

5.1.2 Contributions

The contributions of this chapter are two-folds.

1. We focus on the effect of selecting signal-to-noise-ratio (SNR) vs signal-to-interference-plus-noise-ratio (SINR) as mmWave link quality performance in dense mmWave networks. In fact, in directional communications, the links are sometimes assumed to be interference-free, and the SNR metric is used in simulations. Here, we show that despite the fact that in directional communications, the interference-free assumption is reasonable, however, in cases of occurrence of interference, SNR is not a valid metric and SINR should be considered to make a correct decision.

2. We design a self-organizing algorithm to achieve k-connectivity in a backhaul network. As we mentioned before, redundancy in a backhaul network is one of

the requirements of a fail-safe topology, and connectivity is a key performance factor in topology management. Hence, we use reinforcement learning, Q-learning in specific, to design a transmission range control algorithm to achieve k-connectivity in a backhaul network.

The chapter is organized as follows. In Section 5.2, the system model is presented. Section. 5.3 introduces distributed path selection policies and the effect of using SNR instead of SINR on the resulted topology of the network. Section 5.4, introduced the designed transmission range control algorithm. Finally, Section 5.5 concludes the chapter.

Notation: Lowercase, boldface lowercase, boldface uppercase, and calligraphic symbols represent scalars, vectors, matrices, and sets, respectively.

5.2 System Model

We consider a multi-cell heterogeneous network (HetNet) where multiple macrocells are overlaid with a set of SBSs, $\mathcal{S}$. SBSs are distributed with density $\lambda_s = 100$ SBSs/km^2 on $\mathbb{R}^2$. The location of SBSs are derived according to a Poisson point process (PPP) denoted by Φ_s, however, the derived conclusions in this chapter can be considered for any network generation method. Fig. 5.1 shows the locations of MBSs and SBSs. The network contains 66 wireless SBSs and 6 fixed wired BSs (MBSs). In the following, the antenna, path loss, and interference models are detailed. Further, the value of the system model parameters are presented in TABLE. 5.1.

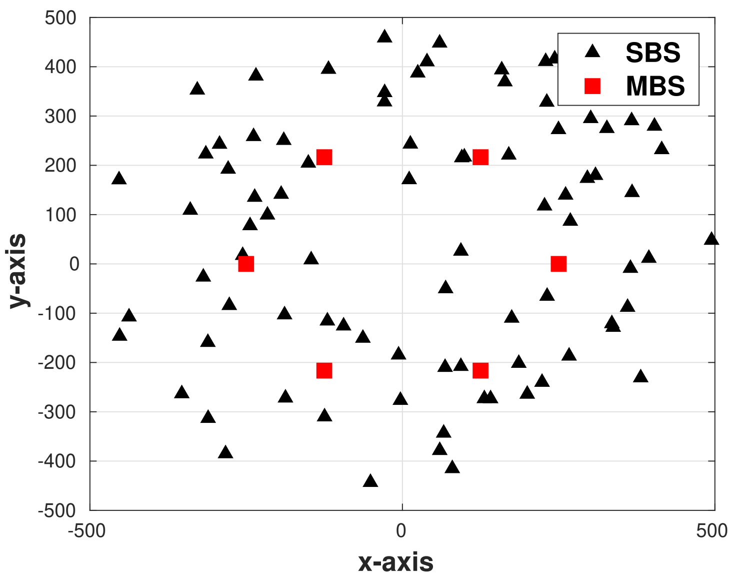

Figure 5.1: Deployment models of mmWave base stations with density of 100 SBS/km^2. MBSs are connected to the core network with a wired backhaul. SBSs use wireless backhauling to reach one of the MBSs. PPP distribution for SBSs and fixed locations for MBSs.

5.2.1 Antenna Model

We assume transmitters and receivers are equipped with directional antennas. Without loss of generality, we assume all BSs are on the same horizon plane. Thus, we do not consider beams variations in the elevation angle θ and define the antenna gain pattern with widely-adopted sectorized-pattern as [16, 101]

$$G(\phi) = \begin{cases} G_{max}, & \text{if } \phi \leq |\phi_m| \\ G_{min}, & \text{otherwise,} \end{cases} \tag{5.1}$$

where, ϕ and ϕ_m denote azimuth angle and antenna main lobe beamwidth, respectively. G_{max} and G_{min} denote the antenna gains at main lobe and side lobes, respectively.

Table 5.1: Notation, Simulation Parameters

Notation	**Parameter**	**Value**
λ_s	SBS density	100 km^{-2}
B	mmWave bandwidth	400 MHz
P_t	mmWave transmit power	30 dBm
f	mmWave carrier frequency	28 GHz
ζ	standard deviation of path loss	LOS = 7.6, NLOS = 7.9
α	path loss exponent	LOS=2.0, NLOS=3.5
β	path loss at 1 m	70 dB
G_{max}	main lobe gain	18 dB
G_{min}	side lob gain	-2 dB
ϕ_m	beam-width	$10°$
NF	Noise Figure	10 dB
σ_N^2	noise power	-174 dBm/Hz+$10\log_{10}(B)$+NF
—	Area of the simulation	1km^2
—	Minimum distance between SBSs	10 m
—	Maximum mmWave transmission range	200 m

5.2.2 Path Loss

The received power at $\mathbf{y} \in \mathbb{R}^2$ from a transmitter at $\mathbf{x} \in \mathbb{R}^2$ with power $p(\mathbf{x})$ is given by $p(\mathbf{x})\,\psi(\mathbf{x},\mathbf{y})\,L(\mathbf{x},\mathbf{y})^{-1}$, where $\psi(\mathbf{x},\mathbf{y})$ is the overall beamforming gain. $L(\mathbf{x},\mathbf{y}) = \beta + 10\alpha\log(\|\mathbf{x}-\mathbf{y}\|) + \chi$ is the associated path loss, where $\chi \sim \mathcal{N}(0,\zeta^2)$. The parameters β, α, and ζ^2 represent the path loss at 1 meter distance, the path loss exponent, and the variance of the shadowing, respectively. For mmWave communications, motivated by the model of [121], we accommodate different path loss parameters for LoS and NLoS links in mmWave band. We assume small-scale fading as Nakagami fading with the shape factor parameter as 2 and 3 for LoS and NLoS links, respectively.

5.2.3 Interference Model

The SINR of the link between the transmitter i and receiver j is calculated as follows Due to directional communication, a few transmitters affect the desired receiver [133]. Considering this fact, the setting for interference is as follows. Assume, small BSs (SBSs) communication over backhaul links. In each time-slot, there are N_T SBSs transmitting. Hence, there are $N_T - 1$ interfering transmitters and I_j number of them are in the interference area of the desired receiver j (SBS$_j$). Therefore, the received SINR of a link from the SBS i (SBS$_i$) to the SBS$_j$ can be expressed as

$$\mathrm{SINR}_{ij} = \frac{H_{ij} G_i G_j L^{-1}(d_{ij})}{N_0/P_t + \sum_{k=1}^{I_j} H_{kj} G_k G_j L^{-1}(d_{kj})}, \tag{5.2}$$

where the received signal and the interference power are normalized by the transmission power P_t. $H_{ij} = |h_{ij}|^2$ is the small-scale fading power of the channel between the SBS$_i$ and the SBS$_j$. d_{ij} is the distance between the two SBSs and N_0 is the thermal noise power. The set $\mathcal{I}_j$ is the interfering nodes active at the same time-slot as the transmitter-receiver i and j. The value of the G_k , $k \in \mathcal{I}_j$, is set by a Bernoulli random variable in such a way that by probability $p = \frac{\phi_m}{2\pi}$, $G_j = G_{\max}$ and otherwise, $G_j = G_{\min}$. By considering the allocated bandwidth between the SBS$_i$ and the SBS$_j$ as B_{ij}, the instantaneous achievable rate for the link is $r_{ij} = B_{ij} \log(1 + \mathrm{SINR}_{ij})$.

5.3 Distributed Path Selection

In reality, the measured signal at a receiver is a combination of the desired signal, the interference, and noise, hence SINR. However, in directional communications, the links are sometimes assumed to be interference-free, and the SNR metric is used in

Table 5.2: Path selection policies for wireless mmWave backhauling.

Policy	**Metric**	**Selection Rule**
High SNR First	SNR	Select the link with the highest SNR.
Wired First	position and SNR	Select a wired BS if possible otherwise use High SNR first.
Position Aware	position and SNR	Select a link with the highest SNR among those links with parent BSs closer to a MBS.
High SINR First	SINR	Select the link with the highest SINR.

simulations. Here, we show that despite the fact that in directional communications, the interference-free assumption is reasonable, however, in cases of occurrence of interference, SNR is not a valid metric and SINR should be considered to make a correct decision. In this regard, first, we implement four path selection policies for wireless backhaul routing as in Table. 5.2. Second, we show the performance effect of selecting SNR and SINR as decision metrics.

5.3.1 Path selection policies

We use four policies for path selection as in Table. 5.2. The *High SNR First*, the *Wired First*, and the *Position Aware* policies are suggested in [134] and [135]. These three policies are defined based on metrics of position and link SNR. To see the effect of decision making based on SINR, we define one more policy named *High SINR First* which uses the SINR as its metric. The selection rule under each policy is defined in Table. 5.2.

5.3.2 Effect of selecting SNR vs SINR as mmWave link quality metric

In order to evaluate the performance of the defined path selection policies, two performance metrics are discussed: (i) required number of hops for a SBS to reach an

MBS, and (*ii*) quality of bottleneck links. These two metrics are discussed below. The location of SBSs and MBSs in Fig. 5.1 are loaded for all simulations. The simulations are implemented using our proposed platform in Chapter 4.

Required number of hops to reach an MBS

For each policy, we evaluate the number of hops that SBSs take to reach a wired BS (MBS). The plot in Fig. 5.2(a) shows the fraction of connected SBSs with respect to the number of hops. Further, the final selected paths for all four policies are visualized in Fig. 5.2 as well. According to Fig. 5.2(a), the two policies relying on just the quality of the link (SNR, SINR) fail to connect all SBSs by increasing the number of hops. In fact, in both cases there are SBSs which fail to reach any wired BS. We see this also in Fig. 5.2(b) and Fig. 5.2(c). On the other hand, in the two policies which use the position of wired BSs, SBSs reach to a wired BS with a maximum of five hops for 90% of the times. The Position aware policy performs slightly better than the Wired first policy in Fig. 5.2(a). Further, the wired first policy results in a star-shape topology as in Fig. 5.2(d). Hence, awareness of the positions of wired BSs enhances the chance of reaching to the wired BSs.

On the comparison of choosing SINR instead of SNR, we can look at the different paths selected by SBSs in Fig. 5.2(b) and Fig. 5.2(c). As shown, choosing SINR metric in the simulations results in different routes which are potentially closer to the reality of the network.

Quality of the bottleneck links

The bottleneck link is defined as the weakest selected link from the selected paths in the network [135], and its quality can be a performance measure for a path selection

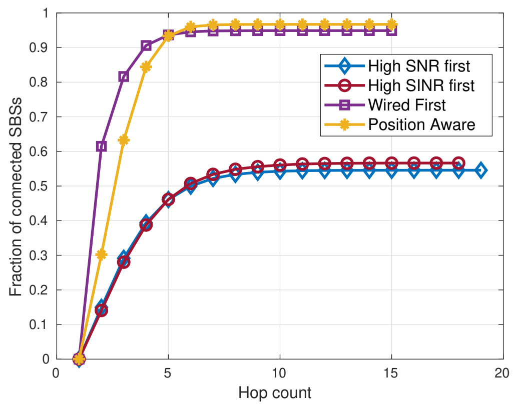

(a) Number of hops to reach an MBS.

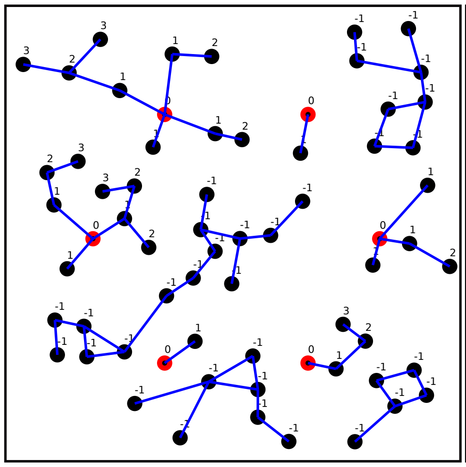

(b) High SNR First.

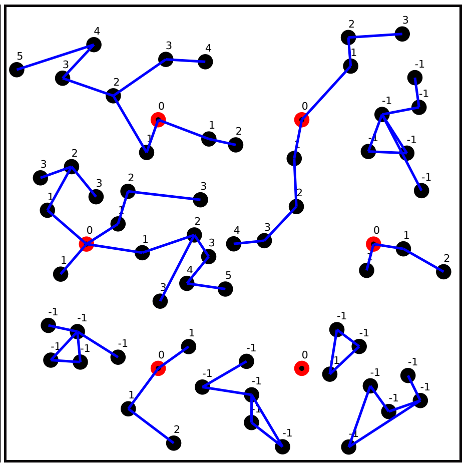

(c) High SINR First.

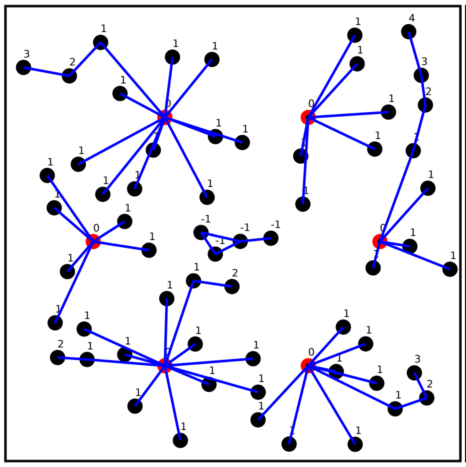

(d) Wired First.

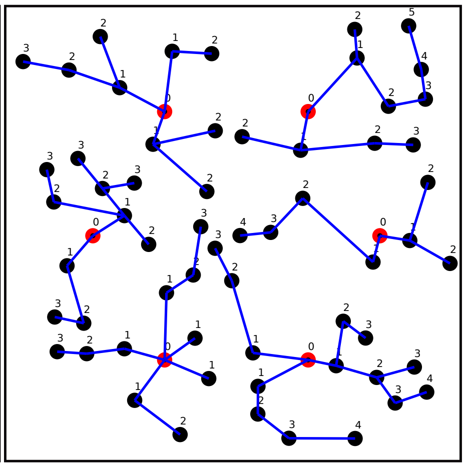

(e) Position Aware.

Figure 5.2: The selected paths by following each of the four policies. The red nodes represent the wired BS, black nodes represent the wireless SBSs. The number on each BS shows the number of hops it takes to reach to a wired BS. This number is zero for a wired BS and -1 for the ones with no route to a wired BS.

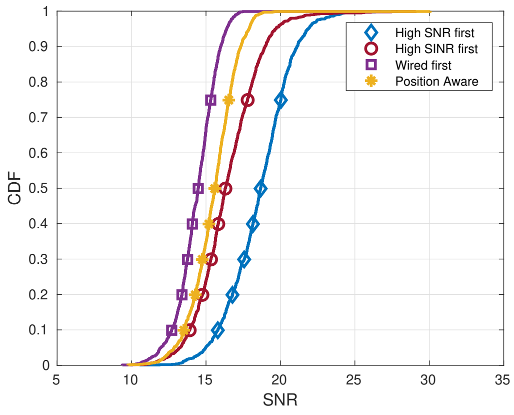

(a) CDF of SNR of the bottleneck link.

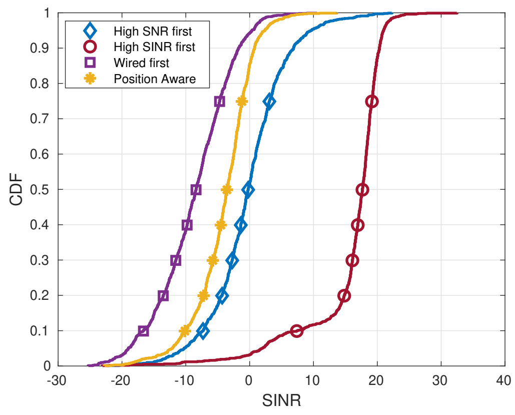

(b) CDF of SINR of the bottleneck link.

Figure 5.3: Empirical CDF over 1000 number of iterations for a fixed topology and 6 number of wired BSs.

policy. The CDF of the bottleneck link's SNR and SINR under the defined policies are plotted in Fig. 5.3(a) and Fig. 5.3(b), respectively. The relative trend of the High SNR first, Wired first, and Position aware policies are the same in both figures. In fact, position aware methods (*Wired First* an *Position Aware*) gain higher performance compared to HQF1. However, the actual quality of the link, i.e., its SINR, is much different than the SNR. Furthermore, the SINR of the bottleneck link under the HQF2 policy has a different trend. This is the result of different decisions under the SINR metric. Therefore, considering SINR as the metric becomes essential in dense networks [59, 102, 136].

Computation wise, calculation of directional interference is much higher than an interference-free scenario, and this is one of the advantages of the proposed platform in Chapter 4 which provides a systematic approach to accelerate the calculation of SINR in highly dense environments. It is important to mention that, it takes about just 12 seconds to provide the 1000 iterations of the above simulations. Each iteration involves neighborhood search and calculation of directional interference for each of the BSs. This is important, since in similar work [134], the CDF of bottleneck link quality is plotted in steps which implies low number of iterations for the simulations due to high computational complexity.

5.4 K-Connectivity with Multi-Agent Reinforcement Learning

In this section, we focus on designing a self-organizing algorithm for SBSs to achieve k-connectivity in a backhaul network. As we mentioned before, redundancy in a backhaul network is one of the requirements of a fail-safe topology. Each SBS needs to hold a certain number of connections to its neighbors to ensure successful transmission of its backhaul data to the core network. We define the degree of a SBS as the number of connections it can establish with its neighbors. In a network of size n, if the degree of a node is on the order of $\log(n)$, the network is connected with high probability [137]. Transmission range control is one of the methods of achieving different connectivity degrees for a node. In fact, with increasing the transmission range (with transmit power control), the node can increase number of its neighbors and hence increase potential connections.

In this section, the range control is presented as a RL problem in which each SBS is an agent which controls its transmission range to achieve a certain connectivity level. Hence, achieving the desired degree with limited transmission power is essential. In the following, we use reinforcement learning, Q-learning in specific, to achieve node degree of k for all SBSs.

5.4.1 Q-learning for range control

In order to use Q-learning, the following definitions are used in our method.

- Agent: each node (SBS) is considered as an agent in the network. The goal of each agent is to learn the minimum transmission range to achieve k as its node degree.

- Environment: The whole network is the environment of the Q-learning. The environment contains all the nodes as its agents. From each node's view, the combination of all other nodes constitutes the environment.

- State set: The state set of each node is defined as the set of degrees that it can hold with its neighbors. Here, we assume a set, $\mathcal{S} = \{0, 1, 2, ..., k_{\max}\}$, as the state set for all the nodes. The goal state for each node is the state $k \in \mathcal{S}$.

- Action set: Each node has a limited transmission range, $R_{\max}$. Each agent selects its transmission range according to a set of actions, $\mathcal{A} = \{\Delta r, 2\Delta r, ..., R_{\max}\}$, $\Delta r = \frac{R_{\max}}{|\mathcal{A}|}$.

- Reward function: The design of the reward function depends on the goal of each agent. Here, the goal of the agent is to reach the state $k \in \mathcal{S}$, i.e., select a minimum transmission range to reach to k neighbors. If a node selects an action a and reaches the state $s \in \mathcal{S}$, the defined reward function is as follows

$$r\left(s, a\right) = e^{-(s-k)^2}. \tag{5.3}$$

The agents act independently. This means each node considers any other node in its transmission range as its potential neighbor. This is due to the definition of topology management in which an algorithm is designed to find potential links for communication. Meanwhile, scheduling the links is the responsibility of scheduler. In the training process, each agent selects a communication range in its current state based on ϵ-greedy policy, transmits a message to find the number of its neighbors in the selected range, and updates the corresponding value of the state-action set in its Q-function according to the temporal-difference method as follows

$$Q\left(s,a\right) \leftarrow Q\left(s,a\right) + \alpha \left(\underbrace{\gamma \max_{a'} Q\left(s',a'\right) + r - Q\left(s,a\right)}_{\text{temporal-difference}} \right), \tag{5.4}$$

in which, s, a, s' represent the current state, the selected action, and the new state, respectively. Also, α and γ are the learning rate and the discount factor. Each agent runs the Q-learning algorithm for L episodes to train its Q-function.

After the training, each agent runs Algorithm 1 to select its neighbors. In Algorithm 1, the goal state, i.e., k, can be selected to configure different connectivity levels for the network. The higher the k, the higher connectivity level is derived for the network. However, the SBSs need to track more links and use more power to increase their transmission range. Hence, the overhead and consumed energy of the network increases as well.

5.4.2 Resulted topology

In order to visualize the resulted topology of the designed algorithm above, a network is generated with the same approach as in Section 5.2 with loading a predefined network. The simulation parameters are presented in Table. 5.3.

Implementation of a MARL algorithm on such a large network is not conventional.

Algorithm 1 Transmission Range Control

```
1: Initialize: $a = R_{\max}$, rounds $= 0$
2: Find the initial state $s$
3: while rounds $> 0$ do
4:     $a = \arg\max_{a'} Q\left(s, a'\right)$
5:     Broadcast a message with $a$
6:     Receive message from others and calculate number of neighbors
7:     Calculate the new state $s'$
8:     if $s' == k$ then
9:         break
10:    else
11:        Update Q-function
12:    end if
13:    rounds $\leftarrow$ rounds $- 1$
14: end while
```

Table 5.3: Simulation Parameters

Parameters	**Value**
Density of nodes	100 km^{-2}
Maximum communication range ($R_{\max}$)	200 m
Goal state (k)	3
Learning rate (α)	0.2
Discount factor (γ)	0.99
ϵ	0.2
Rounds	10

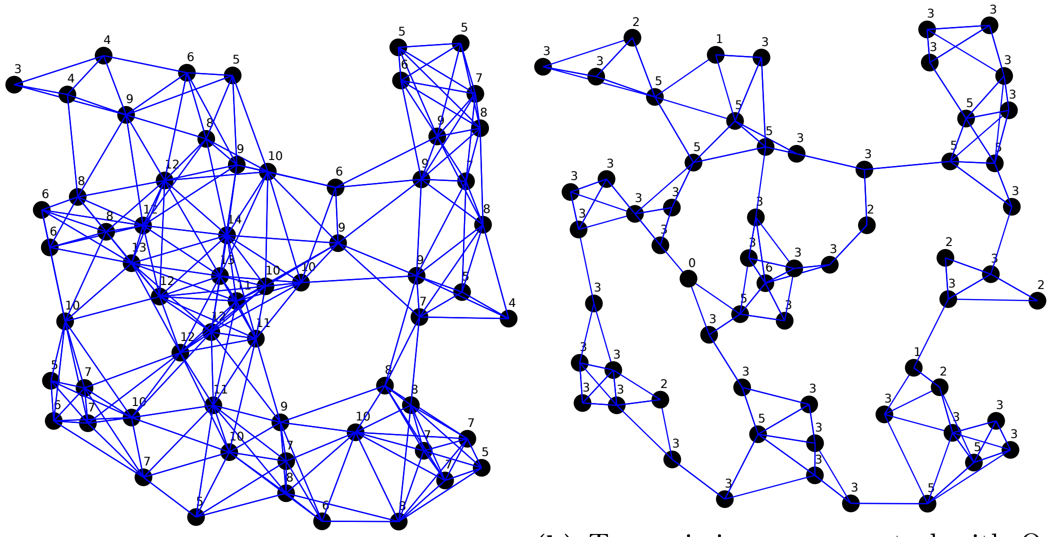

(a) Maximum transmission range.

(b) Transmission range control with Q-learning.

Figure 5.4: Topology of the network. The number on each node represents its degree.

We took advantage of our designed platform in Chapter 4 to integrate RL procedures in each SBS node. Reinforcement learning procedures are implemented with the help of the open-source template-based C++ RLLib [138]. The RLLib template-based classes fit mathematics of RL with the implementations. Further, we illustrate how to implement multi-agent RL training procedure in parallel (asynchronous training) in Appendix C.1. The scalability of the asynchronous multi-agent RL algorithm is investigated in Appendix C.1 as well.

The generated network is shown in Fig. 5.4(a). The degree of each node in Fig. 5.4(a) is the result of using the maximum transmission range. This is the first topology of the network before running the Algorithm 1. The topology of the network after the training and running Algorithm 1 is presented in Fig. 5.4(b).

5.5 Conclusion

In this chapter, we focused on topology management in mmWave backhaul networks. First, we defined distributed path selection policies and illustrated that the effect of using SINR instead of SNR as a metric for mmWave link quality is a necessity in dense networks. We investigated the importance of proper mmWave link quality metric with visualization of the resulted network topologies and CDF of bottleneck links. Second, we focused on k-connectivity of backhaul networks and designed a self-organizing algorithm to achieve k-connectivity via multi-agent reinforcement learning. We used our designed platform in Chapter 4 to implement the designed topology management algorithms. Further, the resulted topologies are visualized as well.

Chapter 6

CONCLUSION

The presented dissertation is an effort to realize, develop, and investigate potential solutions and tools for data-driven decision making in self-organizing networks (SONs) more specifically in cellular networks. We develop an reinforcement learning based framework and develop multiple learning algorithms for transmit power control in heterogeneous networks (HetNets). Generally, training machine learning applications needs large amount of data measurements and there is a need in the communication community of standard data sets such as MNIST [139] in image processing field. Hence, we developed an open-source platform for simulation of large 5G cellular HetNets based on spatial indexing. The platform is able to produce large amount of accurate signal signal-to-interference-plus-noise-ratio (SINR) values in short amount of time. Finally, we take advantage of the developed platform and study topology management of dense millimeter wave (mmWave) backhaul networks. In the following the major contributions of the dissertation are detailed, and possible future directions are presented.

6.1 Summary

- Chapter 2: In this chapter, we focus on realization of self-organizing networks (SONs) with reinforcement learning (RL). We look into transmit power control in a dense heterogeneous network (HetNet) and rely on local SINR measurements to make decisions. We design a general framework for reinforcement learning applications. The proposed framework models a multi-agent network with a single Markov decision process (MDP) that contains the joint action of the all the agents as its action set. Then, we make two main assumption to factorize the global MDP into local ones: (*i*) total reward is linear combination each agents reward, and (*ii*) the transition probability of each agent's MDP depends just on its action. With these two assumptions, we define local independent and cooperative learning (IL, and CL) methods for decision making. Further, we propose a systematic approach to define a reward function that maximizes the summation of achievable transmission rate of the network while satisfying minimum requirements for all agents. Finally, we derive a minimum bound on the sample complexity of the proposed learning methods to achieve ϵ-optimality. The numerical results of this chapter illustrate the performance of different learning configurations and reward functions. This chapter plays a key role in the dissertation as the reinforcement learning framework is used in other chapters as well.

- Chapter 3: In this chapter, we focus on transmit power control in an interference-limited network of small base stations (SBSs). First, we define a global Q-function relating to the whole network. Then, in order to factorize the global Q-function, we feed the interference model of the network to the factorization process. In fact, we investigate the effect of accurate MDP factorization on the optimality of the solution. To di this, we assume each SBS receives most of its interference from one neighbor. Hence, its transition probability function depends on its action and the neighbor. With this assumption, we factorize the global Q-function and use the variable elimination (VE) method to find joint actions in the network. The agents use message-passing for passing conditional solutions to each other. In the simulation section, we illustrate the optimality of the proposed solution for a 2 by 2 transmit-receiver case.

- Chapter 4: In this chapter, we design a new architecture for system-level simulations of large 5G networks. We had two motivations for developing a new simulation platform: (*i*) we needed to design topology management algorithms for large directional networks, and ((*ii*)) we needed a fast simulator to be able to run reinforcement learning algorithms. However, the existing simulators did not provide us with one. Hence, we looked back to the idea of spatial indexing and its advantages, applications, and future potentials in accelerating large 5G network simulations. We introduce a multi-level inheritance based architecture which is used to index all elements of a HetNet on a single geometry tree. Then, we define spatial queries to accelerate searches in distance, azimuth, and elevation. The platform can be used to evaluate and design algorithms related to network issues such as scheduling, mobility management, interference management, and cell planning. Further, the proposed design is implemented as an open source platform freely available to all.

- Chapter 5: In this chapter, we focus on topology management of mmWave backhaul networks. First, we investigate the effect of using signal-to-noise-ratio (SNR) instead of SINR in topology management of dense mmWave networks. In mmWave communications, due to narrow beams, the links are sometimes assumed to be interference-free and the SNR metric is used in simulations. Despite the fact that the interference-free assumption is reasonable, the probability of occurrence of interference increases as the density of the network increases. We investigate the effect of using SNR and SINR on final derived topology of a mmWave backhaul network. Further, we design a multi-agent reinforcement learning algorithm to achieve k-connecitivty as one of the requirements of fail-safe wireless backhauling in mmWave networks.

6.2 Future Research Direction

6.2.1 Deep reinforcement learning for large state sets

As we discussed in simulation section of Chapter 2, there is a performance gap between the proposed approach and the exhaustive search. In fact, we wish to improve and cover this gap by utilizing deep neural networks (DNNs) as the function approximator of the learning method. Neural networks can handle the large state-action spaces more efficiently. Hence, by increasing the state set size we would like to decrease the gap between the RL and the exhaustive search solutions.

6.2.2 Mean-field reinforcement learning in large networks

One of our future works is to extend the proposed message-passing based solution in Chapter 3 to multi transmit-receiver pairs such as [140]. However, the overhead of message passing between the agents would be enormous. Further more, the assumption of one major interferer for each agent might not hold all the times in cellular networks. We propose to use mean-field reinforcement learning [141], to factorize the global Q-function. In fact the transition probability of each agent would depend on its own action and an action which is the average of other agents in the environment. Therefore, we might be able to apply the idea of VE and message-passing in large networks as well.

6.2.3 Spatial correlation of blocking in HetNets

One of the features of the proposed platform in Chapter 4, is ability to introduce blocking in the simulation environment. We believe spatial indexing can accelerate system-level simulations which account for the spatial correlation of blocking as well. Developing an application based on the core of the platform for such studies can be a potential direction for extending the platform.

6.2.4 Graph embedding in topology management

We are currently working on the applications of graph embedding methods in topology management of wireless networks. Topology management can be seen as an algorithm which searches over possible graphs of the network to find one that satisfies all the requirements. Designing an algorithm for search over a graph can be challenging. We wish to overcome this difficulty by using graph embedding methods. In fact, we would like to embed the graph of the wireless network into a fixed-dimensional vector space. This approach helps to search in a vector space in efficient time. Further, the designed machine learning algorithms can become independent of the size of the graphs as well.

Bibliography

[1] SNS.Telecom&IT, "SON (self-organizing networks) in the 5G Era: 2019-2030- opportunities, challenges, strategies forecasts," Tech. Rep., Sep 2018.

[2] R. S. Sutton and A. G. Barto, *Introduction to Reinforcement Learning*, 1st ed. Cambridge, MA, USA: MIT Press, 1998.

[3] J. G. Andrews, S. Buzzi, W. Choi, S. V. Hanly, A. Lozano, A. C. K. Soong, and J. C. Zhang, "What will 5G be?" *IEEE J. Select. Areas Commun.*, vol. 32, no. 6, pp. 1065–1082, Jun. 2014.

[4] R. W. Heath, N. Gonzalez-Prelcic, S. Rangan, W. Roh, and A. M. Sayeed, "An overview of signal processing techniques for millimeter wave MIMO systems," vol. 10, no. 3, pp. 436–453, Apr. 2016.

[5] L. Jiang and H. Jafarkhani, "Multi-user analog beamforming in millimeter wave MIMO systems based on path angle information," *IEEE Trans. Wireless Commun.*, vol. 18, no. 1, pp. 608–619, Jan. 2019.

[6] O. El Ayach, S. Rajagopal, S. Abu-Surra, Z. Pi, and R. W. Heath, "Spatially sparse precoding in millimeter wave MIMO systems," *IEEE Trans. Wireless Commun.*, vol. 13, no. 3, pp. 1499–1513, Mar. 2014.

[7] J. Brady, N. Behdad, and A. M. Sayeed, "Beamspace MIMO for millimeter-wave communications: System architecture, modeling, analysis, and measurements," *IEEE Trans. Antennas Propagat.*, vol. 61, no. 7, pp. 3814–3827, July 2013.

[8] B. He and H. Jafarkhani, "Low-complexity reconfigurable MIMO for millimeter wave communications," *IEEE Trans. Commun.*, vol. 66, no. 11, pp. 5278–5291, Nov. 2018.

[9] M. A. Almasi, R. Amiri, H. Jafarkhani, and H. Mehrpouyan, "Mmwave lens-based MIMO system for suppressing small-scale fading and shadowing," *IEEE Trans. Wireless Commun.*, 2020.

[10] M. A. Almasi, R. Amiri, and H. Mehrpouyan, "A new millimeter wave MIMO system for 5G networks," *arXiv preprint arXiv:1807.04851*, 2018.

[11] M. A. Almasi, R. Amiri, M. Vaezi, and H. Mehrpouyan, "Lens-based millimeter wave reconfigurable antenna NOMA," *in Proc. IEEE ICC Workshops*, pp. 1–5, May 2019.

[12] S. Shad, S. Kausar, and H. Mehrpouyan, "Waveguide-fed lens based beam-steering antenna for 5G wireless communications," *in Proc. IEEE Intern. Symp. on Antennas and Propagation*, pp. 1149–1150, Jul 2019.

[13] S. Kausar, S. Shad, A. Kausar, and H. Mehrpouyan, "Design of high gain low cost beam-steering reflectarray antenna," *in Proc. IEEE Intern. Symp. on Antennas and Propagation*, pp. 315–316, Jul 2019.

[14] ——, "Design of high gain single layer reflectarray antenna using ring and double square elements," *in Proc. IEEE Intern. Symp. on Antennas and Propagation*, pp. 293–294, Jul 2019.

[15] Y. Li, E. Pateromichelakis, N. Vucic, J. Luo, W. Xu, and G. Caire, "Radio resource management considerations for 5G millimeter wave backhaul and access networks," *IEEE Commun. Mag.*, vol. 55, no. 6, pp. 86–92, Jun. 2017.

[16] J. G. Andrews, T. Bai, M. N. Kulkarni, A. Alkhateeb, A. K. Gupta, and R. W. Heath, "Modeling and analyzing millimeter wave cellular systems," *IEEE Trans. Commun.*, vol. 65, no. 1, pp. 403–430, Jan 2017.

[17] M. Gupta, A. Rao, E. Visotsky, M. Cudak, A. Ghosh, and J. G. Andrews, "Learning-based delay optimization for self-backhauled millimeter wave cellular networks," *in Proc. Asilomar Conf. on Signals, Systems and Computers*, pp. 1–5, Nov. 2019.

[18] G. Zhang, T. Q. S. Quek, M. Kountouris, A. Huang, and H. Shan, "Fundamentals of heterogeneous backhaul design–analysis and optimization," *IEEE Trans. Commun.*, vol. 64, no. 2, pp. 876–889, Feb 2016.

[19] S. Haykin, "Cognitive radio: brain-empowered wireless communications," *IEEE J. Select. Areas Commun.*, vol. 23, no. 2, pp. 201–220, Feb 2005.

[20] E. Yanmaz, O. K. Tonguz, and S. Dixit, "Self-organization in cellular wireless networks via fixed relay nodes," *in Proc. IEEE Globecom*, pp. 1–5, Nov 2006.

[21] W. Elmenreich and H. de Meer, "Self-organizing networked systems for technical applications: A discussion on open issues," *Self-Organizing Systems, Springer Berlin Heidelberg*, pp. 1–9, 2008.

[22] 3GPP, "Study on the Self-Organizing Networks for 5G networks," 3rd Generation Partnership Project (3GPP), Technical Specification (TS) 28.861, Dec 2019, version 16.0.0.

[23] O. G. Aliu, "Resource allocation in self organising cellular networks," Ph.D. dissertation, University of Surrey, UK, 2012.

[24] J. Schulman, "Optimizing expectations: From deep reinforcement learning to stochastic computation graphs," Ph.D. dissertation, EECS Department, University of California, Berkeley, Dec 2016. [Online]. Available: http://www2.eecs.berkeley.edu/Pubs/TechRpts/2016/EECS-2016-217.html

[25] C. J. C. H. Watkins and P. Dayan, "Q-learning," *Machine Learning*, vol. 8, no. 3, pp. 279–292, May 1992.

[26] R. Amiri, H. Mehrpouyan, L. Fridman, R. K. Mallik, A. Nallanathan, and D. Matolak, "A machine learning approach for power allocation in HetNets considering QoS," *in Proc. IEEE ICC*, pp. 1–7, May 2018.

[27] R. Amiri, M. A. Almasi, J. G. Andrews, and H. Mehrpouyan, "Reinforcement learning for self organization and power control of two-tier heterogeneous networks," *IEEE Trans. Wireless Commun.*, vol. 18, no. 8, pp. 3933–3947, Aug. 2019.

[28] R. Amiri, H. Mehrpouyan, D. Matolak, and M. Elkashlan, "Joint power allocation in interference-limited networks via distributed coordinated learning," *in Proc. IEEE Veh. Technol. Conf.*, pp. 1–5, Aug 2018.

[29] R. Amiri, E. Balevi, J. G. Andrews, and H. Mehrpouyan, "Spatial Indexing for System-Level Evaluation of 5G Heterogeneous Cellular Networks," to be published.

[30] O. G. Aliu, A. Imran, M. A. Imran, and B. Evans, "A survey of self organisation in future cellular networks," *IEEE Commun. Surv. Tutor.*, vol. 15, no. 1, pp. 336–361, First Quarter 2013.

[31] J. Moysen and L. Giupponi, "From 4G to 5G: Self-organized network management meets machine learning," *CoRR*, vol. abs/1707.09300, 2017. [Online]. Available: http://arxiv.org/abs/1707.09300

[32] J. G. Andrews, S. Buzzi, W. Choi, S. V. Hanly, A. Lozano, A. C. K. Soong, and J. C. Zhang, "What will 5G be?" *IEEE J. Select. Areas Commun.*, vol. 32, no. 6, pp. 1065–1082, Jun 2014.

[33] M. Peng, D. Liang, Y. Wei, J. Li, and H. Chen, “Self-configuration and self-optimization in LTE-advanced heterogeneous networks,” *IEEE Commun. Mag.*, vol. 51, no. 5, pp. 36–45, May 2013.

[34] M. Agiwal, A. Roy, and N. Saxena, “Next generation 5G wireless networks: A comprehensive survey,” *IEEE Commun. Surv. Tutor.*, vol. 18, no. 3, pp. 1617–1655, Thirdquarter 2016.

[35] P. V. Klaine, M. A. Imran, O. Onireti, and R. D. Souza, “A survey of machine learning techniques applied to self-organizing cellular networks,” *IEEE Commun. Surv. Tutor.*, vol. 19, no. 4, pp. 2392–2431, Fourthquarter 2017.

[36] A. Imran, A. Zoha, and A. Abu-Dayya, “Challenges in 5G: how to empower SON with big data for enabling 5G,” *IEEE Network*, vol. 28, no. 6, pp. 27–33, Nov 2014.

[37] R. Li, Z. Zhao, X. Zhou, G. Ding, Y. Chen, Z. Wang, and H. Zhang, “Intelligent 5G: When cellular networks meet artificial intelligence,” *IEEE Wirel. Commun.*, vol. 24, no. 5, pp. 175–183, Oct 2017.

[38] V. Chandrasekhar, J. G. Andrews, T. Muharemovic, Z. Shen, and A. Gatherer, “Power control in two-tier femtocell networks,” *IEEE Trans. Wireless Commun.*, vol. 8, no. 8, pp. 4316–4328, Aug 2009.

[39] Z. Lu, T. Bansal, and P. Sinha, “Achieving user-level fairness in open-access femtocell-based architecture,” *IEEE Trans. Mobile Comput.*, vol. 12, no. 10, pp. 1943–1954, Oct 2013.

[40] H. Claussen, “Performance of macro- and co-channel femtocells in a hierarchical cell structure,” *IEEE 18th Int. Symp. Pers. Indoor Mobile Radio Commun.*, pp. 1–5, Sep 2007.

[41] R. Amiri and H. Mehrpouyan, “Self-organizing mm-wave networks: A power allocation scheme based on machine learning,” *in Proc. IEEE GSMM*, pp. 1–4, May 2018.

[42] Y. S. Nasir and D. Guo, “Multi-agent deep reinforcement learning for dynamic power allocation in wireless networks,” *IEEE J. Select. Areas Commun.*, vol. 37, no. 10, pp. 2239–2250, Oct. 2019.

[43] D. Lopez-Perez, X. Chu, A. V. Vasilakos, and H. Claussen, “Power minimization based resource allocation for interference mitigation in OFDMA femtocell networks,” *IEEE J. Select. Areas Commun.*, vol. 32, no. 2, pp. 333–344, Feb 2014.

[44] M. Yousefvand, T. Han, N. Ansari, and A. Khreishah, "Distributed energy-spectrum trading in green cognitive radio cellular networks," *IEEE Trans. Green Commun.*, vol. 1, no. 3, pp. 253–263, Sep 2017.

[45] H. Yazdani and A. Vosoughi, "On cognitive radio systems with directional antennas and imperfect spectrum sensing," *in Proc. IEEE ICASSP*, pp. 3589–3593, Mar 2017.

[46] A. Galindo-Serrano and L. Giupponi, "Distributed Q-learning for aggregated interference control in cognitive radio networks," *IEEE Trans. Veh. Technol.*, vol. 59, no. 4, pp. 1823–1834, May 2010.

[47] H. Saad, A. Mohamed, and T. ElBatt, "Distributed cooperative Q-learning for power allocation in cognitive femtocell networks," *in Proc. IEEE Veh. Technol. Conf.*, pp. 1–5, Sep 2012.

[48] J. R. Tefft and N. J. Kirsch, "A proximity-based Q-learning reward function for femtocell networks," *in Proc. IEEE Veh. Technol. Conf.*, pp. 1–5, Sep 2013.

[49] M. Bennis, S. M. Perlaza, P. Blasco, Z. Han, and H. V. Poor, "Self-organization in small cell networks: A reinforcement learning approach," *IEEE Trans. Wireless Commun.*, vol. 12, no. 7, pp. 3202–3212, Jul 2013.

[50] B. Wen, Z. Gao, L. Huang, Y. Tang, and H. Cai, "A Q-learning-based downlink resource scheduling method for capacity optimization in LTE femtocells," *in Proc. IEEE. Int. Comp. Sci. and Edu.*, pp. 625–628, Aug 2014.

[51] Z. Gao, B. Wen, L. Huang, C. Chen, and Z. Su, "Q-learning-based power control for LTE enterprise femtocell networks," *IEEE Syst. J.*, vol. 11, no. 4, pp. 2699–2707, Dec 2017.

[52] M. Miozzo, L. Giupponi, M. Rossi, and P. Dini, "Distributed Q-learning for energy harvesting heterogeneous networks," *in Proc. IEEE. ICCW*, pp. 2006–2011, Jun 2015.

[53] R. Barazideh, O. Semiari, S. Niknam, and B. Natarajan, "Reinforcement Learning for Mitigating Intermittent Interference in Terahertz Communication Networks," *arXiv e-prints*, 2020.

[54] B. Hamdaoui, P. Venkatraman, and M. Guizani, "Opportunistic exploitation of bandwidth resources through reinforcement learning," *in Proc. IEEE GLOBECOM*, pp. 1–6, Nov 2009.

[55] G. Alnwaimi, S. Vahid, and K. Moessner, “Dynamic heterogeneous learning games for opportunistic access in LTE-based macro/femtocell deployments,” *IEEE Trans. Wireless Commun.*, vol. 14, no. 4, pp. 2294–2308, Apr 2015.

[56] K.-L. A. Yau, P. Komisarczuk, and P. D. Teal, “Reinforcement learning for context awareness and intelligence in wireless networks: Review, new features and open issues,” *J. Netw. Comput. Appli.*, vol. 35, no. 1, pp. 253 – 267, Jan 2012.

[57] L. Matignon, G. J. Laurent, and N. Le Fort-Piat, “Reward function and initial values: Better choices for accelerated goal-directed reinforcement learning,” *in Proc. ICANN*, pp. 840–849, 2006.

[58] Z.-Q. Luo and W. Yu, “An introduction to convex optimization for communications and signal processing,” *IEEE J. Select. Areas Commun.*, vol. 24, no. 8, pp. 1426–1438, Aug 2006.

[59] S. Niknam and B. Natarajan, “On the regimes in millimeter wave networks: Noise-limited or interference-limited?” *in Proc. IEEE ICCW*, pp. 1–6, May 2018.

[60] H. Sun, X. Chen, Q. Shi, M. Hong, X. Fu, and N. D. Sidiropoulos, “Learning to optimize: Training deep neural networks for interference management,” *IEEE Trans. Signal Processing*, vol. 66, no. 20, pp. 5438–5453, Oct 2018.

[61] C. Boutilier, T. L. Dean, and S. Hanks, “Decision-theoretic planning: Structural assumptions and computational leverage,” *J. Art. Intel. Research*, vol. 11, pp. 1–94, Jul 1999.

[62] Z. Lin and M. van der Schaar, “Autonomic and distributed joint routing and power control for delay-sensitive applications in multi-hop wireless networks,” vol. 10, no. 1, pp. 102–113, Jan 2011.

[63] C. Guestrin, M. G. Lagoudakis, and R. Parr, “Coordinated reinforcement learning,” *in Proc. ICML*, pp. 227–234, Jul 2002.

[64] E. Even-Dar and Y. Mansour, “Learning rates for Q-learning,” *J. Mach. Learn. Research*, vol. 5, pp. 1–25, Dec 2004.

[65] L. Busoniu, R. B. *ŝ*ka, and B. D. Schutter, “A comprehensive survey of multiagent reinforcement learning,” *IEEE Trans. Syst., Man, Cybern. C*, vol. 38, no. 2, pp. 156–172, Mar 2008.

[66] M. J. Kearns and S. P. Singh, “Finite-sample convergence rates for Q-learning and indirect algorithms,” *NIPS*, vol. 11, pp. 996–1002, 1999.

[67] 3GPP, "Evolved Universal Terrestrial Radio Access (E-UTRA); Further advancements for E-UTRA physical layer aspects," 3rd Generation Partnership Project (3GPP), Technical Specification (TS) 36.814, 03 2010, version 9.0.0.

[68] C. C. Zarakovitis, Q. Ni, D. E. Skordoulis, and M. G. Hadjinicolaou, "Power-efficient cross-layer design for OFDMA systems with heterogeneous QoS, imperfect CSI, and outage considerations," *IEEE Trans. Veh. Technol.*, vol. 61, no. 2, pp. 781–798, Feb 2012.

[69] X. Ge, S. Tu, G. Mao, C. X. Wang, and T. Han, "5G ultra-dense cellular networks," *IEEE Wireless Commun. Mag.*, vol. 23, no. 1, pp. 72–79, February 2016.

[70] M. Chen, Y. Hua, X. Gu, S. Nie, and Z. Fan, "A self-organizing resource allocation strategy based on Q-learning approach in ultra-dense networks," in *IEEE Int. Conf. on Network Infrastructure and Digital Content (IC-NIDC)*, Sept 2016, pp. 155–160.

[71] S. Lin, J. Yu, W. Ni, and R. Liu, "Radio resource management for ultra-dense smallcell networks: A hybrid spectrum reuse approach," in *Proc. IEEE Veh. Technol. Conf.*, June 2017, pp. 1–7.

[72] A. Galindo-Serrano and L. Giupponi, "Self-organized femtocells: A fuzzy Q-learning approach," *Wirel. Netw.*, vol. 20, no. 3, pp. 441–455, Apr. 2014. [Online]. Available: http://dx.doi.org/10.1007/s11276-013-0609-6

[73] T. Park, J. Jang, O.-S. Shin, and K. B. Lee, "Transmit power allocation for a downlink two-user interference channel," *IEEE Commun. Lett.*, vol. 9, no. 1, pp. 13–15, Jan 2005.

[74] D. Park, "Optimal power allocation in two-user interference channel under individual power constraint," in *ICTC*, Oct 2016, pp. 530–532.

[75] M. Chiang, C. W. Tan, D. P. Palomar, D. O'neill, and D. Julian, "Power control by geometric programming," *IEEE Trans. Wireless Commun.*, vol. 6, no. 7, pp. 2640–2651, July 2007.

[76] M. J. Osborne and A. Rubinstein, *A course in game theory.* Cambridge, USA: The MIT Press, 1994, electronic edition.

[77] J. R. Kok, M. T. Spaan, and N. Vlassis, "Non-communicative multi-robot coordination in dynamic environments," *Robotics and Autonomous Systems*, vol. 50, no. 2, pp. 99 – 114, 2005.

[78] C. Guestrin, M. G. Lagoudakis, and R. Parr, “Coordinated reinforcement learning,” in *Proc.*, ser. ICML, 2002, pp. 227–234.

[79] J. R. Kok and N. Vlassis, “Sparse cooperative Q-learning,” in *Proc.*, ser. ICML. ACM, 2004, pp. 61–.

[80] C. Guestrin, D. Koller, and R. Parr, “Multiagent planning with factored MDPs,” in *Advances in Neural Information Processing Systems 14*. MIT Press, 2002, pp. 1523–1530.

[81] J. C. Ikuno, M. Wrulich, and M. Rupp, “System level simulation of LTE networks,” *in Proc. IEEE VTC*, pp. 1–5, May 2010.

[82] F. P. Preparata and M. I. Shamos, *Computational Geometry: An Introduction.* Berlin, Heidelberg: Springer-Verlag, 1985.

[83] B. Stroustrup, *The C++ Programming Language*, 4th ed. Addison-Wesley Professional, 2013.

[84] T. Issariyakul and E. Hossain, *Introduction to Network Simulator 2 (NS2), Springer*, pp. 21–40, Boston, MA, 2012.

[85] G. F. Riley and T. R. Henderson, “The NS-3 network simulator,” *Modeling and Tools for Network Simulation*, pp. 15–34, 2010.

[86] M. H. Dunham and V. Kumar, “Location dependent data and its management in mobile databases,” *in Proc. IEEE Workshop on Database and Expert Systems Applications (DEXA)*, pp. 414–419, Aug. 1998.

[87] N. Marsit, A. Hameurlain, Z. Mammeri, and F. Morvan, “Query processing in mobile environments: a survey and open problems,” *in Proc. IEEE Int. Conf. on Distributed Frameworks for Multimedia Applications*, pp. 150–157, Feb. 2005.

[88] A. Y. Seydim, M. H. Dunham, and V. Kumar, “An architecture for location dependent query processing,” *in Proc. IEEE Workshop on Database and Expert Systems Applications (DEXA)*, pp. 549–555, Sep. 2001.

[89] A. Varga, *OMNeT++, Modeling and Tools for Network Simulation, Springer*, pp. 35–59, 2010.

[90] A. Sobeih, J. C. Hou, Lu-Chuan Kung, Ning Li, Honghai Zhang, Wei-Peng Chen, Hung-Ying Tyan, and Hyuk Lim, “J-sim: a simulation and emulation environment for wireless sensor networks,” *IEEE Wireless Commun. Mag.*, vol. 13, no. 4, pp. 104–119, Aug. 2006.

[91] J. Lessmann, T. Heimfarth, and P. Janacik, "ShoX: An easy to use simulation platform for wireless networks," *in Proc. IEEE Int. Conf. on Computer Modeling and Simulation*, pp. 410–415, Apr. 2008.

[92] M. Mezzavilla, M. Zhang, M. Polese, R. Ford, S. Dutta, S. Rangan, and M. Zorzi, "End-to-end simulation of 5G mmWave networks," *IEEE Comm. Surveys Tutorials*, vol. 20, no. 3, pp. 2237–2263, thirdquarter 2018.

[93] B. Zheng, W. Leea, and D. Lee, "Spatial queries in wireless broadcast systems," *Wireless Networks*, vol. 10, no. 6, pp. 723–736, 2004.

[94] W. Ku, R. Zimmermann, and H. Wang, "Location-based spatial query processing with data sharing in wireless broadcast environments," *IEEE Trans. Mobile Comput.*, vol. 7, no. 6, pp. 778–791, Jun. 2008.

[95] K. Mouratidis, "Spatial queries in wireless broadcast environment," *ACM International Workshop on Data Engineering for Wireless and Mobile Access (MobiDE)*, pp. 39–44, May 2012.

[96] R. Cole, A. Ganti, U. Onunkwo, R. Schroeppel, M. Scoggin, and B. V. Leeuwen, "High fidelity simulations of large-scale wireless networks," Sandia National Laboratories, Tech. Rep., Sep. 2016.

[97] R. Fernandes and M. Ferreira, "Scalable VANET simulations with NS-3," *in Proc. IEEE VTC*, pp. 1–5, May 2012.

[98] H. Lee, V. Manshadi, and D. C. Cox, "High-fidelity and time-driven simulation of large wireless networks with parallel processing," *IEEE Commun. Mag.*, vol. 47, no. 3, pp. 158–165, Mar. 2009.

[99] D. Greene, "An implementation and performance analysis of spatial data access methods," *in Proc. Intern. Conf. on Data Engineering*, pp. 606–615, Feb. 1989.

[100] A. Guttman, "R-trees: A dynamic index structure for spatial searching," *in Proc. ACM SIGMOD Int Conf. on Management of Data*, vol. 14, no. 2, pp. 47–57, Jun. 1984.

[101] O. Semiari, W. Saad, M. Bennis, and B. Maham, "Caching meets millimeter wave communications for enhanced mobility management in 5G networks," *IEEE Trans. Wireless Commun.*, vol. 17, no. 2, pp. 779–793, Feb. 2018.

[102] T. Bai and R. W. Heath, "Coverage and rate analysis for millimeter-wave cellular networks," *IEEE Trans. Wireless Commun.*, vol. 14, no. 2, pp. 1100–1114, Feb. 2015.

[103] C. Saha and H. S. Dhillon, "Millimeter wave integrated access and backhaul in 5G: Performance analysis and design insights," *IEEE J. Select. Areas Commun.*, vol. 37, no. 12, pp. 2669–2684, Dec. 2019.

[104] S. Niknam, R. Barazideh, and B. Natarajan, "Cross-layer interference modeling for 5G mmwave networks in the presence of blockage," *in Proc. IEEE Veh. Technol. Conf.*, pp. 1–5, Aug. 2018.

[105] S. Karimi-Bidhendi, J. Guo, and H. Jafarkhani, "Using quantization to deploy heterogeneous nodes in two-tier wireless sensor networks," *in Proc. IEEE ISIT*, pp. 1502–1506, Jul. 2019.

[106] J. Guo, S. Karimi-Bidhendi, and H. Jafarkhani, "Energy efficient node deployment in wireless ad-hoc sensor networks," *CoRR*, vol. abs/1904.06380, 2019. [Online]. Available: http://arxiv.org/abs/1904.06380

[107] R. Jurdi, J. G. Andrews, D. Parsons, and R. W. Heath, "Identifying coverage holes: Where to densify?" *in Proc. IEEE Asilomar Conf. on Signals, Systems, and Computers*, pp. 1417–1421, Nov. 2017.

[108] (2020) GeoNS: Geometric network simulator. [Online]. Available: https://github.com/roamiri/GeoNS

[109] *Mobile backhaul options: Spectrum analysis and recommendations*, ABI research, GSM Association, Nov 2018.

[110] G. Sellin, J. Edstam, A. Olsson, J. Flodin, M. Öhberg, A. Henriksson, J. Hansryd, and J. Ahlberg, "Ericsson Microwave Outlook," Ericsson, Tech. Rep., Dec 2018.

[111] "Small Cell Millimeter Wave Mesh Backhaul," InterDigital Inc., Tech. Rep., Feb 2013.

[112] M. R. Akdeniz, Y. Liu, M. K. Samimi, S. Sun, S. Rangan, T. S. Rappaport, and E. Erkip, "Millimeter wave channel modeling and cellular capacity evaluation," *IEEE J. Select. Areas Commun.*, vol. 32, no. 6, pp. 1164–1179, Jun. 2014.

[113] S. Sur, X. Zhang, P. Ramanathan, and R. Chandra, "BeamSpy: Enabling robust 60 GHz links under blockage," *in Proc. USENIX Networked Systems Design and Implementation (NSDI)*, pp. 193–206, Mar. 2016.

[114] J. Xu, J. Yao, L. Wang, K. Wu, L. Chen, and W. Lou, "Revolution of self-organizing network for 5G mmwave small cell management: From reactive to proactive," *IEEE Wireless Commun. Mag.*, vol. 25, no. 4, pp. 66–73, Aug 2018.

[115] N. Nikaein and C. Bonnet, "Topology management for improving routing and network performances in mobile ad hoc networks," *Mob. Netw. Appl.*, vol. 9, no. 6, pp. 583–594, Dec. 2004.

[116] L. Bao and J. J. Garcia-Luna-Aceves, "Topology management in ad hoc networks," *in Proc. ACM Intern. Symp. on Mobile Ad Hoc Networking and Computing*, pp. 129–140, 2003.

[117] Y. Chiang and W. Liao, "mw-Hierback: A cost-effective and robust millimeter wave hierarchical backhaul solution for HetNets," *IEEE Trans. Mobile Comput.*, vol. 16, no. 12, pp. 3445–3458, Dec. 2017.

[118] 3GPP, "Technical Specification Group Radio Access Network; NR; Study on Integrated Access and Backhaul," 3rd Generation Partnership Project (3GPP), Technical Specification (TS) 38.874, 12 2018, version 16.0.0.

[119] U. Siddique, H. Tabassum, E. Hossain, and D. I. Kim, "Wireless backhauling of 5G small cells: challenges and solution approaches," *IEEE Wireless Commun. Mag.*, vol. 22, no. 5, pp. 22–31, Oct 2015.

[120] H. S. Dhillon and G. Caire, "Wireless backhaul networks: Capacity bound, scalability analysis and design guidelines," *IEEE Trans. Wireless Commun.*, vol. 14, no. 11, pp. 6043–6056, Nov 2015.

[121] S. Singh, M. N. Kulkarni, A. Ghosh, and J. G. Andrews, "Tractable model for rate in self-backhauled millimeter wave cellular networks," *IEEE J. Select. Areas Commun.*, vol. 33, no. 10, pp. 2196–2211, Oct 2015.

[122] M. N. Kulkarni, J. G. Andrews, and A. Ghosh, "Performance of dynamic and static TDD in self-backhauled millimeter wave cellular networks," *IEEE Trans. Wireless Commun.*, vol. 16, no. 10, pp. 6460–6478, Oct 2017.

[123] C. Saha, M. Afshang, and H. S. Dhillon, "Bandwidth partitioning and downlink analysis in millimeter wave integrated access and backhaul for 5G," *IEEE Trans. Wireless Commun.*, vol. 17, no. 12, pp. 8195–8210, Dec 2018.

[124] X. Xu, W. Saad, X. Zhang, X. Xu, and S. Zhou, "Joint deployment of small cells and wireless backhaul links in next-generation networks," *IEEE Commun. Lett.*, vol. 19, no. 12, pp. 2250–2253, Dec 2015.

[125] M. N. Islam, A. Sampath, A. Maharshi, O. Koymen, and N. B. Mandayam, "Wireless backhaul node placement for small cell networks," *in Proc. IEEE CISS*, pp. 1–6, Mar 2014.

[126] T. K. Vu, M. Bennis, M. Debbah, and M. Latva-aho, "Joint path selection and rate allocation framework for 5G self-backhauled mmwave networks," *IEEE Trans. Wireless Commun.*, pp. 2431 – 2445, Apr 2019.

[127] D. Yuan, H. Lin, J. Widmer, and M. Hollick, "Optimal joint routing and scheduling in millimeter-wave cellular networks," *in Proc. IEEE Conf. Comput. Commun.*, pp. 1205–1213, Apr 2018.

[128] M. Selim, A. Kamal, K. Elsayed, H. M. Abdel-Atty, and M. Alnuem, "Self-healing in 5G HetNets: A research and development perspective," pp. 149–177, Apr 2016.

[129] F. Kuo, F. A. Zdarsky, J. Lessmann, and S. Schmid, "Cost-efficient wireless mobile backhaul topologies: An analytical study," *in Proc. IEEE GLOBECOM*, pp. 1–5, Dec 2010.

[130] W. S. Soh, Z. Antoniou, and H. S. Kim, "Improving restorability in radio access network," *in Proc. IEEE GLOBECOM*, vol. 6, pp. 3493–3497 vol.6, Dec 2003.

[131] R. Santos, H. Ghazzai, and A. Kassler, "Optimal steerable mmwave mesh backhaul reconfiguration," *in Proc. IEEE GLOBECOM*, pp. 1–7, Dec 2018.

[132] P. Huang and K. Psounis, "Efficient mmwave wireless backhauling for dense small-cell deployments," pp. 88–95, Feb 2017.

[133] S. Singh, R. Mudumbai, and U. Madhow, "Interference analysis for highly directional 60-GHz mesh networks: The case for rethinking medium access control," *IEEE/ACM Trans. Networking*, vol. 19, no. 5, pp. 1513–1527, Oct. 2011.

[134] M. Polese, M. Giordani, A. Roy, D. Castor, and M. Zorzi, "Distributed path selection strategies for integrated access and backhaul at mmwaves," *in Proc. IEEE GLOBECOM*, pp. 1–7, Dec. 2018.

[135] M. Polese, M. Giordani, T. Zugno, A. Roy, S. Goyal, D. Castor, and M. Zorzi, "Integrated access and backhaul in 5G mmwave networks: Potentials and challenges," *CoRR*, vol. abs/1906.01099, 2019.

[136] M. Rebato, M. Mezzavilla, S. Rangan, F. Boccardi, and M. Zorzi, "Understanding noise and interference regimes in 5G millimeter-wave cellular networks," *in Proc. European Wireless Conf.*, pp. 1–5, May 2016.

[137] P. Balister, A. Sarkar, and B. Bollobás, "Percolation, connectivity, coverage and colouring of random geometric graphs," *Handbook of Large-Scale Random Networks*, pp. 117–142, 2008.

[138] H. Frezza-Buet and M. Geist, “A C++ template-based reinforcement learning library: Fitting the code to the mathematics,” *J. Mach. Learn. Res.*, vol. 14, no. 1, pp. 625–628, Feb. 2013.

[139] Y. LeCun, C. Cortes, and C. Burges, “MNIST handwritten digit database,” *ATT Labs*, vol. 2, 2010. [Online]. Available: http://yann.lecun.com/exdb/mnist

[140] Y. Fan, Z. Zhang, and H. Li, “Message passing based distributed learning for joint resource allocation in millimeter wave heterogeneous networks,” *IEEE Trans. Wireless Commun.*, vol. 18, no. 5, pp. 2872–2885, May 2019.

[141] Y. Yang, R. Luo, M. Li, M. Zhou, W. Zhang, and J. Wang, “Mean field multi-agent reinforcement learning,” *CoRR*, vol. abs/1802.05438, 2018.

[142] A. L. Strehl, L. Li, and M. L. Littman, “Reinforcement learning in finite MDPs: PAC analysis,” *J. Mach. Learn. Res.*, vol. 10, pp. 2413–2444, Dec. 2009.

[143] W. Hoeffding, “Probability inequalities for sums of bounded random variables,” *J. Am. Stat. Assoc*, vol. 58, no. 301, pp. 13–30, 1963.

[144] (2019) Boost C++ libraries/R-tree.

Appendix A

CHAPTER 2

A.1 Proof of Proposition 1

Proof. Assume an MDP represented as $(\mathcal{X}, \mathcal{A}, \Pr(y|x,a), r(x,a))$, a policy π with value-function $V_\pi : \mathcal{X} \to \mathbb{R}$ and Q-function $Q_\pi : \mathcal{Z} \to \mathbb{R}$, $\mathcal{Z} = \mathcal{X} \times \mathcal{A}$. Here, $\mathcal{A}$ refers to action space of one agent and k is the iteration index. According to (2.4), the maximum of the value-function can be fined as $V_{max} = \frac{R_{max}}{1-\beta}$. The Bellman optimality operator is defined as $(\mathtt{T}Q)(x,a) \triangleq r(x,a) + \beta \sum_{y \in \mathcal{X}} \Pr(y|x,a) \max\limits_{b \in \mathcal{A}} Q(y,b)$. $\mathtt{T}Q$ is a contraction operator with factor β, i.e., $\|\mathtt{T}Q - \mathtt{T}Q'\| \leq \beta \|Q - Q'\|$ and Q^* is a unique fixed-point of $(\mathtt{T}Q)(x,a)$, $\forall (x,a) \in \mathcal{Z}$. Further, for the ease of notation and readability the time step notation is slightly changed as Q_k refers to the action-value function after k iterations.

Assume that the state-action pair (x,a) is visited k times and $\mathcal{F}_k = \{y_1, y_2, ..., y_k\}$ are the visiting next states. At time step $k+1$, the update rule of Q-*learning* is

$$Q_{k+1}(x,a) = (1-\alpha_k) Q_k(x,a) + \alpha_k \mathtt{T}_k Q_k(x,a), \tag{A.1}$$

where, $\mathtt{T}_k Q_k$ is the empirical Bellman operator defined as $\mathtt{T}_k Q_k(x,a) \triangleq r(x,a) + \beta \max\limits_{b \in \mathcal{A}} Q(y_k, b)$. (From this point, for simplicity, we remove the dependency on (x,a)). It is easy to show that $E[\mathtt{T}_k Q_k] = \mathtt{T}Q_k$, therefore, we define e_k as the estimation error of each iteration as $e_k = \mathtt{T}_k Q_k - \mathtt{T}Q_k$. By using $\alpha_k = \frac{1}{k+1}$, the update rule of Q-*learning* can be written as

$$Q_{k+1} = \frac{1}{k+1}\left(kQ_k + \mathtt{T}Q_k + e_k\right). \tag{A.2}$$

Now, in order to prove Proposition 1, we need to state the following lemmas.

Lemma 1. For any $k \geq 1$, we have

$$Q_k = \frac{1}{k}\sum_{i=0}^{k-1} \mathtt{T}_i Q_i = \frac{1}{k}\left(\sum_{i=0}^{k-1} \mathtt{T} Q_i + \sum_{i=0}^{k-1} e_i\right). \tag{A.3}$$

Proof. We prove this lemma by induction. The lemma holds for $k = 1$ as $Q_1 = \mathtt{T}_0 Q_0 = \mathtt{T} Q_0 + e_0$. We now show that if the result holds for k, then it also holds for $k+1$. From (A.2) we have

$$\begin{aligned} Q_{k+1} &= \frac{k}{k+1} Q_k + \frac{1}{k+1}\left(\mathtt{T} Q_k + e_k\right) \\ &= \frac{k}{k+1}\frac{1}{k}\left(\sum_{i=0}^{k-1} \mathtt{T} Q_i + \sum_{i=0}^{k-1} e_i\right) + \frac{1}{k+1}\left(\mathtt{T} Q_k + e_k\right) \\ &= \frac{1}{k+1}\left(\sum_{i=0}^{k} \mathtt{T} Q_i + \sum_{i=0}^{k} e_i\right). \end{aligned}$$

Thus (A.3) holds for $k \geq 1$ by induction. □

Lemma 2. Assume that initial action-value function, Q_0, is uniformly bounded by V_{max}. Then, for all $k \geq 1$ we have $\|Q_k\| \leq V_{max}$ and $\|Q^* - Q_k\| \leq 2V_{max}$.

Proof. We first prove that $\|Q_k\| \leq V_{max}$ by induction. The inequality holds for $k = 1$ as

$$\begin{aligned} \|Q_1\| &= \|\mathtt{T}_0 Q_0\| \\ &= \|r + \beta \max Q_0\| \leq \|r\| + \beta\|Q_0\| \leq R_{max} + \beta V_{max} \\ &= V_{max}. \end{aligned}$$

Now, we assume that for $1 \leq i \leq k$, $\|Q_k\| \leq V_{max}$ holds. First, $\|\mathtt{T}_k Q_k\| = \|r + \beta \max Q_k\| \leq \|r\| + \beta\|\max Q_k\| \leq R_{max} + \beta V_{max} = V_{max}$. Second, from Lemma 1 we have

$$\|Q_{k+1}\| = \frac{1}{k+1}\left\|\sum_{i=0}^{k} \mathtt{T}_i Q_i\right\| \leq \frac{1}{k+1}\sum_{i=0}^{k}\|\mathtt{T}_i Q_i\| \leq V_{max}.$$

Therefore, the inequality holds for $k \geq 1$ by induction. Now the bound on $\|Q^* - Q_k\|$ follows $\|Q^* - Q_k\| \leq \|Q^*\| + \|Q_k\| \leq 2V_{max}$. □

Lemma 3. Assume that initial action-value function, Q_0, is uniformly bounded by V_{max}, then, for any $k \geq 1$

$$\|Q^* - Q_k\| \leq \frac{2\beta V_{max}}{k\,(1-\beta)} + \frac{1}{k}\left\|\sum_{i=0}^{k-1} e_i\right\|. \tag{A.4}$$

Proof. From Lemma 1, we have

$$\begin{aligned} Q^* - Q_k &= Q^* - \frac{1}{k}\left(\sum_{i=0}^{k-1}\mathtt{T}Q_i + \sum_{i=0}^{k-1} e_i\right) \\ &= \frac{1}{k}\sum_{i=0}^{k-1}\left(\mathtt{T}Q^* - \mathtt{T}Q_i\right) - \frac{1}{k}\sum_{i=0}^{k-1} e_i. \end{aligned}$$

Therefore, we can write

$$\begin{aligned} \|Q^* - Q_k\| &\leq \frac{1}{k}\left\|\sum_{i=0}^{k-1}\left(\mathtt{T}Q^* - \mathtt{T}Q_i\right)\right\| + \frac{1}{k}\left\|\sum_{i=0}^{k-1} e_i\right\| \\ &\leq \frac{1}{k}\sum_{i=0}^{k-1}\|\mathtt{T}Q^* - \mathtt{T}Q_i\| + \frac{1}{k}\left\|\sum_{i=0}^{k-1} e_i\right\| \\ &\leq \frac{\beta}{k}\sum_{i=0}^{k-1}\|Q^* - Q_i\| + \frac{1}{k}\left\|\sum_{i=0}^{k-1} e_i\right\|. \end{aligned}$$

and according to [142], $\|Q^* - Q_i\| \leq \beta^i\|Q^* - Q_0\|$. Hence, using Lemma 2, we can write

$$\begin{aligned}\|Q^* - Q_k\| &\leq \frac{\beta}{k}\sum_{i=0}^{k-1} 2\beta^i V_{max} + \frac{1}{k}\left\|\sum_{i=0}^{k-1} e_i\right\| \\ &\leq \frac{2\beta V_{max}}{k\left(1-\beta\right)} + \frac{1}{k}\left\|\sum_{i=0}^{k-1} e_i\right\|.\end{aligned}$$

□

Now, we prove Proposition 1 by using the above result in Lemma 3. To this aim, we need to provide a bound on the norm of the summation of errors in the inequality of Lemma 3. First, we can write

$$\frac{1}{k}\left\|\sum_{i=0}^{k-1} e_i\right\| = \frac{1}{k}\max_{(x,a)\in\mathcal{Z}}\left|\sum_{i=0}^{k-1} e_i\right|.$$

For the estimation error sequence $\{e_0, e_1, \cdots, e_k\}$, we have the property that $\mathbb{E}\left[e_k|\mathcal{F}_{k-1}\right] = 0$ which means that the error sequence is a martingale difference sequence with respect to $\mathcal{F}_k$. Therefore, according to Hoeffding-Azuma inequality [143] for a martingale difference sequence of $\{e_0, e_1, \cdots, e_{k-1}\}$ which is bounded by $2V_{max}$, for any $t > 0$, we can write

$$\Pr\left(\left|\sum_{i=0}^{k-1} e_i\right| > t\right) \leq 2\exp\left(\frac{-t^2}{8kV_{max}^2}\right).$$

Therefore, by a union bound over the state-action space, we have

$$\Pr\left(\left\|\sum_{i=0}^{k-1} e_i\right\| > t\right) \leq 2|\mathcal{X}|.|\mathcal{A}|\exp\left(\frac{-t^2}{8kV_{max}^2}\right) = \delta,$$

and then,

$$\Pr\left(\frac{1}{k}\left\|\sum_{i=0}^{k-1} e_i\right\| \le V_{max}\sqrt{\frac{8}{k}\ln\frac{2|\mathcal{X}|.|\mathcal{A}|}{\delta}}\right) \ge 1-\delta.$$

Hence, with probability at least $1-\delta$ we can say

$$\|Q^* - Q_k\| \le \frac{2R_{max}}{(1-\beta)}\left[\frac{\beta}{k\,(1-\beta)} + \sqrt{\frac{2}{k}\ln\frac{2|\mathcal{X}|.|\mathcal{A}|}{\delta}}\right].$$

Consequently, the result in Proposition 1 is proved. $\square$

Appendix B

CHAPTER 4

B.1 Insertion to the R-tree

In order to implement the R-tree, we have used the Boost C++ libraries [144]. Further, we define two variables representing the location and the dimensions of an element of the network respectively as *point* and *box* variables. Without loss of generality, we assume *point* has two-dimensions. The *point* variable can be defined for three-dimensional data if the height of the elements of the network is important as well. Also, The *point* variable is defined over *float* data type to accelerate the simulations. The box variable is a two-dimensional rectangle representing the physical dimensions of the elements of the network. The *Node* contains the above definitions as the spatial information of objects as follows. The above definitions are represented below.

```
namespace bg = boost::geometry;
namespace bgi = boost::geometry::index;
typedef bg::model::point<float,2,bg::cs::cartesian>point;
typedef bg::model::box<point>box;
```

As it is mentioned in Section 4.2.2, leaves of the R-tree hold the information as value pairs. We define the following value pair as the input of the R-tree named as *value*.

```
typedef std::pair<point, boost::shared_ptr<node>> value;
```

The R-tree data structure saves the objects of the network based on their corresponding pairs. This method helps to index all the elements of the network based on their location. Hence, after creating an object, the corresponding *value* pair is created and inserted in the tree as follows. Here, we create a mmWave BS as an example.

```
bgi::rtree< value, bgi::quadratic<16>>m_tree;
boost::shared_ptr<mmWaveBS>BS;
```

```
// Generate shared pointer of a mmWaveBS
BS=boost::shared_ptr<mmWaveBS>(new mmWaveBS(x,y,get_nextID(),def_P_tx));
//Insert the BS to the tree.
m_tree.insert(std::make_pair(BS->get_loc(),BS));
```

In the first line above, the *m_tree* is created as an R-tree over the defined *value* pairs. The second and third line create a mmWaveBS and set its location, x, y, identification number, and its transmit power. Finally, the created mmWaveBS is inserted to the tree with its corresponding *value* in line four (The mmWaveBS contains the get_loc() method which returns the location of the object in *point* format.). Also, since mmWaveBS is inherited from the *Node*, there is no need to cast it to the *Node* object.

B.2 Parallel processing and message-passing

1. Parallel processing: In order to create a parallel process for an object inherited from the *TRX*, the *ThreadMain()* method of the object should be implemented. The desired functionality of the thread can be called from the *Start* method as follows.

```
void Start(){
the_thread=std::thread(&desiredObject::ThreadMain,this);}
```

   In the above, a simple implementation of the *Start* method is presented. The *Start* method calls the *ThreadMain* function as the main function of the thread.

2. Message-passing: Message-passing is implemented using simple signal-slot mechanisms. Any signal-slot mechanism contains three main fields, (*i*) the message structure, (*ii*) the signal to be sent, and (*iii*) the destination function (slot).

You can connect functions to the signal which will be called when the *emit()* method on the signal object is invoked. Any argument passed to *emit()* will be passed to the given functions. For instance, for passing a message from object **O1** to a function in object **O2**, first we need to define the structure of the message as follow.

```
struct Message{char[20] s;};
```

In the above, the Message structure contains an array of characters. The signal is defined in the sender, i.e., **O1** as follow.

```
Signal<Message const &> signal;
```

and the function which handles the received message is defined in the **O2** as follows.

```
void handler(Const Message& msg);
```

After ceating the objects **O1** and **O2**, the signal and the slot are connected to each other as follows.

```
signal.connect_member(&O2, &O2::handler);
```

In order to create an event or emit the signal, we just need to call the emit function of the signal with the Message data as follows.

```
// Create the msg and Fill in the fields.
Message msg; msg.s = "Hello!"
// Emitting the msg.
signal.emit(msg);
```

By emitting the signal from the object **O1**, the *handler* function in the object **O2** receives the Message and is able to process it.

B.3 SINR characterization

In a randomly deployed network or a dynamic network where the active set of transmitters and receivers change with time, deriving the set $\mathcal{I}_j$ (representing the set of directional interferers) for the receiver j is challenging. However, with the proposed architecture, any receiver can find the set $\mathcal{I}_j$ for any transmitter with the defined queries in Section 4.2.3. In Algorithm 1, we illustrate how to calculate SINR of the all possible mmWave links for a network containing a set $\mathcal{N}$ mmWave nodes. Further, the code snippets of the Algorithm 1 is presented afterwards as well.

Algorithm 2 Evaluate SINR of all links in a mmWave network.

```
1:  for $j \in \mathcal{N}$ do
2:      Retrieve desired level of the object $j$ using dynamic_cast
3:      Get position and ID of the node $j$.
4:      perform fixed-radius neighbor query to derive set $\mathcal{O}_j$ (Localizing the search)
5:      for $i \in \mathcal{O}_j$ do
6:          Retrieve desired level of the object $i$ using dynamic_cast
7:          Get position and ID of the node $i$.
8:          Derive the triangular polygon for the pair $j$ and $i$
9:          Perform triangular query over the polygon to derive the set $\mathcal{I}_j$
10:         interference = 0
11:         for $k \in \mathcal{I}_j$ do
12:             Calculate interference of node $k$ and add it to interference
13:         end for
14:         Calculate SINR$_{ij}$
15:     end for
16: end for
```

```
// mmB is the desired receiver SBS, cid and p1 are its ID and location,
    respectively.
uint32_t cid = mmB.get()->getID();
point p1 = mmB->get_loc();
// search for fixed-radius nearest neighbours residing in maximum mmWave
    range.
```

```
std::vector<value> results;
m_tree.query(bgi::satisfies([&](value const& v) {return bg::distance(v.
    first, p1) < def_MAX_MMWAVE_RANGE;}), std::back_inserter(results));
// Search in the resulted SBSs in the maximum range.
BOOST_FOREACH(value const&v, results){
    bs_ptr mmB2 = boost::dynamic_pointer_cast<mmWaveBS>(v.second);
    uint32_t cid2 = mmB2.get()->getID();
    if( cid2 != cid){
        double x2 = mmB2->getX(); double y2 = mmB2->getY(); point p2 =
            mmB2->get_loc();
        // create the interference triangular polygon.
         polygon2D poly = directional_polygon(p1, p2, mmB->get_phi_m());
         std::vector<value> vec_query;
         //Find the interfering SBSs.
         m_tree.query(bgi::intersects(poly), std::back_inserter(vec_query
             ));
         double interf=0.;
         BOOST_FOREACH(value const&mz, vec_query){
             bs_ptr mmB3 = boost::dynamic_pointer_cast<mmWaveBS>(mz.
                 second);
             uint32_t cid3 = mmB3->getID();
             if(cid3!=cid2 && cid3!=cid)
                 interf+= mmB->calculate_Interf_of_link(mmB3->getX(),
                     mmB3->getY());
         }
         // Calculate SNR and SINR of the link.
         double snr = mmB->calculate_SNR_of_link(x2, y2);
         double sinr = mmB->calculate_SINR_of_link(x2,y2, interf);
     }
}
```

Appendix C

CHAPTER 5

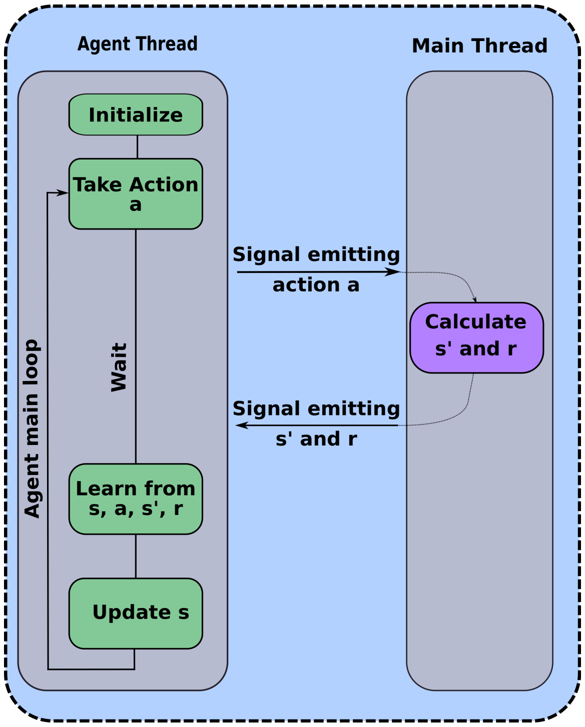

Figure C.1: Independent process of an agent and the main process.

C.1 Synchronous and Asynchronous Learning

Multi-agent RL, in its nature, is based on the interaction of each agent with the environment. Hence, the agents can run their training algorithms separately. From a computation standpoint, the independence of the training of each agent gives us the opportunity to perform this task in parallel. Parallel training of the agents becomes essential as the function approximator of each agent becomes expensive. For instance, if each agent is using a deep neural network (DNN) as its function approximator and backpropagation as the training algorithm, then parallel training and using all resources is essential. Hence, we provide two methods of training for the RL agents, (*i*) synchronous and (*ii*) asynchronous learning. In synchronous learning, agents are trained in a queue by a single process. Synchronous learning can be used in simple

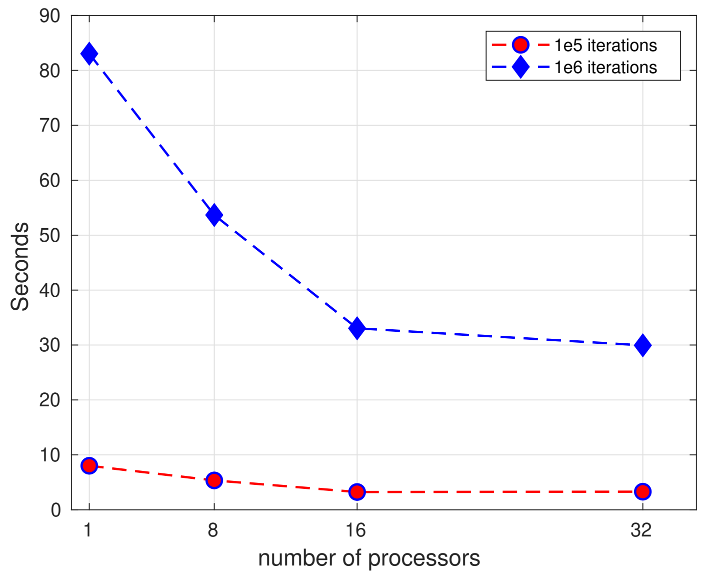

Figure C.2: Running time for training of the WSN with 62 sensors. The running time for one process refers to synchronous learning and the rest are related to asynchronous learning. The machine specification for running the simulations is Intel(R) Xeon(R) CPU E5-2683 v3@2.00GHz.

training algorithms or when the resources are limited. In asynchronous learning, each agent runs its processes independently as a separate thread as in Fig. C.1. According to Fig. C.1, an agent trains its own Q-function with a signal-slot structure. By taking action a, the agent emits a signal containing its action. The environment as the main thread receives this signal and runs the required processes to calculate the reward and the new state of the agent. Meanwhile, the agent waits for the response of the environment. The new state and the reward of the agent are emitted by the environment. Upon receiving the new state and the reward, the agent updates its Q-function, i.e., learning process, and then updates its state. Independent processes for the agents bring scalability, which can be essential in large networks to use all the computation resources.

Further, in order to investigate the scalability, we run the training process on different machines with a different number of processes. Fig. C.2 presents the running time of the training process for one, eight, 16, and 32 number of processes. Fig. C.2 shows the scalability of the simulator for using the existing resources to accelerate the training processes. On the other hand, even for one processor, the running time of the training is just 83.1 seconds for one million iterations. This result shows the efficiency of the platform.